UNIVERSITY OF CALIFORNIA,
IRVINE

Self-interference Cancellation in Full-duplex Wireless Systems

DISSERTATION

submitted in partial satisfaction of the requirements
for the degree of

DOCTOR OF PHILOSOPHY

in Electrical and Computer Engineering

by

Elsayed Ahmed Elsayed Ahmed

Dissertation Committee:
Professor Ahmed M. Eltawil, Chair
Professor Arnold Lee Swindlehurst
Professor Ender Ayanoglu

2014

DEDICATION

To my parents,
my wife,
and my kids.

TABLE OF CONTENTS

LIST OF FIGURES

LIST OF TABLES

ACKNOWLEDGMENTS

I would like to express my deepest gratitude to my advisor, Professor Ahmed M. Eltawil, who provided me with the guidance and support in all aspects of my research at UC Irvine. His guidance and support always helped me to overcome the challenges that I faced in my research. I learnt from him how to face challenges, question thoughts, and express ideas.

I also would like to thank Professor Ashutosh Sabharwal with the Department of Electrical and Computer Engineering, Rice University, Houston, TX, for his guidance and support in the early stage of my research. The numerous insightful discussions with him opened to me several prospects that enriched my contributions.

I would like to acknowledge the support and the cooperative work with the Wireless System and Circuits Lab (WSCL) members. The discussions and technical support provided by Dr. Amr M. A. Hussien, and Dr. Muhammad S. Khairy, were very crucial in the successful completion of this project.

I would also like to thank my parents and my siblings who were always supporting me and encouraging me with their best wishes. I would also like to thank my little daughter Sama Elsayed for scarifying part of her play time for my rest after long work days. Finally, and most importantly, I would like to thank my beloved wife, Nouran Mahmoud. She was always there for me and stood by me through the good and bad times. Her moral and physical support was always a driving force throughout my PhD.

CURRICULUM VITAE

Elsayed Ahmed Elsayed Ahmed

EDUCATION

- **University of California, Irvine** September 2014
  PhD in Electrical Engineering and Computer Science.
  Thesis topic: Self-interference Cancellation Techniques for Full-duplex Systems.

- **Cairo University, Egypt** September 2010
  M.Sc. in Electronics and Communications Engineering.
  Thesis topic: Design and Implementation of Low-complexity Channel Estimation and Equalization Techniques for LTE Systems.

- **Cairo University, Egypt** June 2006
  B.Sc. in Electronics and Communications Engineering.
  Cumulative Grade: Distinction With Degree of Honor.
  Graduation project: FPGA-based Implementation of SPARC Processor.

RESEARCH EXPERIENCE

- **PhD Student Researcher** September 2010 - September 2014
  University of California, Irvine
  Research on the feasibility of full-duplex wireless transmission including theoretical analysis for the system limitations, development of several self-interference cancellation techniques, and experimental analysis for the performance of the developed techniques using different SDR platforms.

- **M.Sc Student Researcher** September 2006 - September 2010
  Cairo University, Egypt
  Design and implementation of low-complexity channel estimation techniques for LTE systems.

WORK EXPERIENCE

- **Digital Design Intern** June 2013 - September 2013
  Newport Media, Inc., Lake Forst, CA
  Architecture and RTL design for a complete multi-mode 802.11a,n,ac transmitter physical-layer, with 20, 40, 80MHz bandwidth options.

- **Digital Design Intern** June 2012 - September 2012
  Newport Media, Inc., Lake Forst, CA
  Architecture and RTL design for 802.11n LDPC encoder.

- **Senior System Design Intern** June 2011 - September 2011
  Newport Media, Inc., Lake Forst, CA
  System level design of LTE physical-layer.

- **Senior System Design Engineer** October 2006 - September 2010
  Newport Media, Inc., Cairo, Egypt
  Design of numerous low-complexity physical-layer algorithms for various mobile TV standards such as DVB-H, MediaFLO, CMMB, ATSC-M/H, and analog TV.

PATENTS

- Elsayed Ahmed, Ahmed M. Eltawil, and Bedri A. Cetiner, "Full-Duplex Systems Using Reconfigurable Antennas". *U.S. Provisional patent application.*

- Elsayed Ahmed, and Ahmed M. Eltawil, "Self-interference Cancellation for Full-duplex Systems". *U.S. Provisional patent application.*

- Elsayed Ahmed, and Nabil Yousef, "Robust Technique for Frame Synchronization in DAB-IP Systems". *U.S. Patent,* No. 7940759.

- Elsayed Ahmed, and Nabil Yousef, "Coarse Frequency Offset Estimation for Digital Multimedia Broadcasting". *U.S. Patent,* No. 8005173.

- Elsayed Ahmed, and Nabil Yousef, "Robust PID Filtering for DVB-H". *U.S. Patent,* No. 8599933.

SELECTED PUBLICATIONS

- E. Ahmed, and A. M. Eltawil "All-Digital Self-interference Cancellation Technique for Full-duplex Systems," submitted to *IEEE Transactions on Wireless Communications.* [Online]. Available: http://arxiv.org/abs/1406.5555.

- E. Ahmed, A. M. Eltawil, Z. Li, and B. A. Cetiner "Full-Duplex Systems Using Multi-Reconfigurable Antennas," submitted to *IEEE Transactions on Wireless Communications.* [Online]. Available: http://arxiv.org/abs/1405.7720.

- E. Ahmed, and A. M. Eltawil, "On Phase Noise Suppression in Full-Duplex Systems," submitted to *IEEE Transactions on Wireless Communications.* [Online]. Available: http://arxiv.org/abs/1401.6437.

- E. Ahmed, A. M. Eltawil, and A. Sabharwal, "Rate Gain Region and Design Tradeoffs for Full-Duplex Wireless Communications, " *Wireless Communications, IEEE Transactions on* , vol.12, no.7, pp.3556,3565, July 2013.

- E. Ahmed, A. M. Eltawil, and A. Sabharwal, "Self-Interference Cancellation with Nonlinear Distortion Suppression for Full-Duplex Systems," *Signals, Systems and Computers, 2013 Asilomar Conference on*, pp.1199,1203, Nov. 2013.

- E. Ahmed, A. M. Eltawil, and A. Sabharwal, "Self-Interference Cancellation with Phase Noise Induced ICI Suppression for Full-Duplex Systems," *Global Communications Conference (GLOBECOM), 2013 IEEE*, pp.3384,3388, Dec. 2013.

- E. Ahmed, A. M. Eltawil, and A. Sabharwal, "Simultaneous transmit and sense for cognitive radios using full-duplex: A first study," *Antennas and Propagation Society International Symposium (APSURSI), 2012 IEEE* , pp.1-2, July 2012.

PEER REVIEW ACTIVITIES

- IEEE Transactions on Wireless Communications.

- IEEE Transactions on Vehicular Technology.

- IEEE Communications Magazine.

- IEEE Journal on Selected Areas in Communications.

HONORS

- Electrical Engineering and Computer Science Department Graduate Fellowship, University of California Irvine 2010.

- Ministry of Communications and Information Technology award for best graduation project in communications, EED (Egypt Engineering Day) 2006 organized by IEEE Egypt Section.

ABSTRACT OF THE DISSERTATION

Self-interference Cancellation in Full-duplex Wireless Systems

By

Elsayed Ahmed Elsayed Ahmed

Doctor of Philosophy in Electrical and Computer Engineering

University of California, Irvine, 2014

Professor Ahmed M. Eltawil, Chair

Due to the tremendous increase in wireless data traffic, one of the major challenges for future wireless systems is the utilization of the available spectrum to achieve better data rates over limited spectrum. Currently, systems operate in what is termed "Half Duplex Mode," where they are either transmitting or receiving, but never both using the same temporal and spectral resources. Full-duplex transmission promises to double the spectral efficiency where bidirectional communications is carried out over the same temporal and spectral resources. The main limitation impacting full-duplex transmission is managing the strong self-interference signal imposed by the transmit antenna on the receive antenna within the same transceiver. Several recent publications have demonstrated that the key challenge in practical full-duplex systems is un-cancelled self-interference power caused by a combination of hardware imperfections, especially Radio Frequency (RF) circuits' impairments.

In this thesis, we consider the problem of self-interference cancellation in full-duplex systems. The ultimate goal of this work is to design and build a complete, real-time, full-duplex system that is capable of achieving wireless full-duplex transmission using practical hardware platforms. Since RF circuits' impairments are shown to have significant impact on the self-interference cancellation performance, first, we present a thorough analysis of the effect of RF impairments on the cancellation performance, with the aim of identifying the main per-

formance limiting factors and bottlenecks. Second, the thesis proposes several impairments mitigation techniques to improve the overall self-interference cancellation capability by mitigating most of the transceiver RF impairments. In addition to impairments mitigation, two novel full-duplex transceiver architectures that achieve significant self-interference cancellation performance are proposed. The performance of the proposed techniques is analytically and experimentally investigated in practical wireless environments. Finally, the proposed self-interference cancellation techniques are used to build a complete full-duplex system with a 90% experimentally proven full-duplex rate improvement compared to half-duplex systems.

Chapter 1

Introduction

1.1 Full-duplex Wireless Transmission

Due to the continuing increase of wireless technology users, wireless data traffic is increasing by a factor of 10 every five years [1, 2]. Coping with such rapid growth is a major challenge for future wireless systems, especially with limited spectrum availability.

One major shortcoming of current deployed systems is the limitation to operate as half-duplex systems employing either a time-division or frequency-division approach to bidirectional communication. Half-duplex transmission requires dividing the temporal and/or spectral resources into orthogonal resources, thus enforcing a limitation on the possible potential of the system to nearly double its spectral efficiency by operating as full-duplex systems. In full-duplex systems [3]-[47], bidirectional communications are carried out over the same temporal and spectral resources.

Recently full-duplex transmission has gained significant attention [3]-[47] due to its potential to double the system's spectral efficiency by allowing simultaneous transmission and

reception over the same frequency band. In addition to spectral efficiency improvement, full-duplex transmission could be used to improve the reliability of multi-users cognitive radio networks [34]. For instance, in cognitive radio networks, collision between users could be avoided by allowing the terminals to simultaneously sense the medium while transmitting a data frame, or receive instantaneous feedback from other terminals.

1.2 Full-duplex Transmission Challenges and Limitations

The main limitation impacting full-duplex transmission is managing the strong self-interference signal imposed by the transmit antenna, on the receive antenna, within the same transceiver. For a full-duplex system to achieve its maximum efficiency, the self-interference signal has to be significantly suppressed to the receiver's noise floor. For instance, in WiFi and femto-cell cellular systems [43, 44], the transmit power can go up to 21dBm and the typical receiver noise floor is -90dBm, which requires more than 111dB of self-interference cancellation for proper operation of a full-duplex system. In case the achieved amount of self-interference cancellation does not reach the receiver noise floor, the residual self-interference power will degrade the System's Signal to Noise Ratio (SNR) and thus negatively impact the system throughput. Achieving such significant self-interference cancellation is the key challenge in full-duplex systems.

Since the transmitted self-interference signal is known at the receiver side, one might think that the self-interference signal could be significantly mitigated by simple subtraction of the transmitted base-band signal from the received signal. However, several publications have demonstrated that simple self-interference signal subtraction achieves limited cancellation amount, mainly due to a combination of hardware imperfections [37]-[41]. In more details,

when the self-interference signal is processed by the transceiver circuitry, additional noise components are introduced to the self-interference signal (e.g. phase noise, nonlinear distortion, quantization noise, etc.). Therefore, simple self-interference signal subtraction can not mitigate the introduced noise components, which limits the amount of cancellable self-interference power to the power level of the introduced noise components. Accordingly, the key challenge in full-duplex systems is mitigating both the self-interference signal as well as the associated noise components.

1.3 Self-interference Cancellation Techniques

Recently, a vast variety of self-interference cancellation techniques for full-duplex systems have been proposed [3]-[47]. Generally, self-interference cancellation techniques are divided into two main categories: passive suppression techniques, and active cancellation techniques. Typical full-duplex systems deploy both passive suppression and active cancellation techniques to achieve significant self-interference cancellation.

In passive suppression techniques, the self-interference signal is suppressed in the propagation domain before it is processed by the receiver circuitry. Passive self-interference suppression could be achieved using antenna separation and/or isolation [17],[29]-[31],[45]-[47], directional antennas [20, 32, 33], or using multiple transmit antennas with careful antenna placement [35, 36]. The self-interference suppression amount achieved using such methods highly depends on the application and the physical constraints of the system. For example, in mobile applications with small device dimensions, the passive suppression achieved using antenna separation and isolation is very limited. However, in others systems (e.g. relay systems) where the transmit and receive antennas are not necessary co-located, antenna separation and isolation could achieve significant passive suppression. For instance, in [45, 46], the use of a single-pattern directional antenna and 4-6 m of antenna separation achieves 85dB of

passive suppression. While in [47], using 5 m of antenna separation in addition to antenna isolation achieves 70dB of passive suppression. This large antenna separation might be acceptable in relay systems, but it is not acceptable in practical mobile applications. A more practical passive self-interference suppression method with relatively small antenna separation was introduced in [33], where antenna directionality is utilized to achieve 45dB of passive self-interference suppression at 35 cm antenna separation.

Active cancellation is the second category of the self-interference cancellation techniques. In active cancellation techniques [3]-[28], the self-interference signal is canceled by leveraging the fact that the transceiver knows the signal it is transmitting, such that the self-interference signal is mitigated by subtracting a processed copy of the transmitted signal from the received signal. Active cancellation techniques are divided into digital and analog cancellation based on the signal domain (digital-domain or analog-domain) where the self-interference signal is actively canceled. The main advantage of the analog cancellation compared to digital cancellation techniques is that the self-interference signal is cancelled in the analog-domain before the signal goes through the receiver Radio Frequency (RF) circuitry. This prevents the receiver from being saturated due to the huge self-interference power. In addition, mitigating the self-interference signal in the analog-domain decreases the effect of the receiver noise and increases the dynamic range allocated for the desired signal.

1.4 Motivation

Generally, self-interference cancellation techniques in full-duplex systems could be characterized by three main factors: (i) cancellation capability, (ii) computational complexity, and (iii) applicability region. Applicability region is the set of applications that the cancellation technique could be practically used with. For example, self-interference cancellation techniques with large antenna separations cannot be used in mobile handheld applications. In

fact, there are tradeoffs between those three factors. For instance, conventional digital self-interference cancellation techniques are the least complex and more applicable techniques. However, their cancellation capability is very limited (i.e. 30-40dB) [3]-[17]. On the other hand, analog cancellation techniques could achieve significant self-interference cancellation at the cost of increased complexity and limited applicability (e.g. due to the increased physical dimensions of the receiver) [23].

Also, the available passive suppression techniques either have good cancellation capability or better applicability, but not both at the same time. For example, the passive suppression techniques in [45]-[47] could achieve up to 85dB of passive suppression. However, since they require large antenna separation, such techniques are not suitable for mobile applications. On the other hand, the passive suppression techniques in [29]-[33] have better applicability range (e.g. due to smaller antenna separation), but at the cost of reduced cancellation capability.

Accordingly, a good self-interference cancellation technique should be applicable to a vast range of applications, and at the same time have significant cancellation capability with relatively low complexity. Such challenging requirements are the main motivation behind the work in this thesis.

1.5 Thesis Contributions

In this thesis, we consider the problem of self-interference cancellation in full-duplex systems. We analytically and experimentally investigate several aspects in full-duplex transmission, focusing on developing novel low-complexity self-interference cancellation techniques to maximize the amount of cancelled self-interference power. The ultimate goal of this work is to design and build a complete, real-time, full-duplex system that is capable of achieving wireless

full-duplex transmission in real wireless environments using practical hardware platforms. The key contributions of the thesis can be summarized as follow:

1. *"Thorough analytical and numerical investigation for i) the full-duplex system limitations and bottlenecks, and ii) the operation regions in which full-duplex systems outperform half-duplex systems in terms of achievable rate, under the same operating conditions".*

   The experimental analyses in [13, 14, 17, 19, 22, 23, 29],[30]-[33] have demonstrated that practical full-duplex systems can improve upon half-duplex systems under certain conditions and using the appropriate self-interference cancellation techniques. However, none of the current full-duplex wireless systems exhibit consistent gains over half-duplex transmission in all operation regimes, largely due to imperfect self-interference cancellation that is mainly limited by hardware imperfections [37]-[41]. Accordingly, a substantial step towards improving the self-interference cancellation capability is the identification of the main performance bottlenecks, and how they affect the overall system performance.

2. *"Comprehensive analytical and experimental analysis of phase noise estimation and suppression in full-duplex systems".*

   Following the identification of the system limitations achieved in the first contribution, mitigating such limitations is the next step towards achieving better self-interference cancellation performance. The analysis in the first contribution, as well as the results presented in [37]-[41] show that, among the various RF circuits' impairments, oscillator phase noise and transceiver nonlinearities are the two main limiting factors in full-duplex systems. The second and third contributions are concerned with mitigating these noise components to achieve better self-interference cancellation capability. In the second contribution, we propose two different phase noise estimation and suppression techniques for full-duplex systems. In addition, we present a comprehensive

numerical and experimental analysis for the feasibility of using phase noise estimation and suppression techniques in full-duplex systems in terms of achieved gain and required complexity.

3. *"Transceiver nonlinearity estimation and suppression technique for full-duplex systems".*

   After phase noise, the second limiting factor in full-duplex systems is the transceiver nonlinearity. Without nonlinearity suppression, the amount of cancellable self-interference power will be limited to the nonlinear distortion power level. In this thesis, we propose a transceiver nonlinearity estimation and suppression technique for full-duplex systems. The proposed technique increases the amount of cancellable self-interference power by suppressing the nonlinear distortion associated with the received self-interference signal.

4. *"Novel digital self-interference cancellation technique that eliminates all transmitter impairments, and significantly mitigates the receiver phase noise and nonlinearity effects".*

   Giving its limiting impact on performance, phase noise reduction is one of the main design targets for full-duplex system designers. The results from the second contribution show that even when using highly complex techniques, only ∼3dB of phase noise suppression could be achieved. Accordingly, phase noise suppression remains a considerable issue in full-duplex systems. To address this issue, we propose a novel all-digital self-interference cancellation technique that significantly mitigates transmitter and receiver impairments. In the proposed technique an auxiliary receiver chain is used to obtain a digital-domain copy of the transmitted RF self-interference signal, which is then used to cancel out the self-interference signal and the associated transmitter impairments. Furthermore, in order to alleviate the receiver phase noise effect, the auxiliary and ordinary receiver chains share a common oscillator. The main

advantage of the proposed technique is that all signal processing is performed in the digital-domain, which significantly reduces the implementation complexity.

5. *"Novel passive self-interference suppression technique using Multi-Reconfigurable Antennas"*.

   Typical full-duplex systems deploy both passive suppression and active cancellation techniques to achieve significant self-interference cancellation. To complete the picture, this thesis concludes with proposing a novel passive self-interference suppression technique using Multi-Reconfigurable Antennas (MRA). MRA is a dynamically reconfigurable antenna that is capable of changing its proprieties (e.g. radiation pattern, polarization, and operating frequency) according to certain input configurations. The proposed technique achieves 65dB of passive self-interference suppression at only 10 cm antenna separation. The proposed passive suppression technique combined with active digital cancellation techniques is experimentally proven to achieve 90% rate improvement over half-duplex systems.

1.6 Thesis Organization

The rest of the thesis is organized as follows. In chapter 2, the full-duplex system bottlenecks and design tradeoffs are analytically investigated. Also, the operation regions in which full-duplex systems outperform half-duplex systems in terms of achievable rate is derived in chapter 2. Chapter 3 presents thorough analytical and experimental analysis for the phase noise estimation and suppression in full-duplex systems. In chapter 4, the transceiver nonlinearity estimation and suppression technique for full-duplex systems is presented. The work in Chapter 2, 3, and 4 was developed in collaboration with Dr. Ashutosh Sabharwal from Rice University. A novel digital self-interference cancellation technique that mitigates the transmitter and receiver impairments is presented in chapter 5. Chapter 6 presents

the MRA based self-interference suppression technique as well as the experimental analysis of the complete MRA-based full-duplex system. The work in Chapter 6 was developed in collaboration with Li Zhouyuan, and Dr. Bedri A. Cetiner from Utah state university. Finally, chapter 7 presents the conclusions.

Chapter 2

Rate Gain Region and Design Tradeoffs for Full-Duplex Systems

2.1 Introduction

The main challenge in full-duplex transmission is due to the large power differential between the self-interference signal caused by the node's own transmission and the signal-of-interest which the receiver intends to decode. A number of recent publications [13, 14, 17, 20, 22, 23, 30] have demonstrated experimentally that practical full-duplex systems can improve upon half-duplex systems under certain conditions and using the appropriate self-interference cancellation techniques. However, none of the current full-duplex wireless systems gains over half-duplex transmission in all operation regimes, largely due to imperfect self-interference cancellation. The analysis in this chapter is inspired by the above observation and aims to analytically understand the bottlenecks in full-duplex systems.

To understand the limits of practical full-duplex systems, we use a signal model for narrow-band full- and half-duplex systems by modeling four significant transceiver noise sources:

(i) transmitter and receiver phase noise, (ii) Low Noise Amplifier (LNA) noise figure, (iii) mixer noise figure, and (iv) Analog-to-Digital Converter (ADC) quantization noise. We use the detailed signal model, with the above mentioned four noise sources, along with different self-interference cancellation mechanisms to analytically investigate the operation regions in which full-duplex systems outperform half-duplex systems in terms of achievable rate, under the same operating conditions.

Another important impairment is the receiver nonlinearity, especially the LNA nonlinearity. Most of the proposed half- and full-duplex signal models assume linear receiver blocks in order to obtain tractable mathematical analysis. Our main goal in this chapter is to obtain a closed form expression for the rate gain region that allows us to better understand the full-duplex system behavior. Including receiver nonlinearity will lead to an intractable mathematical analysis. Therefore, for analysis simplicity, the receiver blocks are assumed to operate in the linear region. This assumption is motivated by the recent work in [59, 60] which proposes a novel low-noise highly-linear receiver architectures that tolerate strong blocker levels (e.g. up to 0dBm). In addition, detailed numerical analysis of the nonlinearity effect on full-duplex systems is presented in Chapter 4.

Using the developed signal model, first, we derive the full-duplex rate gain region under different operating conditions. We define the rate gain region as the region of received signal-of-interest strength at which full-duplex systems outperform half-duplex systems in terms of achievable rate. The key contribution in this chapter is a closed-form piecewise linear approximation, in the log-domain, for the rate gain region under analog and digital self-interference cancellation techniques.[1] The piecewise linear approximation allows us to develop valuable insights in the behavior of full-duplex systems under different operating conditions. Second, we identify the dominant noise components that limit system performance for both analog and digital self-interference cancellation techniques. Third, we investigate

[1]In the log-domain means that the relation is between the logarithm of the variables, e.g. a linear relation between y and x in the log-domain means that $\log(y) = \log(x) + \log(constant)$.

the possible design tradeoffs involved in full-duplex system design, showing that the rate gain region is inversely proportional to the transmit power, i.e. reducing the transmit power makes full-duplex systems more likely to outperform half-duplex systems.

2.2 Signal Model

In this section, we describe the signal models for both half and full-duplex narrowband systems. As illustrated in Figures 2.1 and 2.2, node A and B are separated by distance D meter, and communicating in a full-duplex manner. For conceptual clarity, we have depicted the transmit antenna separate from the receive antenna in Figures 2.1 and 2.2. However, our model and subsequent analysis applies to circulator-based systems which use only one antenna for both transmission and reception. At the transmitter side, the signal is modulated and then up-converted to the carrier frequency f_c, the oscillator at the transmitter side is assumed to have a random phase error represented by $\phi^t(t)$. The signal is then amplified by the transmitter power amplifier.

At the receiver side, the incoming signal level is appropriately adjusted using the LNA which is controlled by an automatic gain control block. The signal is then down-converted from the carrier frequency, the down-conversion mixer is assumed to have a random phase error represented by $\phi^r(t)$. The down-converted signal is then quantized using an m-bits ADC.

For simplicity and without loss of generality, we consider the signal at node A, where, due to hardware symmetry, the same analysis applies to node B. According to the described model, the received signal *without* self-interference cancellation can be written as

$$y[n] = \left(\sqrt{L_A}x_A[n]h_{AA}[n]e^{i\phi_A^t[n]} + \sqrt{L_B}x_B[n]h_{BA}[n]e^{i\phi_B^t[n]}\right)e^{i\phi_A^r[n]} + z[n] + q[n], \quad (2.1)$$

where x_A, x_B are the transmitted signal from node A and B, h_{AA}, h_{BA} are the self-interference

and signal-of-interest channels respectively, L_A, L_B are the propagation losses due to the antenna isolation at the same node and the distance between the two communicating nodes respectively, ϕ_i^t, ϕ_i^r, $i \in [A, B]$ are the carrier phase error at the transmitter and receiver side of node i, z is the receiver noise, and $q \sim \mathcal{U}(0, \frac{1}{2^{m-1}})$ is the uniformly distributed ADC quantization noise, where m is the number of ADC bits.

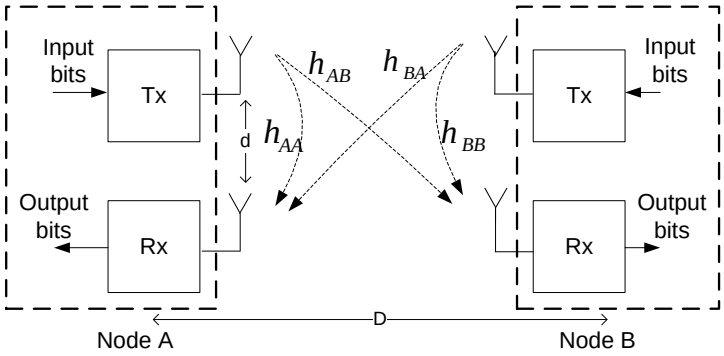

Figure 2.1: Single-input single-output full-duplex system.

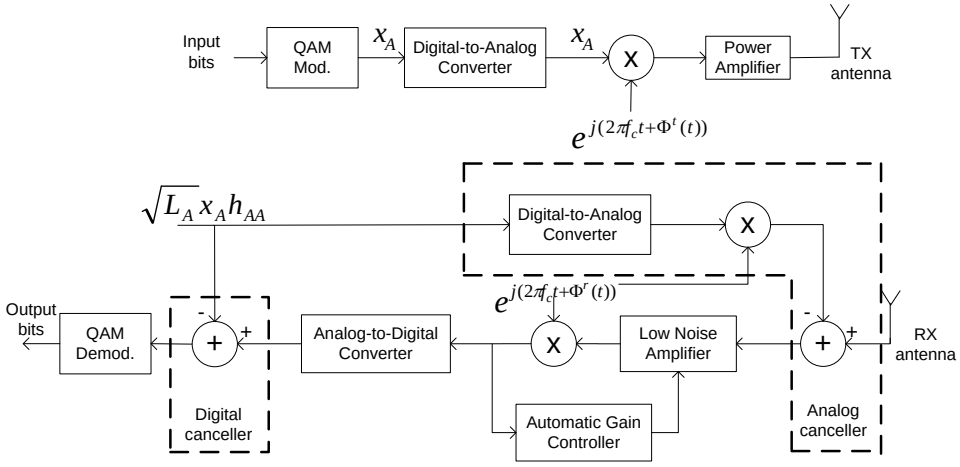

Figure 2.2: Detailed block diagram of a full-duplex transceiver with analog or digital self-interference cancellation.

The receiver noise, $z[n]$, represents the additive noise inherent in the receiver circuits, and specified by the circuit noise figure. The overall receiver noise power can be calculated as [49]

$$P_z = P_{th} N_f = P_{th} \left(N_l + \frac{N_m - 1}{\alpha^2} \right), \tag{2.2}$$

where N_f is the overall receiver noise figure, N_l is the LNA noise figure, N_m is the mixer noise figure, P_{th} is the thermal noise power in a 50ohm source resistance, and α^2 is the LNA power gain. The ADC quantization noise is a uniformly distributed noise introduced by the ADC due to the signal quantization. For an m bits ADC, the total ADC quantization noise power is calculated in terms of the LNA power gain as [50]

$$P_q = \frac{1}{\alpha^2} \frac{1}{12 \cdot 2^{2m-2}} = \frac{\sigma_q^2}{\alpha^2}, \tag{2.3}$$

where $\sigma_q^2 = \frac{1}{12 \cdot 2^{2m-2}}$ is the quantization noise variance.

In a full-duplex system, digital or analog self-interference cancellation technique is used to mitigate the self-interference signal. Both digital and analog cancellation require the knowledge of the transmitted signal and the self-interference channel. In our analysis, the channel is assumed to be frequency-flat fading channel, and the channel state information for all transmitter-receiver links are assumed to be perfectly known at the receiver side.

The main difference between digital and analog canceler is the signal domain, digital or analog domain, where the self-interference signal is cancelled. In digital cancellation technique, the interference signal is eliminated in the digital domain after the received signal goes through the radio section, which forces the LNA to operate at low-gain modes. However, in analog cancellation technique, the base-band self-interference signal is up-converted to the carrier frequency and then subtracted from the received signal in the analog domain. The elimination of the self-interference signal in the analog domain, before the received signal goes through the LNA, allows the LNA to operate at higher gain than in digital cancellation technique.

2.2.1 Digital cancellation technique

In digital cancellation technique, with the knowledge of the interference channel, the self-interference cancellation is done by subtracting the signal $\sqrt{L_A}x_A[n]h_{AA}[n]$ from the received signal in the digital domain. After digital self-interference cancellation, the remaining signal can be written as

$$\begin{aligned} y[n] &= \sqrt{L_A}x_A[n]h_{AA}[n]\left(e^{i(\phi_A^t[n]+\phi_A^r[n])}-1\right) \\ &\quad +\sqrt{L_B}x_B[n]h_{BA}[n]e^{i(\phi_B^t[n]+\phi_A^r[n])}+z[n]+q[n]. \end{aligned} \tag{2.4}$$

Using the approximation of $e^{i\phi} \cong 1+i\phi$ for $\phi \ll 1$, Equation (2.4) can be written as

$$\begin{aligned} y[n] &= \sqrt{L_A}x_A[n]h_{AA}[n]\left(i\phi_A^t[n]+i\phi_A^r[n]\right) \\ &\quad +\sqrt{L_B}x_B[n]h_{BA}[n]\left(1+i\phi_B^t[n]+i\phi_A^r[n]\right)+z[n]+q[n]. \end{aligned} \tag{2.5}$$

The resulting full-duplex Signal-to-Interference plus Noise Ratio (SINR) for digital cancellation technique can be written as

$$\mathsf{SINR}_{\mathsf{DC}}^{\mathsf{FD}} = \frac{P_x L_B |h_{BA}|^2}{P_{\phi,A}+P_{\phi,B}+P_{z,\mathsf{DC}}+P_{q,\mathsf{DC}}}, \tag{2.6}$$

where acronyms DC and FD refers to digital cancellation and full-duplex, respectively. Further, $P_x = E\{|x_A|^2\} = E\{|x_B|^2\}$ is the transmitted signal power, $E\{\}$ denotes expectation process, and $P_{\phi,A}$, $P_{\phi,B}$ are the self-interference and signal-of-interest phase noise power

calculated as

$$P_{\phi,A} = P_x L_A |h_{AA}|^2 \left(\mu_A^t + \mu_A^r\right) = P_x L_A |h_{AA}|^2 \mu, \tag{2.7}$$

$$P_{\phi,B} = P_x L_B |h_{BA}|^2 \left(\mu_B^t + \mu_A^r\right) = P_x L_B |h_{BA}|^2 \mu, \tag{2.8}$$

where μ_i^t, μ_i^r, $i \in [A, B]$ are the total transmitter and receiver normalized phase noise power. In this chapter, we assume that node A and B are hardware symmetrical. Therefore, the *statistics* of the transmitter phase noise are identical, thus $\mu_A^t = \mu_B^t$. The total phase noise power (μ_i^j, $i \in [A, B]$, $j \in [t, r]$) is calculated by integrating the power spectral density (PSD) of the corresponding phase noise process (ϕ_i^j) over the system's bandwidth. Generally, the PSD is a design dependent parameter that depends on the architecture and design parameters of the used phase-locked loop (PLL). Approximate expressions of the phase noise's PSD for different PLL designs could be obtained [58]. However, precise phase noise PSD is usually obtained through measurements of a fabricated tuner involving a PLL.

The receiver and quantization noise power for digital cancellation technique ($P_{z,\mathsf{DC}}$, $P_{q,\mathsf{DC}}$) are calculated in terms of the LNA power gain as in (2.2) and (2.3). The LNA power gain is calculated by the variable gain amplifier circuit in terms of the received signal power at the LNA input as

$$\alpha_{\mathsf{DC}}^2 = \frac{1}{P_x L_A |h_{AA}|^2 + P_x L_B |h_{BA}|^2}. \tag{2.9}$$

Define the instantaneous received signal strength (RSSI) for the self-interference and signal-of-interest respectively as $\mathsf{RSSI}_A = P_x L_A |h_{AA}|^2$, $\mathsf{RSSI}_B = P_x L_B |h_{BA}|^2$, then using (2.2), (2.3), (2.7), (2.8)

and (2.9) in (2.6), we get

$$\mathsf{SINR}_{\mathsf{DC}}^{\mathsf{FD}} = \frac{\mathsf{RSSI}_B}{\eta\mathsf{RSSI}_A + \eta\mathsf{RSSI}_B + \zeta}, \tag{2.10}$$

where

$$\eta = \mu + \sigma_q^2 + P_{th}N_m - P_{th}, \tag{2.11}$$

$$\zeta = P_{th}N_l. \tag{2.12}$$

The parameter ζ can be described as the *system noise power floor* that does not depend on the incoming signal power. On the other hand, the parameter η represents the *signal power dependent noise component*.

2.2.2 Analog cancellation technique

In some of the active analog cancellation techniques, the self-interference cancellation is done by subtracting the up-converted self-interference signal from the received signal in the analog domain, before the received signal goes through the LNA [13]. The residual signal after analog self-interference cancellation can be written as

$$\begin{aligned} y[n] &= \sqrt{L_A}x_A[n]h_{AA}[n]\left(e^{i\phi_A^t[n]} - e^{i\phi_A^r[n]}\right)e^{i\phi_A^r[n]} \\ &\quad + \sqrt{L_B}x_B[n]h_{BA}[n]\; e^{i\phi_B^t[n]}e^{i\phi_A^r[n]} + z[n] + q[n]. \end{aligned} \tag{2.13}$$

Using the approximation of $e^{i\phi} \cong 1 + i\phi$ for $\phi \ll 1$ and collecting terms, Equation (2.13) can be written as

$$\begin{aligned} y[n] &= \sqrt{L_A} x_A[n] h_{AA}[n] \left(i\phi_A^t[n] - i\phi_A^r[n] \right) \\ &\quad + \sqrt{L_B} x_B[n] h_{BA}[n] \left(1 + i\phi_B^t[n] + i\phi_A^r[n] \right) + z[n] + q[n]. \end{aligned} \tag{2.14}$$

The resulting SINR for analog cancellation technique can be written as

$$\mathsf{SINR}_{\mathsf{AC}}^{\mathsf{FD}} = \frac{P_x L_B |h_{BA}|^2}{P_{\phi,A} + P_{\phi,B} + P_{z,\mathsf{AC}} + P_{q,\mathsf{AC}}}, \tag{2.15}$$

where the acronym AC refers to analog cancellation.

Comparing (2.6) and (2.15), it has to be noticed that the only difference between the SINR in digital and analog cancellation techniques is the value of the receiver and quantization noise power. Generally, the receiver and quantization noise power are inversely proportional to the LNA power gain (review (2.2) and (2.3)). In analog cancellation technique the self-interference signal is eliminated before the signal goes through the LNA, which forces the LNA to operate at high-gain mode, and thus reducing the receiver and quantization noise power. The LNA power gain for analog cancelation technique is calculated as

$$\alpha_{\mathsf{AC}}^2 = \frac{1}{P_x L_B |h_{BA}|^2}. \tag{2.16}$$

Substituting from (2.2), (2.3), (2.7), (2.8), and (2.16) in (2.15) we get

$$\mathsf{SINR}_{\mathsf{AC}}^{\mathsf{FD}} = \frac{\mathsf{RSSI}_B}{\mu \mathsf{RSSI}_A + \eta \mathsf{RSSI}_B + \zeta}. \tag{2.17}$$

Equation (2.10), (2.17) describes the full-duplex system SINR for both digital and analog

cancellation techniques. In our analysis, we compare full-duplex system performance against half-duplex system performance. Half-duplex transmission can be considered a special case of the full-duplex transmission, where the received self-interference signal power is equal to zero and the temporal resources are divided between the two nodes. To maintain a fair comparison, the transmitted power is doubled in the case of half-duplex transmission since only one node is transmitting at a time. Accordingly the half-duplex system Signal-to-Noise Ratio (SNR) can be written as

$$\mathsf{SNR}^{\mathsf{HD}} = \frac{2\mathsf{RSSI}_B}{2\eta\mathsf{RSSI}_B + \zeta}. \tag{2.18}$$

2.3 Rate Gain Region for Digital and Analog Cancellation Techniques

In this section, we derive the full-duplex rate gain region for both digital and analog cancellation techniques. Rate gain region is defined as the region of received signal-of-interest strength at which full-duplex system achieves rate gain over half-duplex system. Deriving the rate gain region allows for straightforward exploration of the conditions at which full-duplex systems outperform half-duplex counterparts. The rate gain region can be obtained by solving the following inequality

$$\mathsf{R}^{\mathsf{FD}} > \mathsf{R}^{\mathsf{HD}}, \tag{2.19}$$

where R^{FD} ,R^{HD} are the full-duplex and half-duplex system achievable rates respectively.

Generally, deriving the rate gain region of a full-duplex system depends on how it is defined. For example, the rate gain region could be defined as the region in which the full-duplex *sum* rate is greater than the half-duplex *sum* rate (i.e. $\mathsf{R}^{\mathsf{FD}}_{A\to B} + \mathsf{R}^{\mathsf{FD}}_{B\to A} > \mathsf{R}^{\mathsf{HD}}_{A\to B} + \mathsf{R}^{\mathsf{HD}}_{B\to A}$).

Although this is the general definition, there might be a scenario where the full-duplex sum rate is better than the half-duplex sum rate, while one of the two communication links has smaller full-duplex rate than its half-duplex rate (i.e. $\mathsf{R}^{\mathsf{FD}}_{A\to B}+\mathsf{R}^{\mathsf{FD}}_{B\to A} > \mathsf{R}^{\mathsf{HD}}_{A\to B}+\mathsf{R}^{\mathsf{HD}}_{B\to A}$, while $\mathsf{R}^{\mathsf{FD}}_{A\to B} < \mathsf{R}^{\mathsf{HD}}_{A\to B}$). In this case, one node has to sacrifice part of its rate, which might not be practical especially in symmetric communication scenarios. Another conservative definition for the rate gain region, is the region in which the full-duplex rate for *each* communication link is greater than its half-duplex rate (i.e. $\mathsf{R}^{\mathsf{FD}}_{A\to B} > \mathsf{R}^{\mathsf{HD}}_{A\to B}$ and $\mathsf{R}^{\mathsf{FD}}_{B\to A} > \mathsf{R}^{\mathsf{HD}}_{B\to A}$). In this case the full-duplex sum rate is guaranteed to be greater than the half-duplex sum rate.

In this chapter we analyze the rate gain region based on the second definition. The rate gain region is defined as the region in which the full-duplex rate for each communication link is greater than its half-duplex rate (i.e. $\mathsf{R}^{\mathsf{FD}}_{A\to B} > \mathsf{R}^{\mathsf{HD}}_{A\to B}$ and $\mathsf{R}^{\mathsf{FD}}_{B\to A} > \mathsf{R}^{\mathsf{HD}}_{B\to A}$). Defining the rate gain region that way makes the analysis applicable for other full-duplex systems' architectures such as in [9, 11, 16, 32], where only one node (base-station or relay node) is operating in full-duplex mode and communicating with two half-duplex nodes. Accordingly, we derive the rate gain region for one of the two communicating nodes, and the same results apply to the other node, but with different parameters' values. The per-direction achievable rates at node A is calculated as

$$\mathsf{R}^{\mathsf{FD}} = \log_2\left(1+\mathsf{SINR}^{\mathsf{FD}}\right), \tag{2.20}$$

$$\mathsf{R}^{\mathsf{HD}} = \frac{1}{2}\log_2\left(1+\mathsf{SNR}^{\mathsf{HD}}\right). \tag{2.21}$$

The factor of $\frac{1}{2}$ is due to the fact that node A and B are sharing the available temporal

resources. Substitute from (2.20) and (2.21) in (2.19) we get

$$\log_2\left(1+\mathsf{SINR}^{\mathsf{FD}}\right) > \frac{1}{2}\log_2\left(1+\mathsf{SNR}^{\mathsf{HD}}\right). \tag{2.22}$$

Equation (2.22) could be reduced to

$$\left(1+\mathsf{SINR}^{\mathsf{FD}}\right)^2 > \left(1+\mathsf{SNR}^{\mathsf{HD}}\right), \tag{2.23}$$

then

$$\left(\mathsf{SINR}^{\mathsf{FD}}\right)^2 + 2\mathsf{SINR}^{\mathsf{FD}} > \mathsf{SNR}^{\mathsf{HD}}. \tag{2.24}$$

In the following analysis, Equation (2.24) along with the signal model presented in Section 2.2 are used to derive the rate gain region for both digital and analog cancellation techniques.

2.3.1 Rate gain region for digital cancellation technique

Substituting from (2.10), and (2.18) in (2.24) we get

$$\left(\frac{\mathsf{RSSI}_B}{\eta\mathsf{RSSI}_A+\eta\mathsf{RSSI}_B+\zeta}\right)^2 + \frac{2\mathsf{RSSI}_B}{\eta\mathsf{RSSI}_A+\eta\mathsf{RSSI}_B+\zeta} > \frac{2\mathsf{RSSI}_B}{2\eta\mathsf{RSSI}_B+\zeta}. \tag{2.25}$$

Collecting terms and putting (2.25) in the form of a 2^{nd} order inequality we get

$$a(\mathsf{RSSI}_B)^2 + b\mathsf{RSSI}_B + c > 0, \tag{2.26}$$

where

$$a=\eta(\eta+1),\ b=\zeta(\eta+\frac{1}{2}),\ c=-\eta\mathsf{RSSI}_A(\eta\mathsf{RSSI}_A+\zeta). \tag{2.27}$$

Knowing that RSSI is always a positive quantity and noting that c is always negative, the rate gain region for digital cancellation technique can be written as

$$\mathsf{RSSI}_B > \mathsf{RSSI}_{B,min}, \tag{2.28}$$

where

$$\mathsf{RSSI}_{B,min} = \frac{-b + \sqrt{b^2 - 4ac}}{2a}. \tag{2.29}$$

Equation (2.29) describes the rate gain region in terms of all system parameters and radio impairments. However, due to the complexity of the formula in (2.29), it is difficult to gain insights into system behavior under different operation conditions without resorting to numerical simulations. In the following analysis, we try to simplify the relation in (2.29) by deriving a piecewise linear, in the log-domain, approximation for the rate gain region. The results in Figure 2.3 show that based on the received self-interference signal strength, there are three distinct regions where the linear trend can be observed. Further, it also shows that the region boundaries are not fixed but change with system parameters. In the following analysis, the piecewise linear approximation is derived by solving (2.29) under different operation regimes based on the self-interference signal strength.

Strong self-interference regime

In this case, the received self-interference signal strength is assumed to be strong enough such that the noise introduced due to the presence of the self-interference signal ($\eta\mathsf{RSSI}_A$) is higher than the receiver noise floor i.e. $\eta\mathsf{RSSI}_A > \zeta$ or $\mathsf{RSSI}_A > \frac{\zeta}{\eta}$. Moreover, η is a combination of phase, receiver, and quantization noises; in practical fabricated circuits, all

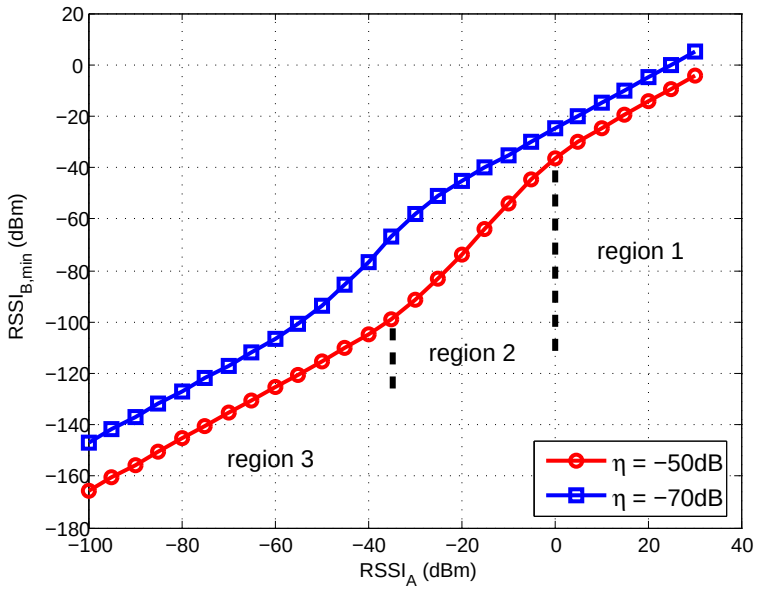

Figure 2.3: Rate gain region for digital cancellation technique.

of these noise components are typically $\ll 1$ (see [51], and [52])[2]. Accordingly, assuming that $\mathsf{RSSI}_A > \frac{\zeta}{\eta}$, and $\eta \ll 1$, Equation (2.27) can be approximated to

$$a \cong \eta,\ b \cong \frac{\zeta}{2},\ c \cong -(\eta \mathsf{RSSI}_A)^2. \tag{2.30}$$

Substituting from (2.30) in (2.29), we get

$$\mathsf{RSSI}_{B,min} \cong \frac{\frac{-\zeta}{2} + \sqrt{\frac{\zeta^2}{4} + 4\eta^3 \mathsf{RSSI}_A^2}}{2\eta}. \tag{2.31}$$

First, we study the case where $4\eta^3 \mathsf{RSSI}_A^2 > \frac{\zeta^2}{4}$ i.e. $\mathsf{RSSI}_A > \frac{\zeta}{4\eta\sqrt{\eta}}$. Using Taylor expansion of

[2]based on the data sheets' numbers in [51, 52], the total inband phase noise μ in a 1MHz bandwidth is ~ -40dB, the total ADC quantization noise $\sigma_q^2 = -77$dB, and the mixer noise figure N_m =10dB. By substituting in (2.11) we get $\eta \simeq -39.9$dB (i.e. $\sim 1e^{-4}$) which is $\ll 1$

$(1+x)^{\frac{1}{2}} \cong 1+\frac{1}{2}x$ when $x<1$, Equation (2.31) can be approximated as

$$\begin{aligned}\mathsf{RSSI}_{B,min} &\cong \frac{-\frac{\zeta}{2}+2\eta\sqrt{\eta}\mathsf{RSSI}_A\sqrt{1+\frac{\zeta^2}{16\eta^3\mathsf{RSSI}_A^2}}}{2\eta} \\ &\cong \frac{-\frac{\zeta}{2}+2\eta\sqrt{\eta}\mathsf{RSSI}_A+\frac{\zeta^2}{16\eta\sqrt{\eta}\mathsf{RSSI}_A}}{2\eta}. \end{aligned} \tag{2.32}$$

Using the case condition $\mathsf{RSSI}_A > \frac{\zeta}{4\eta\sqrt{\eta}}$, equation (2.32) can be approximated as

$$\mathsf{RSSI}_{B,min} \cong \frac{\eta\mathsf{RSSI}_A}{\sqrt{\eta}}. \tag{2.33}$$

Now, considering the opposite case where $4\eta^3\mathsf{RSSI}_A^2 < \frac{\zeta^2}{4}$ i.e. $\mathsf{RSSI}_A < \frac{\zeta}{4\eta\sqrt{\eta}}$, Equation (2.31) can be approximated as

$$\begin{aligned}\mathsf{RSSI}_{B,min} &\cong \frac{-\frac{\zeta}{2}+\frac{\zeta}{2}\sqrt{1+\frac{16\eta^3\mathsf{RSSI}_A^2}{\zeta^2}}}{2\eta} \\ &\cong \frac{2\eta^2\mathsf{RSSI}_A^2}{\zeta}, \end{aligned} \tag{2.34}$$

where $\frac{\zeta}{\eta} < \mathsf{RSSI}_A < \frac{\zeta}{4\eta\sqrt{\eta}}$.

Weak self-interference regime

In this case the received self-interference signal strength is assumed to be weak enough such that the noise introduced due to the presence of the self-interference signal ($\eta\mathsf{RSSI}_A$) is lower than the receiver noise floor i.e. $\eta\mathsf{RSSI}_A < \zeta$ or $\mathsf{RSSI}_A < \frac{\zeta}{\eta}$. Assuming that $\mathsf{RSSI}_A < \frac{\zeta}{\eta}$, and

$\eta \ll 1$, Equation (2.27) can be approximated to

$$a \cong \eta,\ b \cong \frac{\zeta}{2},\ c \cong -\zeta\eta\mathsf{RSSI}_A. \tag{2.35}$$

Substituting from (2.35) in (2.29), we get

$$\mathsf{RSSI}_{B,min} \cong \frac{-\frac{\zeta}{2} + \sqrt{\frac{\zeta^2}{4} + 4\zeta\eta^2\mathsf{RSSI}_A}}{2\eta}. \tag{2.36}$$

For additional simplification, first, assume that $4\zeta\eta^2\mathsf{RSSI}_A > \frac{\zeta^2}{4}$ i.e. $\mathsf{RSSI}_A > \frac{\zeta}{16\eta^2}$. Knowing that typically $\eta \ll 1$, this condition contradicts the weak self-interference condition above, and thus $4\zeta\eta^2\mathsf{RSSI}_A$ should be $< \frac{\zeta^2}{4}$. Accordingly, equation (2.36) can be approximated as

$$\begin{aligned} \mathsf{RSSI}_{B,min} &\cong \frac{-\frac{\zeta}{2} + \frac{\zeta}{2}\sqrt{1 + \frac{16\eta^2\mathsf{RSSI}_A}{\zeta}}}{2\eta} \\ &\cong 2\eta\mathsf{RSSI}_A, \end{aligned} \tag{2.37}$$

where $\mathsf{RSSI}_A < \min(\frac{\zeta}{\eta}, \frac{\zeta}{16\eta^2})$. Since $\eta \ll 1$ for practical systems, it can be assumed that $16\eta^2 < \eta$. Therefore, the condition for this operation regime is $\mathsf{RSSI}_A < \frac{\zeta}{\eta}$

As a conclusion, using (2.33), (2.34), and (2.37), the simplified rate gain region for digital cancellation technique can be written as

$$\mathsf{RSSI}_{B,min} \cong \begin{cases} \frac{\eta\mathsf{RSSI}_A}{\sqrt{\eta}} & ,\ \mathsf{RSSI}_A \geq \frac{\zeta}{4\eta\sqrt{\eta}}, \\ \frac{2\eta^2\mathsf{RSSI}_A^2}{\zeta} & ,\ \frac{\zeta}{\eta} \leq \mathsf{RSSI}_A < \frac{\zeta}{4\eta\sqrt{\eta}}, \\ 2\eta\mathsf{RSSI}_A & ,\ \mathsf{RSSI}_A < \frac{\zeta}{\eta}. \end{cases} \tag{2.38}$$

2.3.2 Rate gain region for analog cancellation technique

Due to the similarity of the SINR relations in both digital and analog cancellation techniques, the rate gain region for analog cancellation technique can be derived following the same steps as in Section 2.3.1 above by using Equation (2.17) instead of (2.10). Thus, for simplicity, we present the final results without going into derivation details. Equation (2.39) describes the piecewise linear approximation for the rate gain region in analog cancellation technique.

$$\mathsf{RSSI}_{B,min} \cong \begin{cases} \frac{\mu \mathsf{RSSI}_A}{\sqrt{\eta}} & , \ \mathsf{RSSI}_A \geq \frac{\zeta}{4\mu\sqrt{\mu}}, \\ \frac{2\mu^2 \mathsf{RSSI}_A^2}{\zeta} & , \ \frac{\zeta}{\eta} \leq \mathsf{RSSI}_A < \frac{\zeta}{4\mu\sqrt{\mu}}, \\ 2\mu \mathsf{RSSI}_A & , \ \mathsf{RSSI}_A < \frac{\zeta}{\mu}. \end{cases} \tag{2.39}$$

Using (2.38) and (2.39), one can straightforwardly predict the region where full-duplex systems outperform half-duplex systems for any given combination of system parameters and operating conditions. The accuracy of the approximated rate gain region described by (2.38) and (2.39) is confirmed by comparing it to the un-approximated rate gain region at different system parameters. Furthermore, the accuracy of the analysis is verified by comparing both the approximated and the un-approximated rate gain regions to the simulation results. The comparison results are shown in Figures 2.4. It is clear that the results from simulation closely match the un-approximated analysis, which validates the accuracy of the analysis. In addition, the results also show that the approximated rate gain region is an excellent fit to the un-approximated one except at the transition between different operation regions where a small error (0 - 3dBm) exists.

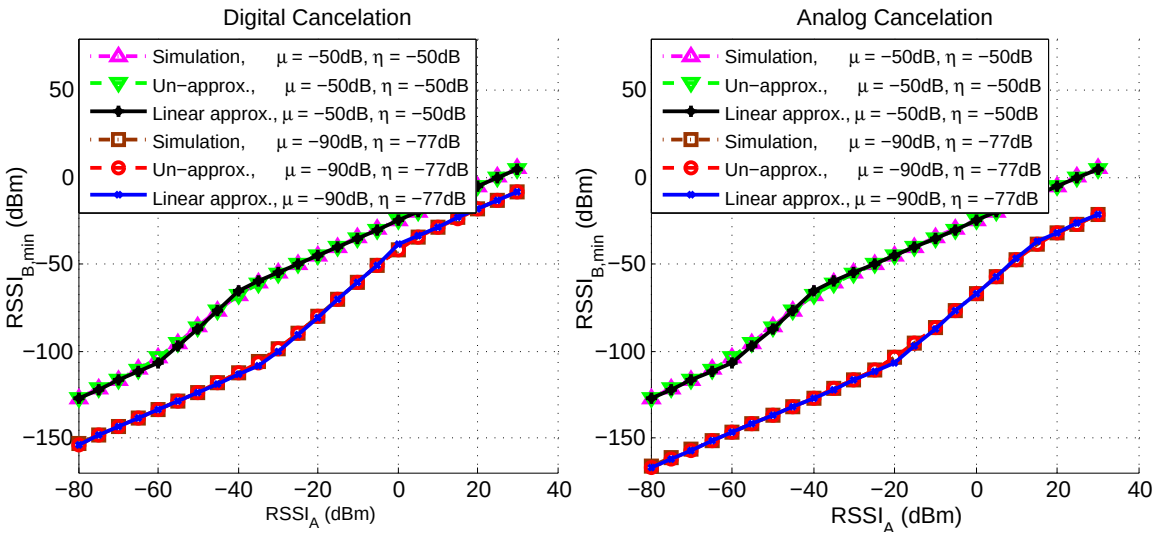

Figure 2.4: Comparison between simulation and analytical results for digital and analog cancellation technique.

2.4 Key Observations and Design Tradeoffs

In this section, we highlight several key observations regarding full-duplex system behaviour under analog and digital self-interference cancellation techniques.

Observation 1: *Analog cancellation reduces the effect of both mixer and quantization noise.* According to (2.38) and (2.39), the rate gain region for the digital cancellation technique depends on the combined noise power associated with the self-interference signal ($\eta\mathsf{RSSI}_A$) which consists of all noise components. However, in the analog cancellation technique, the rate gain region only depends on the phase noise power ($\mu\mathsf{RSSI}_A$). This observation implies that using the analog cancellation technique reduces the effect of all noise components except phase noise. The reason is that analog cancellation eliminates most of the self-interference power at the LNA input allowing it to operate at a high-gain mode, and thus reducing the effect of both mixer and quantization noise (review (2.2) and (2.3)). On the other hand, changing the LNA gain does not affect the phase noise associated with the incoming self-interference signal.

Observation 2: *Analog cancellation is most useful for low phase noise systems.* As a consequence of the previous observation, when phase noise dominates other noise components (i.e. $\mu \gg \sigma_q^2 + P_{th}N_m$, and therefore $\eta \cong \mu$), the rate gain region will be identical for both digital and analog cancellation techniques. On the other hand, if $\mu \ll \sigma_q^2 + P_{th}N_m$ (i.e. either quantization or mixer noise dominates), the analog cancellation technique outperforms the digital cancellation technique. Therefore, the advantage of using analog cancellation is evident only when either quantization or mixer noise dominates the phase noise. Accordingly, in high phase noise systems, performing analog cancellation requires additional hardware complexity [13, 37, 40] without achieving performance gain over digital cancellation technique.

Looking at Observations 1 and 2 one can conclude that current full-duplex systems are limited by the oscillator phase noise. From a noise perspective, the results in (2.38) and (2.39) shows that, for analog cancellation technique, the rate gain region is limited by the total phase noise μ. While, for digital cancellation technique, the rate gain region is limited by the combined noise parameter η, which consists of all phase, quantization, and mixer noise. Therefore, the system bottleneck for analog cancellation technique is the phase noise.

On the other hand, in the digital cancellation technique, the bottleneck is the dominant component of phase, quantization, and mixer noise. Typically, in today's wireless technology, down-conversion mixer's noise figure is $\sim$10dB [52] resulting in a normalized mixer noise power ($P_{th}N_m$) of -104dBm in a 1MHz bandwidth. Further, assuming a 12 bits ADC is used, the resulting normalized quantization noise power is ~ -77dBm. However, the in-band oscillator phase noise is usually much higher than those values, for example, the 2.4GHz oscillators in [53] has a total in-band phase noise of -50dBc in a 1MHz bandwidth. Thus, the in-band oscillator phase noise dominates other noise components, and is considered a bottleneck for current full-duplex systems with either analog or digital cancellation technique.

Observation 3: *Significant performance improvement requires both passive suppression and hardware enhancement.* According to (2.38) and (2.39), improving the rate gain region

could be achieved through one/both of two main techniques, i) reducing the received self-interference signal strength and/or ii) improving analog circuits to reduce noise. Each technique has tradeoffs that might limit its applicability and practicality. For example, one way to reduce self-interference RSSI is to passively suppress the self-interference in the spatial domain before it is processed by the receiver radio-frequency section. However, passive self-interference suppression techniques usually have a limited mitigation capability [29]-[36]. The second improvement technique is to reduce the noise introduced by the analog front-end through either technology, device or architectural innovations. From a practical viewpoint, noise reduction in analog circuits is very challenging, and the improvement could be very limited. Therefore, achieving wide rate gain region require a hybrid approach that combines contributions from both techniques.

The first tradeoff: *Increasing the rate gain region at the cost of hardware complexity.* According to observation 1 and 2, in some cases when either mixer or quantization noise dominates the phase noise, performing analog cancellation reduces the noise effect and improves the overall system performance. However, this performance enhancement comes at the cost of additional hardware required to perform analog cancellation [18]-[28].

The second tradeoff: *Increasing the rate gain region by reducing the transmission range.* According to (2.38) and (2.39), reducing the received self-interference signal strength increases the rate gain region. One way to reduce self-interference RSSI is to reduce the transmitted signal power. However, reducing the transmit power also reduces the signal-of-interest power at the desired node, which in effect reduces the transmission range. From a practical point of view, improving the rate gain region by trading the transmission range might be beneficial for short range applications or for applications where symmetrical transmit and receive rates are not necessary.

The third tradeoff: *Increasing the passive suppression to allow for higher noise levels.* Equation (2.38) and (2.39) show that for same design target (rate gain region), there exists a

tradeoff between noise reduction and passive self-interference suppression. In other words, additional passive self-interference suppression allows for having higher noise values while maintaining the same performance and vice versa. For example, for analog cancellation technique, Equation (2.39) shows that there is a linear relation (in the log-domain) with a slope of one between the self-interference RSSI and the phase noise required to achieve certain performance. Accordingly, an xdB additional passive self-interference suppression allows the phase noise to be higher by the same x amount while achieving the same performance.

2.5 Numerical Results

In this section we numerically investigate the full-duplex system performance, design trade-offs, and rate gain region for practical indoor applications. First, we use the rate gain region to investigate the design requirements to enable full-duplex transmission with rate gains as compared to half-duplex transmission. Then, we characterize the rate gain achieved by using full-duplex instead of half-duplex as a communication technique. In this analysis, the cluster-based channel model introduced in [54] is used to model the wireless channel. The signal-of-interest and self-interference channel Rician factors are chosen according to the experimental results in [17] to be 0dB and 35dB respectively. The propagation loss is assumed to follow the log-normal model with shadowing effect introduced in [55]. System parameters are chosen to reflect industry standard chipsets [51, 52] operating in the ISM band as follows: the carrier frequency f_c =2.4GHz, system BW =1MHz, LNA noise figure N_l =4dB, mixer noise figure N_m =10dB, and number of ADC bits m =12bits.

2.5.1 Design requirements for feasible full-duplex transmission

Achieving higher full-duplex rate gain over a larger range requires full-duplex systems to have a wide rate gain region such that the received signal strength falls within the rate gain region. According to (2.38) and (2.39), the full-duplex rate gain region is mainly controlled by the system noise level and the received self-interference signal strength. The received self-interference signal strength could be written as a multiplication of the transmit power and the passive self-interference suppression as $\mathsf{RSSI}_A = P_x C$, where C is the passive self-interference suppression due to antenna separation and/or other passive suppression techniques. The rate gain region becomes a function of three main parameters: the noise level, the transmit power, and the passive suppression. In fact, to achieve a certain rate gain region, different combinations could be used.

As a design example, we quantify the requirements for full-duplex systems to achieve a better rate than half-duplex systems in practical indoor applications such as Bluetooth. According to the experimental results in [56], the average received signal strength for typical Bluetooth signal is in the range of -65dBm to -80dBm. Therefore, choosing a design target of $\mathsf{RSSI}_{B,min} = -80$dBm guarantees that most of the incoming signal power in such application falls within the rate gain region. Figure 2.5 shows the combination of the total phase noise (μ), transmit power, and passive suppression required to achieve -80dBm rate gain region for both analog and digital cancellation techniques.

The results illustrate the tradeoffs discussed in Section 2.4. It shows that at high phase noise values (when phase noise dominates other noises), analog and digital cancellation techniques achieve the same performance. While at low phase noise values, the analog cancellation technique outperforms the digital cancellation technique. For example, at phase noise of -85dB and transmit power of 10dBm, the analog cancellation technique requires 8dB less passive suppression than digital cancellation. The results also show the tradeoff between the

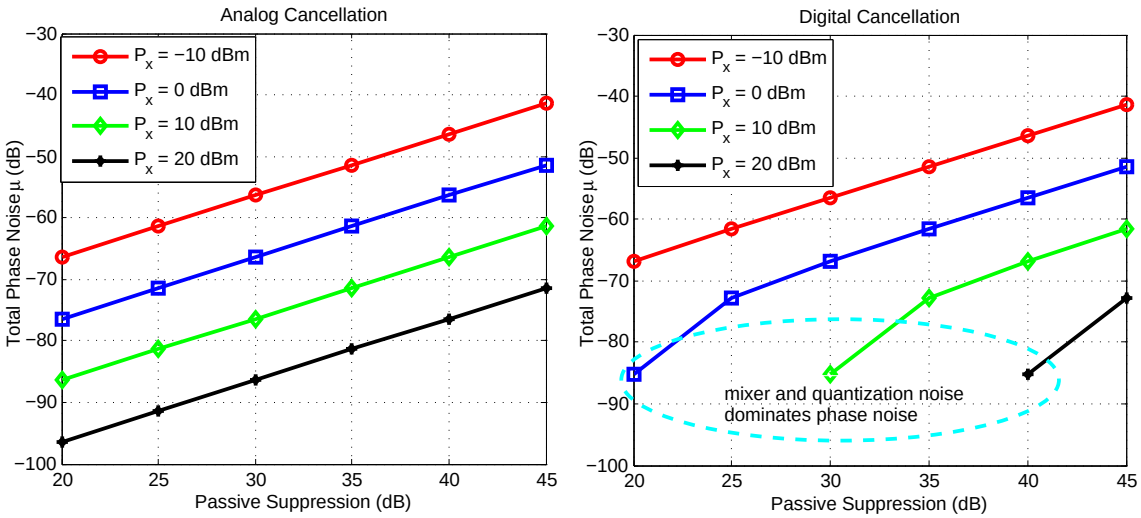

Figure 2.5: Requirements on phase noise level and passive self-interference suppression for rate gain region of −80dBm in case of analog and digital cancellation techniques.

transmit power, the system noise, and the passive suppression. The exact relation between the three parameters could be derived using (2.38), (2.39) along with the assumed system parameters at the beginning of this section. It can be shown that for a rate gain region of −80dBm, the relation between the transmit power, the noise level and the amount of passive suppression for both digital and analog cancellation techniques respectively can be written as

$$P_x + \eta + C = -96.5, \tag{2.40}$$

$$P_x + \mu + C = -96.5, \tag{2.41}$$

where all parameters are in dB units. Equation (2.40) and (2.41) show that the transmit power, the noise level and the passive suppression could be traded with each other to achieve the same design target. For example, we can trade some additional passive suppression (that could be achieved by increasing the antenna separation implying larger device sizes) with

more transmit power (i.e. more transmission range) or having higher noise (i.e. less hardware complexity). We could also lower the transmit power (i.e. less transmission range) while trading the passive suppression (i.e. smaller devices) and the noise level.

To better articulate these observations, we consider the example of Bluetooth system as a practical application and study different design tradeoffs. The three Bluetooth system's classes are considered in this analysis [57]. The Bluetooth application is operating in the 2.4GHz band, thus the oscillator in [53], which has a ~ -50dBc total in-band phase noise (μ) is assumed.

In class-3 Bluetooth systems, the transmit power is 0dBm and achieves $\sim$1 meters transmission range. Substituting in (2.41), we find that a $\sim$46dB passive self-interference suppression is required to achieve -80dBm rate gain region. For wider transmission range (e.g. $\sim$10 meters), class-2 Bluetooth could be used. However, the transmit power in this case is 4dBm, which means 4dB more passive suppression is required. In class-1 Bluetooth systems, a much wider transmission range of $\sim$100 meters could be achieved at transmit power of 20dBm. However, in this case, a $\sim$66dB passive suppression is required. This example illustrates the tradeoff between the transmission range and the amount of passive suppression. However, a possible means to avoid the aggressive requirements on the amount of passive suppression is to trade it with the oscillator phase noise. According to (2.41), each xdB reduction in the oscillator in-band phase noise reduces the requirements on the passive suppression by the same amount, thus promoting aggressive in-band noise reduction techniques for oscillator circuits.

2.5.2 Achievable rate gain

Another important aspect to investigate is the improvement in spectral efficiency when full-duplex transmission is employed by evaluating the achievable rate gain at different signal-

of-interest RSSI values. Figure 2.6 shows the achievable rate for both full-duplex and half-duplex systems at different passive self-interference suppression amounts with transmit power of 0dBm and 20dBm. The results show that, at 0dBm transmit power, a total of 40dB passive self-interference suppression could achieve −87dBm rate gain region, while achieving a rate of ∼1.2x and ∼1.4x times the half-duplex rate at −80dBm and −70dBm signal-of-interest strengths respectively, which is considered a significant improvement in the system throughput. The results also show that, at 20dBm transmit power, the full-duplex system requires 20dB more passive suppression to achieve the same performance as the case of 0dBm transmit power, which is consistent with the results in (2.41).

On the other hand, the half-duplex rate is identical in both simulation cases. The reason is that, half-duplex system's performance depends on the received signal-of-interest strength, which is the same in both simulation cases. In this specific simulation, in order to keep the same received signal-of-interest strength, the transmission range (distance between the two communicating nodes) is increased along with the increase of the transmit power.

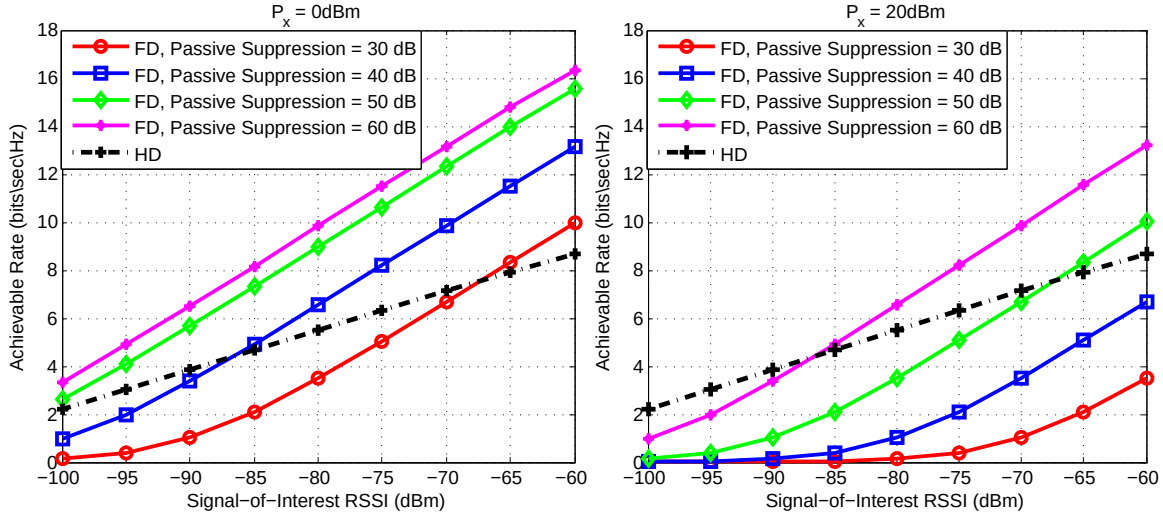

Figure 2.6: Achievable rate for full-duplex and half-duplex systems with total phase noise μ=−60dB, and transmit power of 0dBm and 20dBm.

Figure 2.6 implicitly show that, increasing the transmit power worsens the full-duplex system

performance. In the following simulation, we numerically investigate the effect of changing the transmit power (while keeping constant distance (D) between the two communicating nodes) on both full-duplex and half-duplex system's performance. Figure 2.7 shows the full-duplex and half-duplex achievable rate at different transmit power values. The results show that, the full-duplex rate gain decreases with the increase of the transmit power, which implies that, for a given distance D, lowering the transmit power makes full-duplex systems more likely to outperform half-duplex systems. This conclusion consists with the second tradeoff discussed in section 2.4. The results also show that, as the transmit power increases the full-duplex rate increases until it reaches a saturation point. The reason is that, as the transmit power increases, the received self-interference signal strength increases, and the full-duplex SINR starts to be totally limited by the un-cancelled self-interference power ($\eta \mathsf{RSSI}_A$). At this point, increasing the transmit power will increase both signal-of-interest and un-cancelled self-interference power with the same amount, keeping the SINR constant.

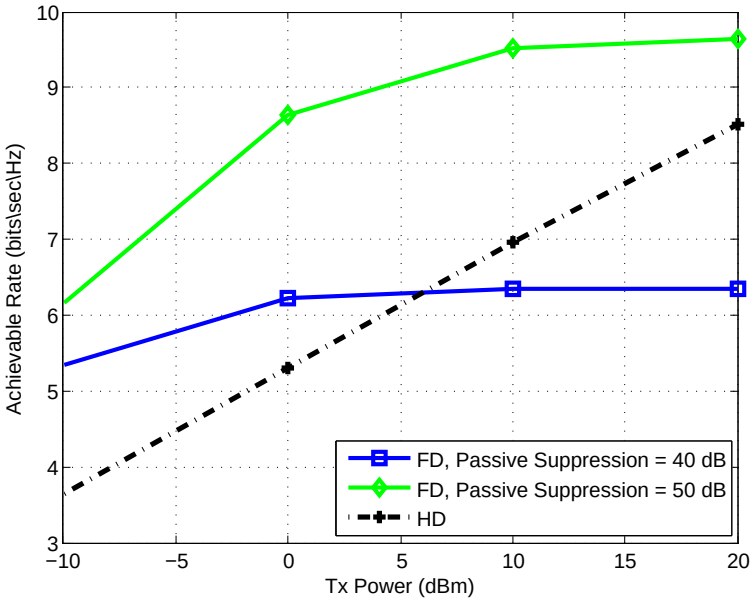

Figure 2.7: Achievable rate for full-duplex and half-duplex systems at different transmit power values, with total phase noise μ=−60dB, and distance $D = 50$ meters between the two communicating nodes.

2.6 Conclusion

In this chapter, we introduced a signal model for single input single output narrowband full-duplex system by modeling different transmitter and receiver radio impairments. More specifically, transmitter and receiver phase noise, LNA noise figure, mixer noise figure, and analog-to-digital converter quantization noise. The signal model is used to analytically derive a piecewise linear, in the log domain, approximation for the rate gain region in terms of all system parameters, as well as radio impairments under both analog and digital self-interference cancellation techniques. A study of full duplex system behaviour under different operation conditions is presented illustrating the system design space and possible tradeoffs. Finally, we numerically investigate the design requirements to enable full-duplex transmission with rate gains as compared to half-duplex transmission in typical indoor environments. The results show that, for low-transmit power applications (e.g. 0dBm), a -60dBc in-band phase noise combined with 40dB passive self-interference suppression could achieve a rate of $\sim$1.2x to $\sim$1.4x times that of half-duplex systems.

Chapter 3

Phase Noise Suppression in Full-Duplex Systems

3.1 Introduction

The analysis in chapter 2 along with the results presented in [37],[39]-[41] show that among the various RF circuits' impairments, oscillator phase noise is found to be one of the main self-interference cancellation limiting factors in full-duplex systems. Without phase noise suppression, the amount of cancellable self-interference power will be limited to the phase noise power level. Giving its limiting impact on performance, phase noise suppression is one of the main design targets for full-duplex system designers.

In this chapter, we analytically and experimentally investigate the problem of phase noise estimation and suppression in full-duplex systems in the presence of both transmitter and receiver oscillator phase noise. First, we study the impact of oscillator phase noise on full-duplex Orthogonal Frequency Division Multiplexing (OFDM) systems. For practical system considerations, both free-running and phase locked loop (PLL) based oscillators are consid-

ered. Second, we propose two different phase noise estimation and suppression techniques. Detailed complexity comparison between the two proposed techniques is introduced. Third, the effect of channel estimation error on the phase noise estimation performance is discussed. Fourth, a real-time experimental framework is used to confirm the conclusions derived from the numerical analysis. For additional diversity, the experimental results are obtained using two different research platforms (e.g. WARP [63], and USRP [64]). Finally, the overall system performance is investigated to study the feasibility of using phase noise estimation and suppression techniques in full-duplex systems in terms of achieved gain and required complexity.

Generally, the presence of phase noise in OFDM systems introduces common phase error (CPE) and intercarrier interference (ICI) [65]-[66]. Most of the current self-interference cancellation techniques compensate only for the CPE and ignore the ICI effect, which limits the amount of cancellable self-interference power to the ICI power level. Therefore, improving self-interference cancellation capability requires the ICI signal to be estimated and suppressed. In fact, conventional half-duplex frequency-domain ICI suppression techniques [65]-[67] could be used in full-duplex systems with the following two exceptions; first, in full-duplex systems, while suppressing the ICI associated with the self-interference signal, the signal-of-interest is considered as unknown noise signal. Second, in full-duplex systems, the self-interference signal is known at the receiver side, thus eliminating the need to use decision feedback techniques to obtain the transmitted signal.

In addition to the frequency domain ICI estimation techniques, conventional time-domain ICI estimation techniques introduced in [68, 69] could be modified and used in full-duplex systems. In [68, 69] a low-complexity Least Square (LS) plus filtering technique is used for ICI estimation in half-duplex systems. Despite its low complexity, using LS techniques in full-duplex systems has to be carefully considered, mainly due to the fact that the ICI has to be estimated in the presence of the signal-of-interest which is typically higher than the ICI

power in typical operating scenarios. This high signal-of-interest noise power will negatively impact the LS estimator quality.

Since the ICI suppression amount depends on the accuracy of the estimated ICI signal, which is proportionally related to the computational complexity; the main challenge in full-duplex systems is achieving sufficient ICI suppression at reasonable computational complexity. The analysis in this chapter shows that in full-duplex systems, two main factors affect the achieved ICI suppression amount: first, the fact that the signal-of-interest is considered as a noise signal during the ICI estimation process significantly degrades the quality of the estimated ICI signal, especially in the cases where the signal-of-interest power is higher than the ICI signal power. Second, the results also show that using different oscillator types (e.g. free-running or PLL based oscillator) affect the achieved ICI suppression amount, mainly due to the different phase noise power spectral density shapes in different oscillator types.

Notation: In this chapter, we use $(*)$ to denote convolution, $(.)^H$ to denote conjugate transpose, $E[.]$ to denote expectation. We use boldface letters $(\mathbf{A})$ for matrices, $\mathbf{A}(m,n)$ to denote the element on the m^{th} row and n^{th} column of the matrix $\mathbf{A}$, and $diag(\mathbf{A})$ to denote a diagonal matrix whose diagonal is constructed from the vector $\mathbf{A}$.

3.2 Signal Model

In this section, a signal model for full-duplex systems including the transmitter and receiver phase noise is introduced. Figure 3.1 illustrates a block diagram for a full-duplex OFDM transceiver using passive self-interference suppression (i.e. antenna separation) followed by digital self-interference cancelation. The oscillator at the transmitter side is assumed to have a random phase error represented by $\phi^t(t)$. At the receiver side, the received signal consists of the self-interference signal and the signal-of-interest (the signal to be decoded)

down-converted from the carrier frequency to the base-band. The down-conversion mixer is assumed to have a random phase error represented by $\phi^r(t)$[1]. The received base-band time domain signal can be written as

$$y_n = \left[\left(x_n^I e^{j\phi_n^{t,I}} * h_n^I\right) + \left(x_n^S e^{j\phi_n^{t,S}} * h_n^S\right)\right] e^{-j\phi_n^r} + z_n, \tag{3.1}$$

where n is the sample index, x^I, x^S are the transmitted self-interference signal and signal-of-interest respectively, $\phi^{t,I}$, $\phi^{t,S}$ are the self-interference and signal-of-interest transmitter phase noise processes, ϕ^r is the receiver phase noise process, h^I, h^S are the self-interference and signal-of-interest channels, and z is the receiver noise.

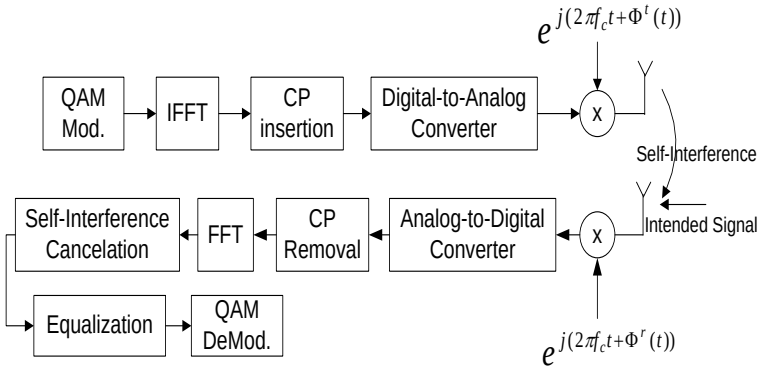

Figure 3.1: Block diagram of full-duplex OFDM transceiver.

Performing Discrete Fourier Transform (DFT) on both sides of (3.1) we get

$$\begin{aligned} Y_k &= \underbrace{\sum_{m=0}^{N-1}\sum_{l=0}^{N-1} X_l^I H_m^I J_{m-l}^{t,I} J_{k-m}^r}_{Y_k^I} + \underbrace{\sum_{m=0}^{N-1}\sum_{l=0}^{N-1} X_l^S H_m^S J_{m-l}^{t,S} J_{k-m}^r}_{Y_k^S} + Z_k \\ &= Y_k^I + Y_k^S + Z_k, \end{aligned} \tag{3.2}$$

[1]In this chapter, we consider the general case of using different transmitter and receiver local oscillators. The analysis is also valid (with slight modifications) for the special case where the transmitter and the receiver share the same local oscillator [39, 41].

where k is the subcarrier index, N is the total number of subcarriers per OFDM symbol, Y_k^I, Y_k^S represents the self-interference and signal-of-interest parts of the received signal, Z_k is the Fourier transform of the receiver noise, and J^i, $i \in [(t,I),(t,S),r]$ represents the DFT coefficients of the phase noise signal calculated as

$$J_k^i = \sum_{n=0}^{N-1} e^{j\phi_n^i} e^{-j2\pi nk/N}. \tag{3.3}$$

In experimental results published in [33], it was shown that for full-duplex systems, the self-interference channel follows a Rician distribution with a coherence bandwidth ranging from 3−15MHz depending on the experimental environments. Accordingly, compared to the narrowband phase noise process, the self-interference channel could be assumed constant over the phase noise bandwidth. It has to be noticed that this assumption is only used during the development of the algorithms. However, the entire numerical analysis is performed using typical channel models for indoor environments. In addition, the experiments are conducted in typical indoor environments. This assumption is commonly used in phase noise suppression approaches [67]-[69]. Accordingly, Equation (3.2) can be simplified as

$$Y_k = \sum_{l=0}^{N-1} X_l^I H_l^I \sum_{m=0}^{N-1} J_{m-l}^{t,I} J_{k-m}^r + Y_k^S + Z_k = \sum_{l=0}^{N-1} X_l^I H_l^I J_{k-l}^c + Y_k^S + Z_k, \tag{3.4}$$

where J^c is the DFT coefficients of the combined transmitter and receiver phase noise calculated as the circular convolution of $J^{t,I}$ and J^r.

Rewriting (3.4) in a more detailed form we get

$$Y_k = X_k^I H_k^I \underbrace{J_0^c}_{CPE} + \underbrace{\sum_{l=0, l\neq k}^{N-1} X_l^I H_l^I J_{k-l}^c}_{ICI} + Y_k^S + Z_k, \tag{3.5}$$

where J_0^c is the DC coefficient that acts on all subcarriers as a CPE, and the second term represents the ICI associated with the self-interference signal. The time-domain representation

of (3.5) can be written as

$$y_n = (x_n^I * h_n^I) j_n^c + y_n^S + z_n, \tag{3.6}$$

where $j_n^c = e^{j\left(\phi_n^{t,I} - \phi_n^r\right)}$ is the time domain representation of the combined phase noise process.

In order to proceed with the analysis, a closed form model for the phase noise process is required. In this chapter, we consider the two commonly used oscillator types: free-running oscillators and PLL based oscillators. In free-running oscillators the phase noise could be modeled as a Wiener process where the phase error at the n^{th} sample is related to the previous one as $\phi_n = \phi_{n-1} + \alpha$, where α is a Gaussian random variable with zero mean and variance $\sigma^2 = 4\pi^2 f_c^2 C T_s$ [62]. In this notation T_s describes the sample interval and C is an oscillator dependent parameter that determines its quality. The oscillator parameter C is related to the 3dB bandwidth f_{3dB} of the phase noise Lorentzian spectrum by $C = f_{3dB}/\pi f_c^2$ [65]. As shown in [65], the phase noise auto-correlation for free-running oscillators is calculated as

$$E\left[e^{j\phi_m} e^{-j\phi_n}\right] = E\left[e^{j\Delta\phi_{mn}}\right] = e^{\frac{-4\pi^2 f_c^2 C T_s |m-n|}{2}}. \tag{3.7}$$

In PLL based oscillators, as shown in figure 3.2, the voltage controlled oscillator (VCO) output is controlled through a feed-back loop that involves a phase detector and low-pass filter (LPF). The purpose of the feed-back loop is to lock the phase of the VCO output with the phase of a high quality reference oscillator. As shown in [58], the PLL output phase noise can be modeled as Ornstein-Uhlenbeck process with auto-correlation function calculated as

$$E\left[e^{j\Delta\phi_{mn}}\right] = e^{\frac{-4\pi^2 f_c^2}{2}\left(C T_s |m-n| + 2\sum_{i=0}^{n_0}(\mu_i + v_i)\left(1 - e^{-\lambda_i T_s |m-n|}\right)\right)}, \tag{3.8}$$

where (n_0, μ , v, λ) are PLL specific parameters that are function of the PLL loop filter design[2].

[2]See [58] for detailed description on how these parameters are calculated.

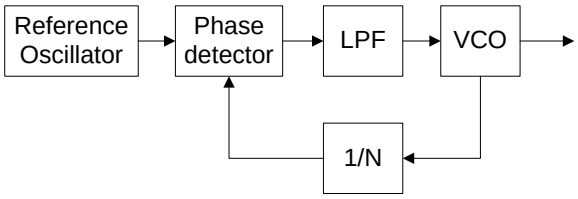

Figure 3.2: PLL based oscillator.

3.3 Self-Interference Cancellation with Phase Noise Suppression

According to (3.5), total self-interference cancellation requires both the CPE and the ICI components to be suppressed. Conventional digital self-interference cancellation techniques only consider the suppression of the CPE component and neglects the ICI component, which limit the amount of cancellable self-interference power to the ICI power level. In this section, we introduce two different phase noise estimation and suppression techniques that are used to enhance self-interference cancellation capability in full-duplex systems.

Generally, self-interference cancellation requires the knowledge of both transmitted self-interference signal (X^I) and self-interference channel (H^I). Since it is transmitted from the same transceiver, the transmitted self-interference signal is assumed to be known at the receiver side. An accurate estimation for the self-interference channel (H^I), as well as the signal-of-interest channel (H^S) could be obtained using orthogonal training sequences sent at the beginning of each transmission frame. Detailed analysis for the channel estimation error effect on the system performance is introduced in section 3.4.

3.3.1 Frequency-domain phase noise estimation and suppression

In this technique, the DFT coefficients of the phase noise process (J_k^c) is estimated in the frequency-domain, and then used to suppress both the CPE and ICI components. The estimation-suppression process consists of four main steps:

- Estimating the DC coefficient (J_0^c).
- Suppressing the CPE component by subtracting $X_k^I H_k^I J_0^c$ from the received signal.
- Estimating the remaining phase noise coefficients ($J_i^c, i \neq 0$).
- Suppressing the ICI component by reconstructing the signal $\sum_{l=0,l\neq k}^{N-1} X_l^I H_l^I J_{k-l}^c$ then subtract it from the received signal.

For the DC coefficient estimation, the LS estimator is used as follows

$$\hat{J}_0^c = \frac{1}{N_u} \sum_{k=0,k\in U}^{N_u-1} \frac{Y_k}{X_k^I H_k^I}, \tag{3.9}$$

where U is a set that contains the pilot positions within the OFDM symbol, and N_u is the number of pilot subcarriers. After estimating the DC coefficient, the CPE component is subtracted from the received signal in (3.5) as follows

$$Y_k - X_k^I H_k^I \hat{J}_0^c = \sum_{l=0,l\neq k}^{N-1} X_l^I H_l^I J_{k-l}^c + Y_k^S + Z_k. \tag{3.10}$$

In order to perform ICI suppression, the remaining coefficients of J^c have to be estimated. Based on (3.10), the problem of estimating J^c is considered as a linear estimation problem, where J^c is a parameter vector distributed by Gaussian noise and the signal-of-interest (Y^S).

For an estimation order M, Equation (3.10) can be written in a matrix form as

$$\begin{bmatrix} B_{l_1} \\ B_{l_2} \\ : \\ B_{l_p} \end{bmatrix} = \begin{bmatrix} A_{l_1} & ... & A_{l_1+M} \\ A_{l_2} & ... & A_{l_2+M} \\ : & : & : \\ A_{l_p} & ... & A_{l_p+M} \end{bmatrix} \begin{bmatrix} J^c_{M/2} \\ : \\ J^c_1 \\ J\_1^c \\ : \\ J^c_{-M/2} \end{bmatrix} + \begin{bmatrix} Y^S_{l_1} \\ Y^S_{l_2} \\ : \\ Y^S_{l_p} \end{bmatrix} + \begin{bmatrix} \gamma^{ICI}_{l_1} \\ \gamma^{ICI}_{l_2} \\ : \\ \gamma^{ICI}_{l_p} \end{bmatrix} + \begin{bmatrix} Z_{l_1} \\ Z_{l_2} \\ : \\ Z_{l_p} \end{bmatrix}, \quad (3.11)$$

where $B_k = Y_k - X^I_k H^I_k \hat{J}^c_0$, $A_k = X^I_k H^I_k$, and γ^{ICI} is the residual ICI beyond the estimation order M. The set $[l_1 \quad l_2 \quad ... \quad l_p]$ has to be of length $\geq M$ in order to solve (3.11) for M unknowns. The cancellation order M represents the number of estimated phase noise frequency coefficients. It also determines the computational complexity of the algorithm. As M increases, the estimation quality improves and the complexity increases. Summarizing (3.11) in a compact form we get

$$\mathbf{B} = \mathbf{A}\mathbf{J^c} + \boldsymbol{\eta}, \quad (3.12)$$

where $\boldsymbol{\eta}$ represents the effective noise that combines all of the signal-of-interest, the residual ICI, and the receiver noise. Using (3.12), the minimum mean square error (MMSE) estimate of $\mathbf{J^c}$ is given by

$$\hat{\mathbf{J}}^c = \mathbf{W}\mathbf{B}, \quad (3.13)$$

$$\mathbf{W} = \mathbf{R_{JJ}}\mathbf{A^H}(\mathbf{A}\mathbf{R_{JJ}}\mathbf{A^H} + \mathbf{R}_{\eta\eta})^{-1}, \quad (3.14)$$

where $\mathbf{R_{JJ}}$ represents the correlation matrix of the vector $\mathbf{J^c}$, and $\mathbf{R}_{\eta\eta}$ represents the correlation matrix of the vector $\boldsymbol{\eta}$.

Using equation (3.3), the (p,q) element of the correlation matrix $\mathbf{R_{JJ}}$ can be calculated as

$$\mathbf{R_{JJ}(p,q)} = \mathbf{E}\left[\mathbf{J_p J_q^*}\right] = \frac{\mathbf{1}}{\mathbf{N^2}} \sum_{\mathbf{m=0}}^{\mathbf{N-1}} \sum_{\mathbf{n=0}}^{\mathbf{N-1}} \mathbf{E}\left[\mathbf{e^{j\Delta\phi_{mn}}}\right] \mathbf{e}^{-\mathbf{j}\frac{\mathbf{2\pi}}{\mathbf{N}}\mathbf{(pm-qn)}}, \tag{3.15}$$

where $E\left[e^{j\Delta\phi_{mn}}\right]$ is calculated as in (3.7), (3.8) for free-running and PLL based oscillators.

Assuming that the data symbols and the receiver noise are not correlated, the correlation matrix $\mathbf{R}_{\eta\eta}$ can be written as

$$\mathbf{R}_{\eta\eta} = \mathsf{diag}(\mathbf{E}\left[\left|\mathbf{Y_{l_1}^S}\right|^{\mathbf{2}}\right] + \mathbf{E}\left[\left|\gamma_{\mathbf{l_1}}^{\mathbf{ICI}}\right|^{\mathbf{2}}\right] + \sigma_{\mathbf{z}}^{\mathbf{2}}, ..., \mathbf{E}\left[\left|\mathbf{Y_{l_p}^S}\right|^{\mathbf{2}}\right] + \mathbf{E}\left[\left|\gamma_{\mathbf{l_p}}^{\mathbf{ICI}}\right|^{\mathbf{2}}\right] + \sigma_{\mathbf{z}}^{\mathbf{2}}), \tag{3.16}$$

where σ_z^2 is the receiver noise variance, $E\left[\left|\gamma_{l_i}^{ICI}\right|^2\right]$ is the power of the residual ICI at subcarrier l_i calculated as [65]

$$E\left[\left|\gamma_{l_i}^{ICI}\right|^2\right] = \sum_{p=0, p>|M|}^{N-1} \mathbf{R_{JJ}(p,p)}, \tag{3.17}$$

and $E\left[\left|Y_{l_1}^S\right|^2\right]$ is the power of the received signal-of-interest at subcarrier l_i. For simplicity, $E\left[\left|Y_{l_1}^S\right|^2\right]$ can be approximated to the average received signal-of-interest power as follows

$$E\left[\left|Y_{l_i}^S\right|^2\right] = E\left[\left|X_{l_i}^S H_{l_i}^S\right|^2\right] = E\left[\left|H_{l_i}^S\right|^2\right], \tag{3.18}$$

where the transmitted signal are assumed to be M-QAM modulated with a unity average power. In the end, the estimated phase noise vector $\hat{\mathbf{J}}^c$ is constructed by placing the M estimated coefficients in their corresponding positions and placing zero elsewhere.

In the ICI cancellation phase, the ICI component is reconstructed as

$$\hat{ICI}_k = \sum_{l=0, l\neq k}^{N-1} X_l^I H_l^I \hat{J}_{k-l}^c, \tag{3.19}$$

and then subtracted from the received signal.

Regarding the computational complexity, the most computation consuming part in the discussed frequency-domain technique is the calculation of the weighting matrix $\mathbf{W}$ which involves matrix inversion. Although the correlation matrix $\mathbf{R_{JJ}}$ is a symmetric matrix, however, due to the fact that $\mathbf{A}$ is a general matrix with no special properties, the matrix $(\mathbf{AR_{JJ}A^H}+\mathbf{R}_{\eta\eta})$ is also a general MxM matrix, which sets the complexity of such technique to $O(M^3)$. The high complexity order will limit the use of such technique to small M cases which directly affects the accuracy of the estimated phase noise vector, and thus the amount of suppressed ICI power.

In addition to matrix inversion, reconstructing the ICI component involves a convolution process of order $O(NM)$, which also limits the use of such technique to systems with a small number of subcarriers N. For complexity reduction, lower complexity time-domain phase noise estimation and suppression technique is proposed in the following subsection.

3.3.2 Time-domain phase noise estimation and suppression

Referring back to (3.6), since the self-interference channel H^I and the self-interference signal X^I are known, a time-domain MMSE estimator could be used to solve (3.6) for the unknown vector j^c that is distributed by Gaussian noise and the signal-of-interest (y^S). For an M

order MMSE estimator, equation (3.6) can be written in a matrix form as

$$\begin{bmatrix} y_{l_1} \\ y_{l_2} \\ : \\ y_{l_M} \end{bmatrix} = \begin{bmatrix} a_{l_1} & 0 & ... & 0 \\ 0 & a_{l_2} & ... & 0 \\ : & : & : & \\ 0 & 0 & ... & a_{l_M} \end{bmatrix} \begin{bmatrix} j^c_{l_1} \\ j^c_{l_2} \\ : \\ j^c_{l_M} \end{bmatrix} + \begin{bmatrix} y^S_{l_1} \\ y^S_{l_2} \\ : \\ y^S_{l_M} \end{bmatrix} + \begin{bmatrix} z_{l_1} \\ z_{l_2} \\ : \\ z_{l_M} \end{bmatrix}, \tag{3.20}$$

or in a compact form as

$$\mathbf{y} = \mathbf{a}\mathbf{j}^{\mathbf{c}} + \boldsymbol{\zeta}, \tag{3.21}$$

where the diagonal elements of the matrix $\mathbf{a}$ represents the time domain self-interference signal after going through the self-interference channel and can be calculated as $a_n = IDFT(X^I_k H^I_k)$, $\boldsymbol{\zeta}$ represents the effective noise vector that combines Gaussian noise $\mathbf{z}$, and signal-of-interest $\mathbf{y}^{\mathbf{S}}$. In the time-domain technique, the cancellation order M represents the number of estimated phase noise time samples and also defines the computational complexity.

Comparing (3.21) with (3.12) we note that in the time-domain technique, the matrix $\mathbf{a}$ is a diagonal matrix and the noise vector $\boldsymbol{\zeta}$ contains only the Gaussian noise $\mathbf{z}$, and the signal-of-interest $\mathbf{y}^{\mathbf{S}}$. However, in the frequency-domain technique, $\mathbf{A}$ is a full matrix and the noise vector $\boldsymbol{\eta}$ has an additional term (γ^{ICI}) which is the residual ICI beyond the estimation order M. The reason is that the phase noise is a multiplicative process in the time-domain, which means that the received signal at time n is only affected by the phase noise at that time instant, while, in the frequency-domain, due to the ICI effect, the received signal at each subcarrier is affected by the phase noise at that subcarrier and all other subcarriers.

Using (3.21), the MMSE estimate of $\mathbf{j}^{\mathbf{c}}$ is given by

$$\hat{\mathbf{j}}^c = \mathbf{w}\mathbf{y}, \tag{3.22}$$

$$\mathbf{w} = \mathbf{R_{jj}a^H}(\mathbf{aR_{jj}a^H} + \mathbf{R}_{\zeta\zeta})^{-\mathbf{1}}, \tag{3.23}$$

where $\mathbf{R_{jj}}$ represents the time-domain correlation matrix of the vector $\mathbf{j^c}$, and $\mathbf{R}_{\zeta\zeta}$ represents the correlation matrix of the vector $\boldsymbol{\zeta}$. The (m,n) element of the correlation matrix $\mathbf{R_{jj}}$ can be calculated as

$$\mathbf{R_{jj}}(\mathbf{m},\mathbf{n}) = \mathbf{E}\left[\mathbf{j_m j_n^*}\right] = \mathbf{E}\left[\mathbf{e^{j\Delta\phi_{mn}}}\right], \tag{3.24}$$

where $E\left[e^{j\Delta\phi_{mn}}\right]$ is calculated as in (3.7), (3.8) for free-running and PLL based oscillators respectively. The noise correlation matrix $\mathbf{R}_{\zeta\zeta}$ can be calculated as in (3.16) with the exception that $\boldsymbol{\gamma}^{ICI} = \mathbf{0}$ in the time-domain problem.

In cases where $M < N$ (the number of estimated samples is less than the overall number of samples per OFDM symbol), the remaining un-estimated samples could be set to the value of one. However, for better estimation quality, the estimated samples are linearly interpolated to get an estimate for the phase noise at the un-estimated time positions. For lower interpolation errors, the estimation positions $[l_1 \quad l_2 \quad ... \quad l_M]$ are chosen to be equally-spaced in the time-domain. For the cancellation phase, the self-interference signal is reconstructed in the time-domain as $y_n^I = \left(x_n^I * h_n^I\right)\hat{\jmath}_n^c$, then subtracted from the received signal.

From a performance perspective, two main advantages make the time-domain technique expected to outperform the frequency-domain technique: first, in the frequency-domain technique, the remaining ICI beyond the cancellation order is considered as a noise term that negatively affects the estimation quality. However, in the time-domain technique there is no ICI effect. Second, the linear interpolation performed in the time-domain technique results in a good estimate for the un-estimated samples beyond the estimation order, thus

improving the overall estimation performance.

In terms of complexity, the complexity of the proposed time-domain technique is at least one order of magnitude lower than the complexity of the frequency-domain technique. In more details, the complexity advantage of the time-domain technique is a result of three main factors: first, in the calculation of the weighting matrix ($\mathbf{w}$), the time-domain phase noise correlation matrix $\mathbf{R_{jj}}$ is a real symmetric matrix and ($\mathbf{a}$) is a diagonal matrix which results in $(\mathbf{aR_{jj}a^H} + \mathbf{R}_{\zeta\zeta})^{-\mathbf{1}}$ being a symmetric matrix with an inversion complexity order $O(M^2)$ instead of $O(M^3)$ in the frequency-domain technique. Second, in the cancellation phase of the time-domain technique, the self-interference signal is reconstructed using $O(N)$ multiplication process instead of the $O(NM)$ convolution process used in the frequency-domain technique. Finally, performing time-domain phase noise interpolation helps to achieve better performance at a lower estimation order (M), and thus reduces the complexity.

On the other hand, performing time-domain MMSE estimation requires additional inverse discrete Fourier transform (IDFT) process to calculate $a_n = IDFT(X_k^I H_k^I)$. For $N = 2^m$, the complexity of the IDFT process is $O(N \log_2 N)$. Performing time-domain phase noise interpolation is an additional $O(N)$ process that does not exist in the frequency-domain technique. As a conclusion, table 3.1 summarizes the computational complexity of both time-domain and frequency-domain techniques.

Table 3.1: Complexity order of time-domain and frequency-domain phase noise estimation and suppression techniques

	Frequency-domain technique	Time-domain technique
Estimation Phase	$O(M^3)$	$O(M^2)$ For matrix inversion + $O(N \log_2 N)$ to calculate a_n
Cancellation Phase	$O(NM)$	$O(N)$ for Interpolation + $O(N)$ for Cancellation

3.3.3 Discussion on the use of LS-based estimators

Despite the low complexity of LS-based estimators, using LS techniques for ICI estimation in full-duplex systems might result is a negative gain compared to the case when only the CPE is estimated. For more clarification of the "negative gain" issue, consider the following simplified example.

Referring back to equation (3.6), a LS estimate for the combined phase noise process j_n^c is obtained as follows

$$\hat{j}_n^c = \frac{y_n}{h_n * x_n} = j_n^c + \frac{y_n^S + z_n}{h_n * x_n} = j_n^c + e_j \tag{3.25}$$

where e_j is the phase noise estimation error. In this case the phase noise estimation error is directly proportional to the signal-of-interest power, which limits the phase noise cancellation amount to the signal-of-interest power level. This limitation implies that, if the signal-of-interest power is higher than the ICI component of the phase noise, performing LS-based suppression will achieve negative gain compared to the case when only the CPE is mitigated. This is why LS-based techniques can not be used alone in full-duplex systems.

The filtering technique proposed in [68] is could be used to reduce the LS estimation error by relying on the fact that the 3dB BW of the phase noise process is smaller than the system BW, thus using LPF could help filter-out part of the LS estimation noise and improve the performance. In fact, using LPF will not eliminate the "negative gain" issue of the LS estimator; the issue still exists, but will appear at a different signal-of-interest power level. The signal-of-interest power level at which the LS estimator starts to negatively impact the overall performance is a function of the ratio between the system BW and the filter BW. The higher the ratio, the better the performance is. On the other hand, using LPF degrades the phase noise estimation quality by filtering-out part of the phase noise itself. This tradeoff becomes more challenging in the case of PLL-based oscillators where (as will be discussed

in section 3.4) the phase noise spectrum is more flattened than the case of free-running oscillator.

As a conclusion, the "negative gain" issue of the LS-based estimators is the main reason why LS-based estimators should be carefully considered when it comes to full-duplex systems; especially with the knowledge that the typical operating point for a full-duplex system is at high signal-to-ICI power ratios. Generally, full-duplex systems are supposed to achieve significant capacity improvement when the self-interference signal is suppressed near to the noise floor. Giving that the typical SNR values in half-duplex systems is in the range of 20dB, ICI suppression technique is generally useful when the ICI power is close to the noise floor such that the ICI suppression gain mitigates the ICI near to the noise floor. In this case, the ICI suppression algorithm should be properly working at such high signal-of-interest to ICI power values. The main advantage of the proposed MMSE algorithms over the LS-based algorithms is that at high signal-of-interest to ICI power ratios, the MMSE algorithm performance approaches the CPE only performance without having the "negative gain" issue.

3.4 Analysis and Discussions

In this section, the performance of the proposed phase noise estimation and suppression techniques is experimentally and numerically investigated under different operating conditions. In addition, the effect of channel estimation error on the performance is also investigated. For reference, the performance of the proposed techniques is compared to the case where no phase noise suppression is performed. Following the analysis, the feasibility of using phase noise estimation and suppression techniques in full-duplex systems is discussed in terms of achieved gain and required complexity.

A 20MHz wireless LAN system is used as a framework for the analysis. The system is assumed to operate in full-duplex mode, where the wireless terminals are transmitting and receiving at the same time, using the same carrier frequency. The transmitted frame consists of orthogonal training sequences used for channel estimation purposes, followed by data OFDM symbols with 64 subcarriers in each symbol. Each OFDM symbol contains 4 pilot subcarriers used for CPE estimation. The carrier frequency f_c is set to 2.4GHz with a system bandwidth of 20MHz. The indoor TGn channel model D [54] is used to model the self-interference and signal-of-interest channels. The self-interference and signal-of-interest channel's Rician factors are set to 30dB and 3dB respectively.

In the analysis, the self-interference cancellation gain is used as a performance metric. Self-interference cancellation gain is defined as the incoming self-interference power divided by the remaining self-interference power after performing all cancellation and suppression processes. For more clarity, following is the definition of terms used in this section: i) self-interference to signal-of-interest ratio (ISR) is defined as the ratio between the incoming self-interference power and the signal-of-interest power. ii) Total phase noise induced ICI power (P_{ICI}) is defined as the total power of the ICI component relative to the received self-interference power in dBc units. As an example, an ISR of -40dB and P_{ICI} of -30dBc means that the signal-of-interest and the ICI component are below the self-interference signal by 40dB and 30dB respectively, it also means that the ICI power is higher than the signal-of-interest power by 10dB.

3.4.1 Time-domain vs frequency-domain phase noise suppression

In this subsection, the proposed reduced complexity time-domain phase noise estimation and suppression technique is compared to the frequency-domain technique. A free-running oscillator and exact channel knowledge are assumed in this analysis. However, the PLL

based oscillator and channel estimation error effects are studied separately in the following subsections.

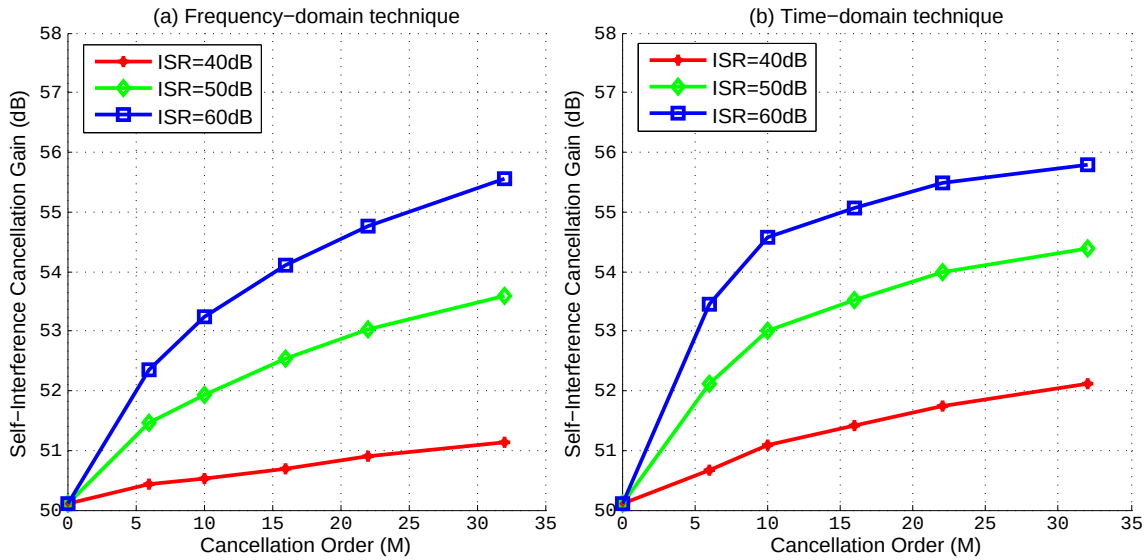

Figure 3.3: Self-interference cancellation gain for time- and frequency-domain phase noise estimation and suppression techniques at $P_{ICI} = -50$dBc, with free-running oscillator.

Figure 3.3 shows the performance of time- and frequency-domain techniques at different cancellation orders (M), and different ISR values with a total ICI power of -50dBc. It has to be noticed that $M = 0$ means that only the CPE component is suppressed, and no ICI suppression is performed. In fact, suppressing the CPE component only is exactly what most of the existing digital self-interference cancellation techniques are doing. The conclusions from this analysis are multifold: first, as described in section 3.3, performing only CPE suppression limits the amount of cancellable self-interference power to the ICI power level (i.e. -50dBc in our case). Second, according to (3.12), (3.21) the variance of the noise vectors $\boldsymbol{\eta}$ and $\boldsymbol{\zeta}$ are directly proportional to the signal-of-interest power, therefore, increasing the signal-of-interest power (i.e. decreasing the ISR) increases the estimator noise variance, thus degrading the estimator performance. Finally, in addition to its complexity advantage, the proposed time-domain technique achieves better performance ($\sim$1dB more cancellation

gain) compared to the frequency-domain technique. The performance superiority of the time-domain technique is mainly due to the linear interpolation performed using the estimated samples to get an estimate for the remaining samples in each OFDM symbol.

3.4.2 Free-running vs. PLL based oscillators

As a matter of fact, most of the current wireless system transceivers use PLL based oscillators; mainly due to its phase stability compared to the continuous phase drift in free-running oscillators. In order to understand the effect of using PLL based oscillators on the proposed phase noise estimation and suppression techniques, first we investigate the main differences between free-running and PLL based oscillators.

First, in free-running oscillators the phase error is modeled as a Wiener process [62] with a continuous phase drift. However, in PLL based oscillators [58], the feed-back loop tends to stabilize the output phase error which results in very small CPE compared to free-running oscillators. Therefore, in case of using PLL based oscillators the CPE estimation could be omitted or estimated over long time periods. Second, as shown in [62, 58], generally the phase noise power spectral density (PSD) has a low pass shape with a decay rate proportional to $1/f_o^2$ (f_o is the frequency offset from the main carrier). However, in PLL based oscillators, due to the existence of the loop filter, the phase noise PSD of the output Flatter over the bands of interest. Figure 3.4 [58] shows a typical example for the phase noise PSD in free-running and PLL based oscillators[3]. From an OFDM perspective, in the free-running oscillator case, the subcarriers centered around the carrier frequency will have large phase noise power, and this power will decay fast when you go towards the edge subcarriers. On the other hand, in PLL based oscillator case, the phase noise power starts at a lower value and decays slower than free-running oscillators. Figure 3.5 shows the phase noise power per subcarrier for both

[3]In Figure 3.4 [58], the legend "Reference" and "VCO Open Loop" refers to free-running oscillators and "PLL VCO" refer to PLL based oscillator.

free-running and PLL based oscillators with the same total in-band phase noise power. The question to consider is how does this impact the performance of the proposed techniques?

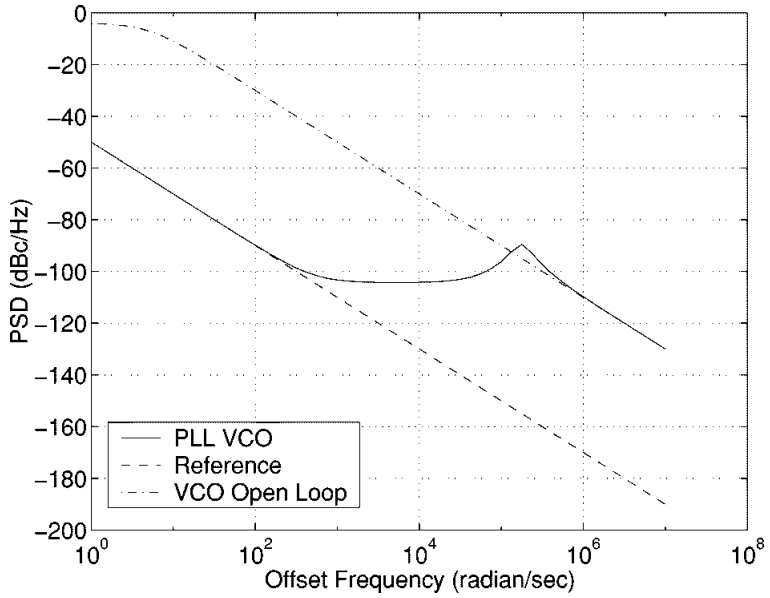

Figure 3.4: PSD for free-running and PLL based oscillators [58], free-running is the dashed lines and PLL is the solid line

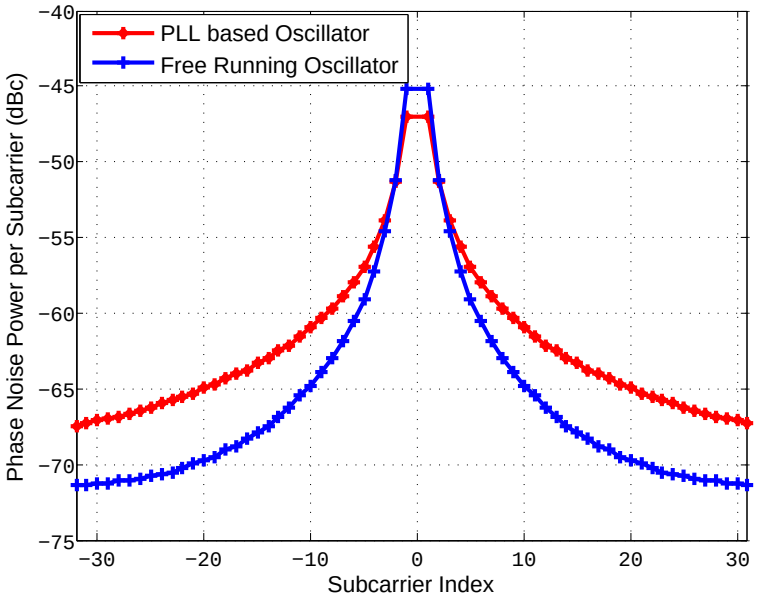

Figure 3.5: Phase noise power per subcarrier for free-running and PLL based oscillators at $P_{ICI} = -40$dBc.

In the frequency-domain estimation technique, at a given estimation order M, the power of the estimated phase noise will be larger in the case of free-running than PLL based oscillator. Therefore, the ICI suppression amount will be higher in the case of free-running oscillators. In addition, for small cancellation orders (M), the remaining ICI power beyond the estimation order will be smaller in case of free-running as compared to the PLL based oscillator, which means lower noise variance, and thus better estimation quality in the case of free-running oscillators. As a conclusion, using PLL based oscillators degrades the overall cancellation performance. Figure 3.6a shows the performance of the frequency-domain estimation technique using free-running and PLL based oscillators. The results show that using free-running oscillators approximately doubles the achieved ICI suppression amount compared to the case where PLL based oscillators are used.

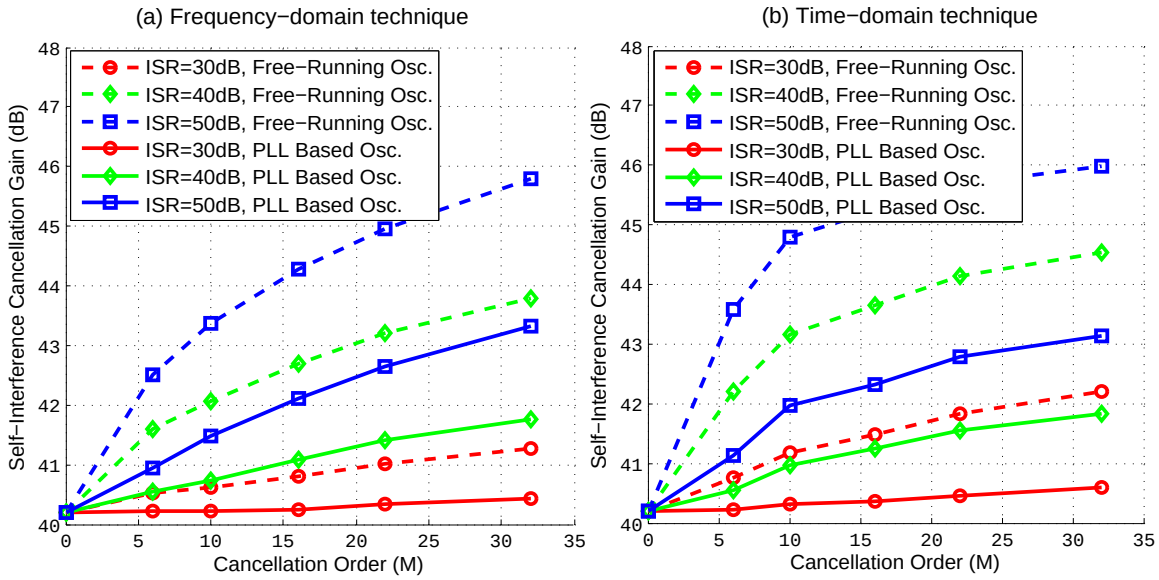

Figure 3.6: Self-interference cancellation gain for free-running and PLL based oscillators using frequency- and Time-domain phase noise estimation techniques at $P_{ICI} = -40$dBc.

For the time-domain estimation technique, the flatness in the phase noise PSD is equivalent to lower correlation between time-domain samples. Since the time-domain estimation technique uses linear interpolation to get an estimate for the remaining phase noise samples

beyond the estimation order, lower time correlation means higher interpolation errors and thus lower estimation quality. Figure 3.6b shows the performance of the time-domain estimation technique using free-running and PLL based oscillators. The results also show that using PLL oscillators degrades the ICI suppression performance. On the other hand, comparing figure 3.6a and 3.6b we notice that even with PLL based oscillators, the time-domain technique still outperforms the frequency-domain technique.

3.4.3 Effect of channel estimation error

In practical systems, exact channel information is not available at the receiver side. Rather, the channel has to be estimated, which typically results in channel estimation error that affects the overall system performance. In this analysis, we investigate two things: i) the effect of the phase noise on the channel estimation error, and ii) the effect of the channel estimation error on the phase noise estimation performance. The channel is estimated using L OFDM training symbols transmitted at the beginning of each data frame. The training symbols have the same structure as the long preamble of the 802.11n standard. The training symbols for the self-interference and the signal-of-interest channels are orthogonal in the time-domain.

During the training period of the self-interference channel, Equation (3.5) can be rewritten as

$$Y_k = X_k^I H_k^I J_0^c + \sum_{l=0, l\neq k}^{N-1} X_l^I H_l^I J_{k-l}^c + Z_k, \tag{3.26}$$

where the term Y_k^S is eliminated because the signal of-interest is not transmitted during the self-interference training interval. Since J_0^c is constant across the subcarriers, it can be considered part of the channel. Therefore, the LS estimate for the self-interference channel

(including J_0^c) can be written as

$$\hat{H}_k^I = \frac{Y_k}{X_k^I} = H_k^I J_0^c + \sum_{l=0, l\neq k}^{N-1} \frac{X_l^I}{X_k^I} H_l^I J_{k-l}^c + \frac{Z_k}{X_k^I} = H_k^I J_0^c + \delta_k^I, \tag{3.27}$$

where δ_k^I is the self-interference channel estimation error. Assuming no correlation between the noise and the data symbols, the variance of the channel estimation error can be written as

$$\sigma_\delta^2 = E\left[\left|H_k^I\right|^2\right] \sum_{p=1}^{N-1} \mathbf{R_{JJ}}(\mathbf{p}, \mathbf{p}) + \sigma_{\mathbf{Z}}^{\mathbf{2}}, \tag{3.28}$$

where the first term in right hand side of (3.28) represents the total ICI power. As shown in (3.28), the variance of the channel estimation error is directly proportional to the phase noise power (ICI component) and the AWGN noise power.

One way to reduce the channel estimation error is by averaging the estimated channel over multiple OFDM symbols. Such that

$$\hat{H}_k^{I,avg} = \sum_{l=1}^{L} \hat{H}_{l,k}^I, \tag{3.29}$$

where L is the number of training symbols. Since the correlation between the phase noise at different OFDM symbols is very small, averaging over multiple OFDM symbols achieves $\sim 10log(L)$ dB reduction in the channel estimation error. However, increasing the number of training symbols negatively impacts the overall system capacity.

Another technique that could be used to reduce the channel estimation error is the IDFT based channel estimation technique proposed in [70]. In this technique, an estimate for the channel impulse response (CIR) is obtained as $\hat{h}_n^I = \mathsf{IDFT}\{\hat{H}_k^I\}$. Then, by leveraging the fact that the channel information is contained in the first T samples of the CIR, a better estimate for the channel is obtained by taking the first T samples of $\hat{h}_n^I$ while forcing other

samples to zero as follows

$$\hat{h}_n^{I,nulling} = \begin{cases} \hat{h}_n^I & , \ 0 \leq n \leq T-1, \\ 0 & , \ \text{otherwise}, \end{cases} \tag{3.30}$$

then

$$\hat{H}_k^{I,nulling} = \mathsf{DFT}\left\{\hat{h}_n^{I,nulling}\right\}. \tag{3.31}$$

By doing this, the channel estimation error is reduced by a factor of T/N. The key challenge in such technique is the choice of T. Since the cyclic prefix in practical systems is designed to be larger than the channel length, a good choice for T is to be equal to the cyclic prefix length. For better performance, the IDFT nulling algorithm could be combined with the averaging technique.

Figure 3.7 shows the Mean Square Error (MSE) of the self-interference channel at different phase noise power values. The results show that without averaging or IDFT nulling, the channel estimation error will be at the phase noise power level. However, by averaging over two symbols and using IDFT nulling, the channel estimation error is reduced by 5.5dB below the phase noise power.

From a phase noise suppression perspective, the channel estimation error will negatively affect the estimation of the CPE as well as the ICI components. Since CPE is estimated using LS techniques, the degradation in the CPE estimation will be directly proportional to the channel estimation error σ_δ^2. For example, at a total phase noise power of -50dBc, the channel estimation error using averaging plus IDFT nulling is -55.5dBc, thus, the CPE estimation error will be in the range of $(-50\text{dB}) + (-55.5\text{dB}) \sim= -49\text{dB}$ which is 1dB higher than the CPE estimation error in case of using perfect channel knowledge. The ICI estimation techniques discussed in section 3.3 could be slightly modified to account for

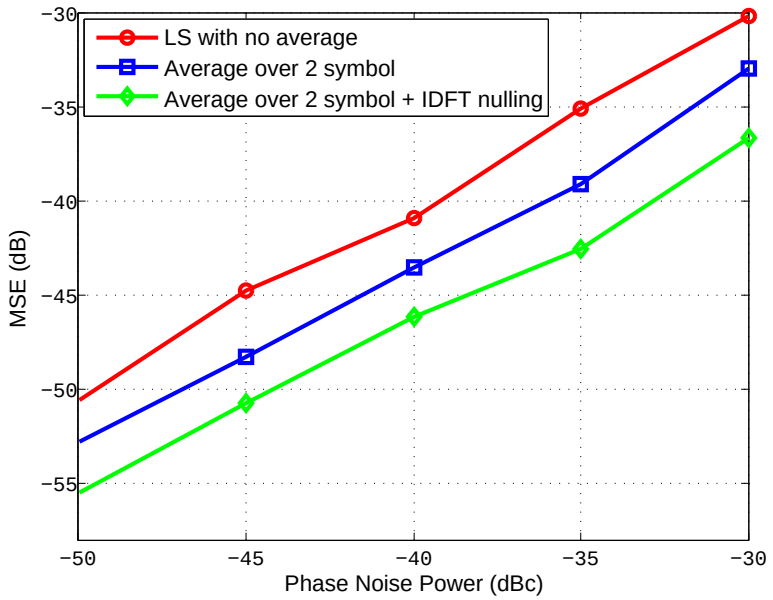

Figure 3.7: Self-interference channel MSE at different phase noise power values.

the channel estimation error by using $\hat{H}_k^I$ instead of H_k^I, and adding another noise element (represents the channel estimation error) to the composite noise vectors η and ζ in (3.12) and (3.21) respectively. In case of using symbol averaging plus IDFT nulling, the added noise element will be $= \frac{T}{N.L}(\sigma_\delta^2 + \sigma_Z^2)$.

Figure 3.8 shows the effect of the channel estimation error on the overall cancellation performance using the averaging plus IDFT nulling channel estimation algorithm. The results show that, the channel estimation error could results in a total of ∼1.5dB loss in the overall cancellation performance. It has to be noticed that out of the 1.5dB degradation, 1dB is due to degradation in the estimation of the CPE component and only 0.5dB due to degradation in the estimation of the ICI component (compare the performance loss at $M = 0$ and $M = 32$ in figure 3.8). Second, at least 1dB performance degradation exists even with no ICI suppression (case with $M = 0$), which means that conventional self-interference cancellation techniques are also affected by the channel estimation errors.

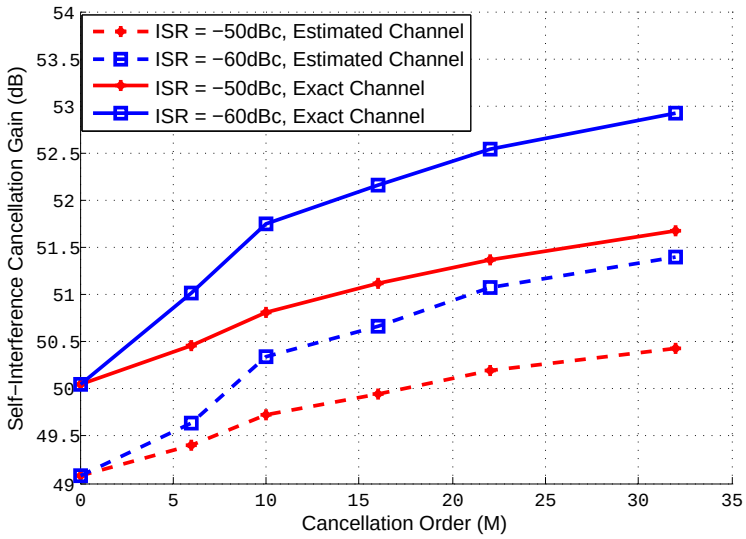

Figure 3.8: Self-interference cancellation gain for PLL based oscillators with time-domain phase noise estimation technique at $P_{ICI} = -50$dBc, using estimated and exact channels.

3.4.4 Experimental analysis

In this section, experimental analysis is performed to verify the accuracy and validity of the presented numerical analysis. A real time experimental framework is constructed to investigate the performance of the proposed phase noise estimation and suppression techniques. For analysis diversity, two commonly used open access wireless platforms (e.g. WARP and USRP) are used in the analysis. Figure 3.9 shows the experimental setup, where a full-duplex communication link is established using two research platforms namely node-A and node-B. Each node has one transmitter and one receiver connected to a separate antenna[4]. The transmitter and receiver base-band processing is done over a host PC, while analog-domain and RF processing is done over the platform. Both platforms are configured to transmit and receive at the same time using the same carrier frequency. Based on the datasheet, both WARP and USRP platforms are using PLL based oscillator for the up- and down-conversion processes. In the experimental analysis, the performance is evaluated at different ISR ratios. At the beginning of each transmission frame, orthogonal training sequences are sent

[4]note that one antenna and circulator could be used instead of two antennas.

for channel estimation proposes. The training sequences are also used to measure the ISR ratio at the receiver input. All the presented results are averaged over several transmission frames. Therefore, the presented results are the ergodic expectation of the instantaneous values.

First, in order to validate our experimental setup, our results are compared to the experimental results reported in [13]. In [13] the WARP platform is used to characterize the cancellation capability of different self-interference cancellation techniques under different antenna configurations. The cancellation techniques used in [13] only consider the suppression of the CPE component, therefore, it has to be compared with our results at $M = 0$. Figure 3.10 shows the cancellation performance of the digital self-interference cancellation technique in [13] compared to our digital self-interference cancellation technique at $M = 0$.

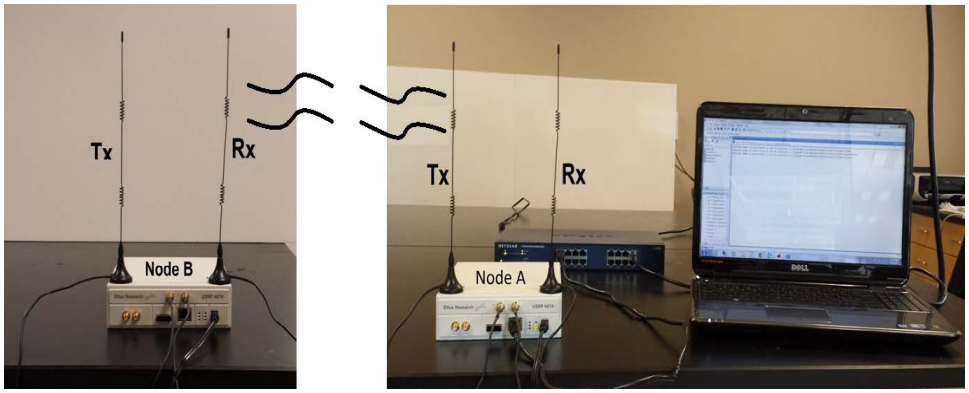

Figure 3.9: Experimental setup using USRP platform.

Now we investigate the performance of the proposed phase noise estimation and suppression techniques. Figure 3.11 show the achieved self-interference cancellation gain at different ISR values for the proposed frequency-domain cancelation technique running over WARP and USRP platforms respectively. The results confirm the conclusions derived from the numerical analysis, where performing ICI suppression improves the cancellation performance (up to 3dB more cancellation) especially at high ISR values. The results also show that the USRP platform achieves better performance than the WARP platform, which means that

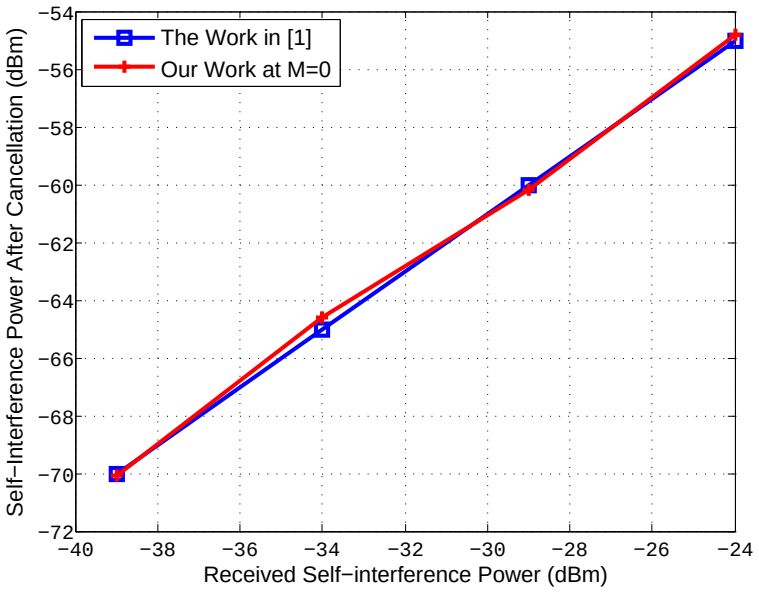

Figure 3.10: Experimental results at $M = 0$ compared to the experimental results in [13].

the quality of the RF circuits and connectors used in the USRP may be better than those used in the WARP platform.

In order to measure the accuracy of the numerical analysis presented earlier in this section, the system model is simulated using the same system parameters used in the USRP platform, and the results are then compared to the experimental results. As shown in Figure 3.12, the simulation results highly matches the experimental results with <0.2dB error. With this matching, all the conclusions derived from the numerical analysis are now confirmed.

3.4.5 Performance limitations

The previous analytical and experimental analyses show that phase noise estimation and suppression techniques in full-duplex systems achieve relatively small gain compared to the required computational complexity. For example, a maximum of 6dB more self-interference cancellation with free-running oscillators (reduced to 3dB in case of PLL based oscillators) is

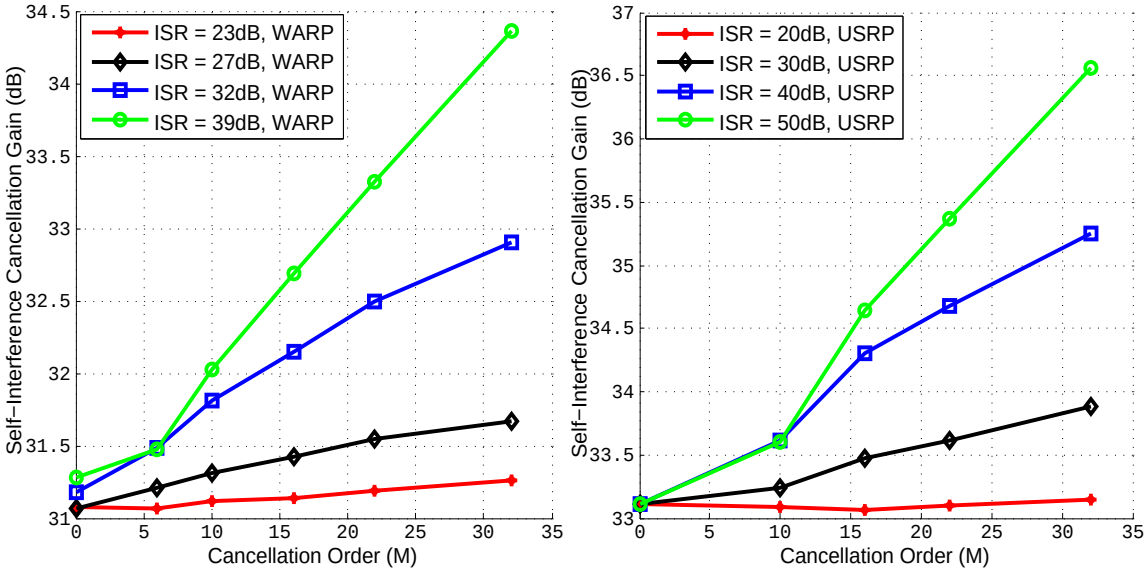

Figure 3.11: Self-interference cancellation gain for frequency-domain phase noise suppression technique using different platforms.

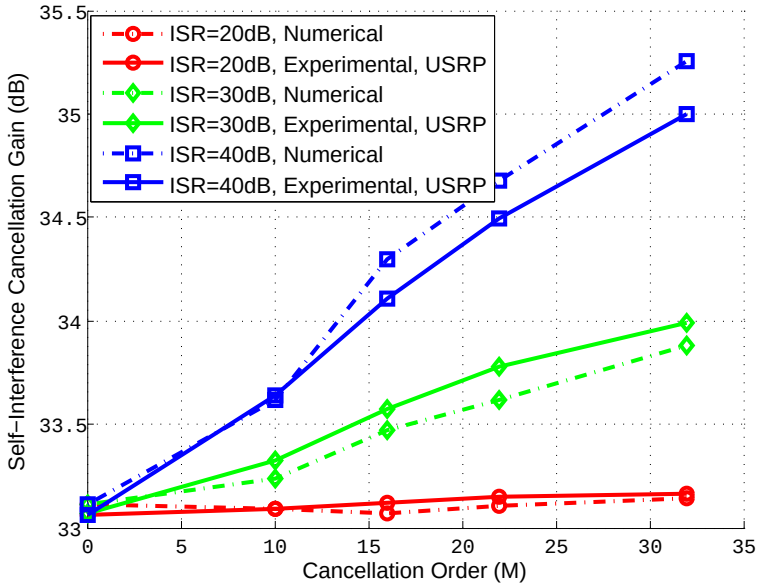

Figure 3.12: Experimental vs numerical results for frequency-domain phase noise suppression at $P_{ICI} = -33$dBc.

achieved at a computational complexity order $O(M^2), M = 32$. This gain is further reduced with the decrease of the ISR.

Three main reasons explain the low gain achieved, and the high complexity required for phase noise estimation and suppression in full-duplex systems: first, the most important reason is that phase noise in full-duplex systems has to be estimated in the presence of the unknown signal-of-interest, which significantly affects the estimator performance, especially at high signal-of-interest powers. Second, the channel estimation error. The results in figure 3.7 show that even using efficient channel estimation techniques, the channel estimation MSE is $\sim$6dB below the phase noise level, this error acts as another noise source during the phase noise estimation process. Finally, the un-estimated phase noise coefficients. In the case when part of the phase noise coefficients are estimated, the remaining ICI due to the un-estimated coefficients acts as another noise component during the estimation process, which negatively affects the estimation performance, especially when PLL based oscillators are used, due to the phase noise spectrum flatness. In order to overcome this issue, all phase noise coefficients have to be estimated, which results in significant complexity especially in OFDM systems with a large number of subcarriers.

In addition to those three factors, the frequency-flat channel approximation used in Equation (3.4) to simplify the phase noise estimation problem might also affect the estimation performance. However, the following analysis shows that, the error due to such approximation is negligible compared to the previously mentioned limiting factors, even at severe channel conditions.

In order to investigate the accuracy of the frequency-flat channel approximation, we first calculate the approximation error. According to (3.2) and (3.4), the frequency-flat channel

approximation error (β_k) can be written as

$$\begin{aligned}\beta_k &= \sum_{l=0}^{N-1}\sum_{m=0}^{N-1} X_l^I H_m^I J_{m-l}^{t,I} J_{k-m}^r - \sum_{l=0}^{N-1} X_l^I H_l^I \sum_{m=0}^{N-1} J_{m-l}^{t,I} J_{k-m}^r \\ &= \sum_{l=0}^{N-1}\sum_{m=0}^{N-1} X_l^I \left(H_m^I - H_l^I\right) J_{m-l}^{t,I} J_{k-m}^r, \end{aligned} \tag{3.32}$$

and the approximation MSE is written as

$$MSE = E\left[|\beta_k|^2\right] = \sum_{l=0}^{N-1}\sum_{m=0}^{N-1} E\left[\left|X_l^I\right|^2\right] E\left[\left|H_m^I - H_l^I\right|^2\right] E\left[\left|J_{m-l}^{t,I}\right|^2\right] E\left[\left|J_{k-m}^r\right|^2\right]. \tag{3.33}$$

Typically, the correlation between the channel frequency responses at different subcarriers is determined by the coherence bandwidth (CBW) of the channel. By definition, the CBW is defined as the frequency band in which the channel could be considered frequency flat. According to this definition, equation (3.33) can be rewritten as

$$MSE = \sum_{l=0}^{N-1} \sum_{\substack{m=0,\\ |m-l|>CBW}}^{N-1} E\left[\left|X_l^I\right|^2\right] E\left[\left|\left(H_m^I - H_l^I\right)\right|^2\right] E\left[\left|J_{m-l}^{t,I}\right|^2\right] E\left[\left|J_{k-m}^r\right|^2\right]. \tag{3.34}$$

where $H_m^I - H_l^I = 0$ within the CBW of the channel. Furthermore, as shown in figure 3.5, the phase noise process has a decaying power spectral density, such that the majority of the phase noise power is located around the DC carrier (i.e. J_0). Accordingly, the remaining terms where $|m-l| > CBW$ will be weighted by small phase noise values $\left|J_{m-l}^{t,I}\right|^2$.

Equation (3.34) shows that the approximation error depends on two main factors: the CBW of the self-interference channel, which is a function of the maximum delay spread, and the quantity $\left|H_m^I - H_l^I\right|^2$, which is a function of the self-interference channel Rician factor. The larger the Rician factor, the smaller the quantity $\left|H_m^I - H_l^I\right|^2$. Figure 3.13 shows the

approximation MSE for different channel models with different Rician factors. The MSE is normalized to the total phase noise power. The simulated channel models are the 'B', 'C', and 'D' TGn channel models defined in [54]. The 'B', 'C', and 'D' channel models have a maximum delay spread of 80, 200, and 390ns respectively. The results show that, even at very small Rician factors, the approximation error is at least two orders of magnitudes below the phase noise level. In addition, the approximation error linearly decrease with the increase of the channel Rician factor. As a conclusion, this results show that, even at severe channel conditions (e.g. large delay spread and small Rician factor), the approximation error is negligible compared to other limiting factors such as channel estimation error and un-estimated phase noise coefficients.

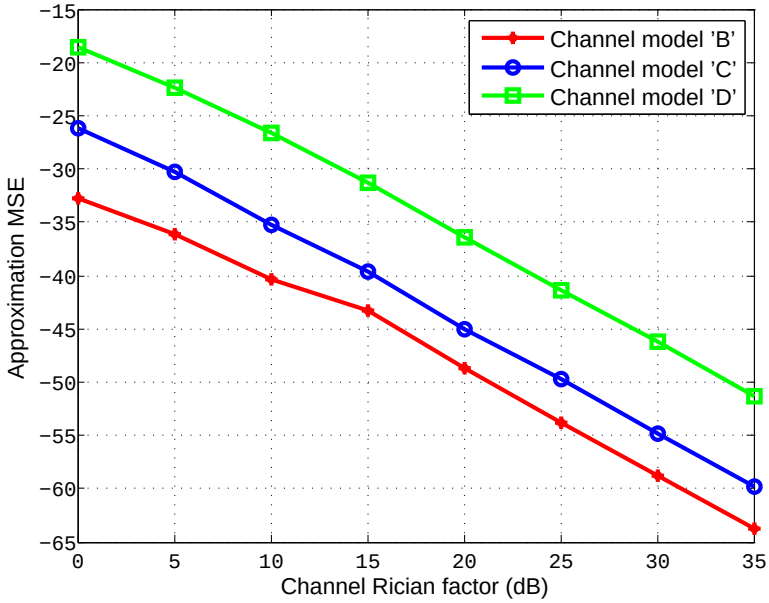

Figure 3.13: MSE due to the frequency-flat channel approximation at different Rician factors with different channel models.

3.4.6 Overall system performance

The previous discussion raises the following important questions; In practical scenarios does phase noise suppression improve the overall system performance? If yes, by how much? And is it worth the extra complexity? In order to answer these questions, we numerically investigate the overall system performance of a practical system in typical operating conditions.

Assume a 20MHz WiFi system with a 20dBm transmit power, −90dBm noise floor, and −40dBc total in-band phase noise power (i.e. $P_{ICI} = -40$dBc). In this example, an average of 60dB passive self-interference suppression gain is assumed [33]. Following the passive suppression, the proposed self-interference cancellation and phase noise suppression techniques are used for digital cancellation. After self-interference cancellation, the signal to interference plus noise ratio (SINR) is calculated for each data subcarrier. The overall SINR is calculated by averaging the instantaneous SINR over both OFDM subcarriers and transmission frames. The overall SINR is then used as a performance metric to characterize the overall system performance. The full-duplex system performance is compared to the corresponding half-duplex system performance at different signal to noise ratios (SNR). The SNR is defined as the signal-of-interest power divided by the noise floor (i.e. SNR of the corresponding half-duplex system). Figure 3.14, shows the overall SINR for both half-duplex and full-duplex systems. The performance is evaluated using a PLL based oscillator model.

In this example, the signal is transmitted at 20dBm power; the passive suppression has an average of 60dB gain, which results in average received self-interference power of -40dBm. The ICI power is −40dB below the self-interference, that is −80dBm. The system is simulated at SNR ranging from 0 to 30dB, which corresponds to signal-of-interest power ranging from −90dBm to −60dBm respectively (the noise floor is −90dBm). First, without ICI suppression ($M = 0$), the remaining self-interference power will be limited by the ICI power level (−80dBm in this case). As a result, the full-duplex system noise floor will be increased to

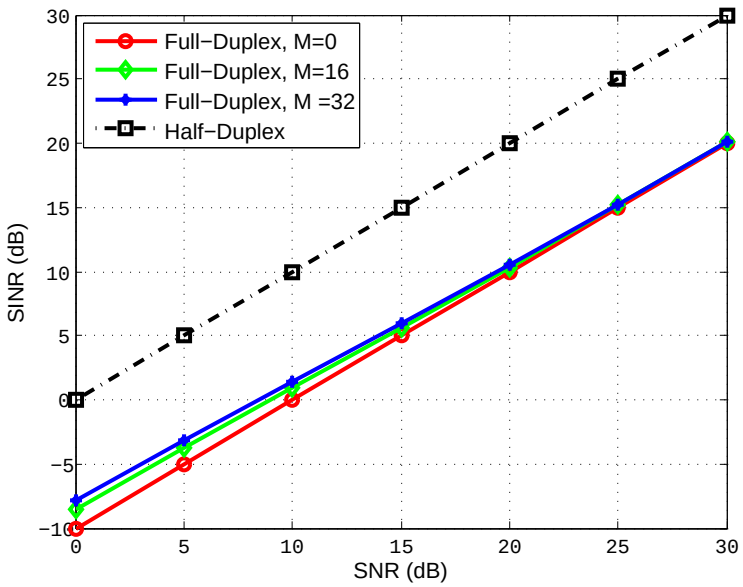

Figure 3.14: Overall SINR for time-domain phase noise suppression technique at different SNR values with 60dB passive self-interference suppression and P_{ICI} of -40dBc, using PLL based oscillator and estimated channel.

-80dBm, resulting in a 10dB difference in SINR between full- and half-duplex performance. The results in Figure 3.14 also show that the maximum ICI suppression gain is achieved at low SNR scenarios; this is where the ICI power is greater than the signal-of-interest power. However, the achieved suppression gain (e.g. $\sim$2.5dB) is not enough to fill the gap between the full-duplex and half-duplex performances.

3.4.7 Discussion on other phase noise mitigation schemes

The previous analyses settle an important question on the feasibility of using phase noise estimation and suppression techniques in full-duplex systems. The analyses show that, the gain achieved by performing phase noise estimation and suppression is relatively small compared to the required complexity. Furthermore, the phase noise suppression gain decreases significantly at high SNR scenarios. Accordingly, phase noise suppression based on linear estimation of the phase noise process is shown to be inefficient in full-duplex systems.

Another way to mitigate the phase noise effect in full-duplex systems is using specific transceiver architectures that are inherently mitigate the phase noise effect without the need of estimating the phase noise process. Three different examples of such modified architectures are briefly discussed in this section.

First, using extensive passive self-interference suppression. One of the main advantages of passive suppression is that it mitigates the self-interference signal and the associated transmitter noise (e.g. phase noise). Since passive suppression reduces the self-interference power at the receiver input, the receiver phase noise effect is also reduced. The analysis in chapter 2 identifies, for a given phase noise power, how much passive suppression is required to achieve full-duplex rate gain compared to half-duplex systems.

Second, using RF-to-RF cancellation techniques [23]. In this architecture, a copy of the transmitted RF signal (including the transmitter noise) is used to cancel-out the received self-interference signal in the RF-domain. Since the canceller signal inherently includes the transmitter phase noise, subtracting it from the incoming self-interference signal significantly mitigates the transmitter phase noise. The receiver phase noise effect is also mitigated by the means of reducing the self-interference power at the RF section.

Finally, sharing the local oscillator between the transmitter and the receiver sides. The analysis in [41] shows that, sharing the same local oscillator between the transmitter and the receiver sides in a full-duplex system achieves $\sim$25dB of phase noise suppression compared to the separate oscillator case. This architecture uses the fact that the phase noise process slightly changes within the self-interference channel delay spread, such that when the same transmitter phase noise process is used at the receiver side, the correlated parts of the phase noise and the delayed phase noise processes cancel each other. The main limitation of such architecture is that, in certain applications, when the transmitter and the receiver are not necessarily collocated (e.g. relay networks and femtocell applications), sharing the local oscillator is practically challenging. At such high RF frequency, if the local oscillator

signal is transferred over relatively large distances, it will suffer from huge attenuation, synchronization, and skew issues that significantly affect the overall system performance. As a conclusion (if possible), sharing the same local oscillator between the transmitter and the receiver sides is more efficient than using estimation-based techniques (e.g. the proposed techniques) to mitigate the phase noise effect. According to the results in [41], sharing the same local oscillator is shown to achieve ∼25dB of phase noise suppression, which is much better than the gain achieved using estimation-based techniques.

Now, the basic question is, could the proposed estimation and suppression techniques combined with these transceiver architectures to achieve more phase noise suppression? The answer is "theoretically" yes. With some modifications in the problem formulation and the used assumptions, one can develop other phase noise estimation techniques (using the same principal as in the proposed techniques) to achieve additional phase noise suppression. However, the achieved gain is expected to be significantly small (or even zero). The reason is that, when the phase noise is mitigated using such transceiver architectures, the phase noise (the signal to be estimated) is expected to be significantly lower than the signal-of-interest (the noise signal), which significantly decrease the estimation quality and thus the performance. Furthermore, when the phase noise is initially mitigated using such transceiver architectures, other noise components (e.g. transceiver nonlinearities) start to dominate the full-duplex system performance [23].

3.5 Conclusion

In this chapter, the problem of phase noise estimation and suppression in OFDM full-duplex systems is analytically and experimentally investigated. A frequency-domain and a lower complexity time-domain ICI suppression techniques are proposed. The feasibility of performing ICI suppression in full-duplex systems is investigated in terms of required complex-

ity and achieved gain. Both free-running and PLL based oscillators are considered. The results show that ICI suppression in OFDM based full-duplex systems is a very challenging and complexity consuming problem. More specifically, the results show that at a complexity of order $O(32^2)$ a maximum of 6dB more self-interference cancellation is achieved compared to the case where no ICI suppression in performed. This gain is reduced to 3dB when PLL based oscillator is used, mainly due to the flatter spectrum of the phase noise in PLL oscillators. Furthermore, the results show that this gain is conditioned; it can be achieved only at low SNR scenarios where the phase noise power is greater than the signal-of-interest power. However, at high SNR scenarios, ICI suppression does not add any gain. Accordingly, phase noise suppression remains a key challenge in full-duplex systems. Conventional phase noise estimation and suppression techniques are shown to be ineffective for mitigating the phase noise. Therefore, researchers have to find other solutions to suppress the phase noise. One novel solution is proposed in chapter 5 of this thesis.

Chapter 4

Nonlinear Distortion Suppression in Full-Duplex Systems

4.1 Introduction

In addition to the oscillator phase noise, the work in [23, 38] shows that transceiver nonlinearity is another major self-interference cancellation limiting factor in full-duplex systems. Along the same line of improving the self-interference cancellation capability by mitigating the RF impairments, transceiver nonlinearity is another impairment that needs to be mitigated.

In this chapter, we consider the problem of transceiver nonlinearity estimation and suppression in full-duplex systems. A digital-domain self-interference cancellation technique that accounts for the transmitter and receiver nonlinearity effect is proposed. The proposed technique increases the amount of cancellable self-interference power by suppressing the nonlinear distortion associated with the received self-interference signal.

Suppressing the nonlinear distortion requires the self-interference channel as well as nonlinearity coefficients to be estimated. However, due to the presence of the nonlinear distortion while the self-interference channel is being estimated, the channel estimation error will be distortion limited. To overcome this problem, we propose an iterative technique to jointly estimate the self-interference channel and the nonlinearity coefficients required to perform self-interference cancellation and distortion suppression. The performance of the proposed technique is numerically investigated and compared against the case of a linear full-duplex system. The results show that after three to four iterations, the nonlinear distortion is significantly suppressed such that the proposed technique achieves a performance that is less than 0.5dB off the performance of a linear full-duplex system.

4.2 Signal Model

Figure 4.1 illustrates a block diagram for a full-duplex OFDM transceiver, where the transmitter and the receiver are operating simultaneously over the same carrier frequency. At the transmitter side, the base-band signal is modulated using an OFDM modulator and then up-converted to the carrier frequency f_c, then amplified using a power amplifier. The oscillator at the transmitter side is assumed to have a random phase error represented by $\phi^t(t)$. At the receiver side, the amplitude of the received signal is properly adjusted using a low-noise amplifier (LNA). The signal is then down-converted from the carrier frequency to the base-band. The down-conversion mixer is assumed to have a random phase error represented by $\phi^r(t)$. The base-band signal is then quantized and converted to the frequency domain using Fourier transform.

In practical systems, the main sources of the system nonlinearity are the power amplifier at the transmitter side and the LNA at the receiver side. In this chapter, we consider both the power amplifier and LNA nonlinearities. Generally, for any nonlinear block, the output

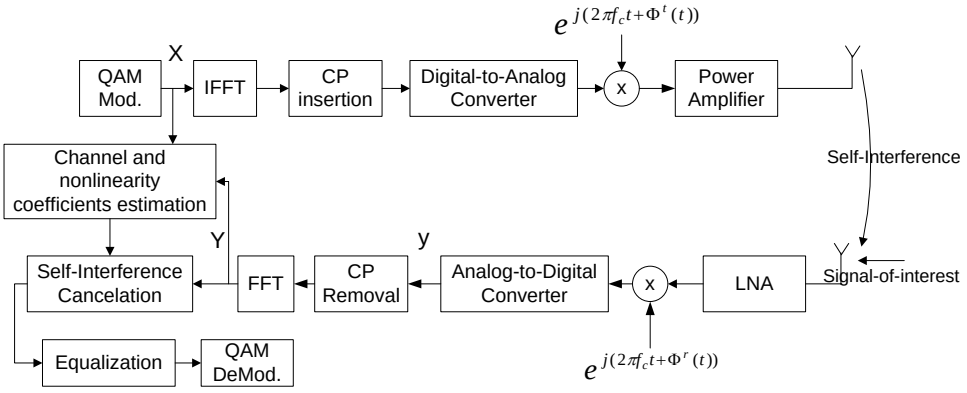

Figure 4.1: Block diagram of a full-duplex OFDM transceiver.

signal y can be written as a polynomial function of the input signal x as follows [48]

$$y = \sum_{m=0}^{M-1} \alpha_{m+1} x^{m+1}. \tag{4.1}$$

It can be shown that for practical wireless systems [48], only the odd orders of the polynomial contribute to the in-band distortion. Furthermore, only a limited number of orders contribute to the distortion and higher orders could be neglected. In practical systems, the nonlinearity is typically characterized by the third-order intercept point (IP3), which is defined as the point at which the power of the third harmonic is equal to the power of the first harmonic [49]. Accordingly, in this chapter we limit our analysis to the third-order nonlinearity where the output of any nonlinear block can be simplified as

$$y = x + \alpha_3 x^3, \tag{4.2}$$

assuming a unity linear gain (i.e. $\alpha_1 = 1$).

Following the block diagram in Figure 4.1 and using the assumption that $e^{j\phi} = 1 + j\phi$, $\phi \ll 1$, the base-band representation of the received signal at the ADC output can be written as

$$y_n = x_n^I * h_n^I + x_n^S * h_n^S + d_n + \phi_n + q_n + z_n, \tag{4.3}$$

where '$*$' denotes convolution process, n is the sample index, x^I, x^S are the transmitted self-interference and signal-of-interest respectively, h^I, h^S are the self-interference and signal-of-interest channels, d_n is the total transmitter and receiver nonlinear distortion, ϕ_n is the total phase noise, q_n is the ADC quantization noise, and z_n is the receiver Gaussian noise. The receiver Gaussian noise represents the noise inherent in the receiver circuits, and usually specified by the circuit noise figure, which is implicitly a function of the LNA gain [49].

Using the nonlinearity model in (4.2), and ignoring the nonlinearity associated with the signal of interest because of its small power compared to the self-interference signal, the total distortion d_n can be written as

$$d_n = \underbrace{\alpha_3^t \left(x_n^I\right)^3 * h_n^I}_{\text{Transmitter nonlinearity}} + \underbrace{\alpha_3^r \left(x_n^I * h_n^I + \alpha_3^t \left(x_n^I\right)^3 * h_n^I\right)^3}_{\text{Receiver nonlinearity}}, \tag{4.4}$$

where α_3^t, α_3^r are the transmitter and receiver third-order nonlinearity coefficients. Expanding (4.4) we get

$$\begin{aligned} d_n \;=\; & \alpha_3^t \left(x_n^I\right)^3 * h_n^I + \alpha_3^r \left(x_n^I * h_n^I\right)^3 \\ & + 3\alpha_3^t \alpha_3^r \left(x_n^I * h_n^I\right)^2 \left(\left(x_n^I\right)^3 * h_n^I\right) \\ & + 3\alpha_3^r \left(x_n^I * h_n^I\right) \left(\alpha_3^t \left(x_n^I\right)^3 * h_n^I\right)^2 \\ & + \left(\alpha_3^t \left(x_n^I\right)^3 * h_n^I\right)^3, \end{aligned} \tag{4.5}$$

According to (4.4), the main difference between the transmitter and receiver nonlinearity is that the transmitter nonlinearity affects the signal only, while the receiver nonlinearity affects both the signal and the wireless channel. Also, it has to be noted that, although only 3^{rd} order harmonics are considered at both transmitter and receiver sides, the coexistence of the transmitter and receiver nonlinearity introduces 5^{th}, 7^{th}, and 9^{th} order harmonics (the

3^{rd}, 4^{th}, and 5^{th} terms in (4.5)). The 7^{th} and 9^{th} order harmonics are much smaller than other harmonics, thus can be ignored. Accordingly, the distortion signal can be simplified as

$$\begin{aligned} d_n &= \alpha_3^t \left(x_n^I\right)^3 * h_n^I + \alpha_3^r \left(x_n^I * h_n^I\right)^3 \\ &\quad +3\alpha_3^t \alpha_3^r \left(x_n^I * h_n^I\right)^2 \left(\left(x_n^I\right)^3 * h_n^I\right). \end{aligned} \tag{4.6}$$

Finally, the received frequency-domain signal can be written as

$$Y_k = X_k^I H_k^I + X_k^S H_k^S + D_k + \Phi_k + Q_k + Z_k, \tag{4.7}$$

where k is the subcarrier index, and upper-case notation refers to the discrete Fourier transform (DFT) of the corresponding time-domain signals.

In order to show the significance of each noise term, the system is simulated using parameter values for practical wireless transceiver [51]. Figure 4.2 shows the strength of each noise source at different received self-interference signal strengths. The results show that the nonlinear distortion is the main limiting factor, followed by the phase noise, then the receiver Gaussian noise and quantization noise.

4.3 Self-interference Cancellation with Distortion Suppression

The results in Figure 4.2 imply that, eliminating the nonlinear distortion increases the self-interference mitigation capability. According to (4.6), distortion elimination requires the knowledge of the self-interference channel (h^I) as well as the nonlinearity coefficients (α_3^t, α_3^r). In the proposed technique, the self-interference channel is estimated using an orthogo-

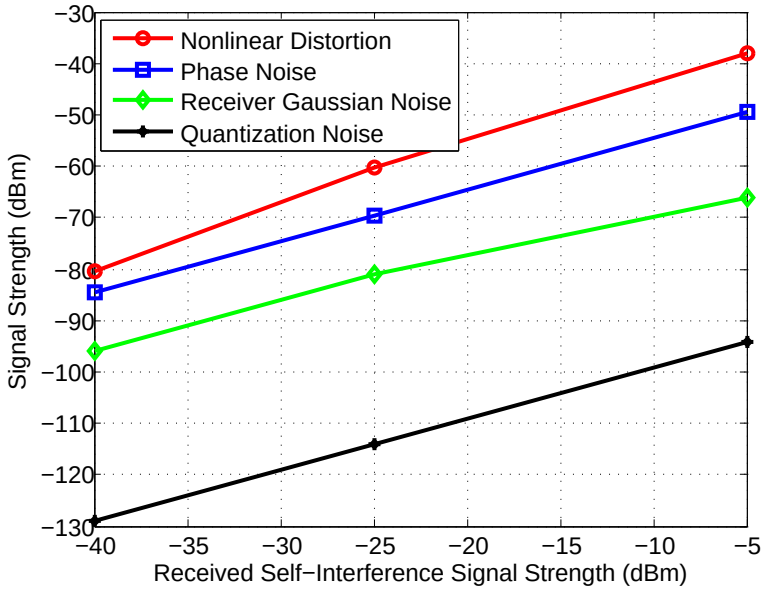

Figure 4.2: Noise powers at different received self-interference signal strengths for the transceiver in [51].

nal training sequence at the beginning of each transmission frame. The estimated channel along with the knowledge of the self-interference signal (x^I) are then used to estimate the nonlinearity coefficients.

The main problem is that due to the presence of the distortion signal at the training time, the channel estimation error will be limited by the distortion signal, which impacts the estimation accuracy and thus the overall cancellation performance. To overcome this problem, we propose an iterative technique to jointly estimate the self-interference channel and the nonlinearity coefficients. The proposed technique consists of four main steps: (i) an initial estimate for the self-interference channel ($\hat{H}_k^I$) is obtained, (ii) the estimated channel is used to estimate the nonlinearity coefficients (α_3^t, α_3^r), (iii) the estimated coefficients are used to construct an estimate for the distortion signal $\hat{D}_k$, and (iv) the estimated distortion signal $\hat{D}_k$ is subtracted from the received signal. The four steps are then repeated for a number of iterations. An illustrative block diagram for the proposed iterative technique is shown in Figure 4.3.

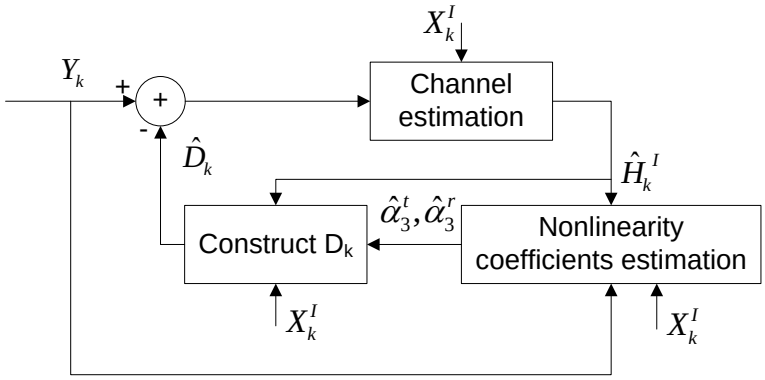

Figure 4.3: Block diagram for the iterative channel and nonlinearity coefficients estimation technique.

After channel and nonlinearity coefficients estimation, the self-interference signal ($X_k^I \hat{H}_k^I$) and the distortion signal ($\hat{D}_k^I$) are subtracted from the received signal at each data OFDM symbol to construct the interference-free signal. In the following subsections, detailed analysis for the channel and nonlinearity coefficients estimation techniques is presented.

4.3.1 Channel estimation

It has to be noted that for the iterative technique in Figure 4.3 to work properly, the mean square error of the channel estimation should be less than the distortion power, otherwise the performance will be limited by the channel estimation error and there will be no gain achieved by the iterative technique. The DFT based channel estimation technique proposed in [70] is one of the low complexity channel estimation techniques that achieve relatively small mean square error. In this technique, first, an estimate for the channel impulse response (CIR) is obtained using the least square (LS) estimator as follows

$$\hat{h}_n^{LS} = \mathsf{IDFT}\left\{\frac{Y_k}{X_k}\right\}. \tag{4.8}$$

Then, by leveraging the fact that the channel information is contained in the first L samples of the CIR, a better estimate for the channel is obtained by taking the first L samples of $\hat{h}_n^{LS}$ while forcing other samples to zero as follows

$$\hat{h}_n = \begin{cases} \hat{h}_n^{LS} & , \ 0 \leq n \leq L-1, \\ 0 & , \ \text{otherwise}, \end{cases} \tag{4.9}$$

then

$$\hat{H}_k = \mathsf{DFT}\left\{\hat{h}_n\right\}. \tag{4.10}$$

By doing this, the estimation error is reduced by a factor of $\frac{L}{N}$, where N is the number of subcarriers per OFDM symbol. The key challenge in such technique is the choice of L. Since the cyclic prefix in practical systems is designed to be larger than the channel length, a good choice for L is to be equal to the cyclic prefix length.

4.3.2 Nonlinearity coefficients estimation

At the self-interference training symbol, the signal-of-interest is not present. Therefore, Equation (4.3) can be written as

$$y_n = x_n^I * h_n^I + d_n + \phi_n + q_n + z_n. \tag{4.11}$$

Since the transmitted self-interference signal x_n^I and the self-interference channel $\hat{h}_n$ are now known, the problem in (4.11) can be recognized as a linear estimation problem with the unknown coefficients $[\alpha_3^t, \alpha_3^r, 3\alpha_3^t\alpha_3^r]$.

Rewriting (4.11) in a matrix form we get

$$\begin{bmatrix} \bar{y}_0 \\ \bar{y}_1 \\ : \\ \bar{y}_N \end{bmatrix} = \underbrace{\begin{bmatrix} A_1 & B_1 & C_1 \\ A_2 & B_2 & C_2 \\ : & : & : \\ A_N & B_N & C_N \end{bmatrix}}_{W} \begin{bmatrix} \alpha_3^t \\ \alpha_3^r \\ 3\alpha_3^t\alpha_3^r \end{bmatrix} + \begin{bmatrix} \eta_0 \\ \eta_1 \\ : \\ \eta_N \end{bmatrix}, \tag{4.12}$$

where $\bar{y}_n = y_n - x_n^I * \hat{h}_n^I$, $\eta_n = \phi_n + q_n + z_n$, $A_n = (x_n^I)^3 * \hat{h}_n^I$, $B_n = (x_n^I * \hat{h}_n^I)^3$, and $C_n = (x_n^I * \hat{h}_n^I)^2((x_n^I)^3 * \hat{h}_n^I)$. Rewrite (4.12) in a compact form we get

$$\bar{y} = W\alpha + \eta. \tag{4.13}$$

An estimate for the nonlinearity coefficients α can be found using the LS estimator as

$$\hat{\alpha} = W^{-1}\bar{y}. \tag{4.14}$$

The main problem with the LS estimator is that the matrix W is often ill-conditioned, thus, the inversion of the matrix will incur numerical errors. To overcome this problem, we propose a successive one-by-one estimation technique to avoid matrix inversion. The proposed technique is similar to the successive interference cancellation technique where one coefficient (e.g α_3^t) is estimated assuming that other two are equal to zero. The estimated coefficient is multiplied by its corresponding signal and subtracted from the received signal, then the next coefficient is estimated. Since the third coefficient ($3\alpha_3^t\alpha_3^r$) is function of the first two, estimating α_3^t, and α_3^r is sufficient to get the three coefficients. Furthermore, for better estimation accuracy iterative techniques could be used.

A common problem with any successive technique is the determination of the coefficient to start with. If there is prior knowledge about the relative strength of the transmitter and

receiver nonlinearity, the optimum choice is to start with the coefficient that corresponds to the stronger nonlinearity. For example, if the transmitter nonlinearity is stronger than receiver nonlinearity, the algorithm should start with α_3^t and vise versa. However, if there is no prior knowledge, wrong starting point might result in performance degradation. In order to overcome this problem, the proposed algorithm selects the start coefficient based on the residual distortion power. In other words, the coefficient that results in smaller residual distortion power will be selected as the start coefficient. The iterative successive nonlinearity coefficients estimation technique is summarized in algorithm 1. The equations in algorithm 1 assume that α_3^t is selected as the start coefficient. Finally, it has to be mentioned that, to compute A_n, B_n, and C_n up-sampling is required in order to prevent aliasing

Algorithm 1 Successive nonlinearity coefficients estimation

1: set $\bar{y}_n = y_n - x_n^I * \hat{h}_n^I$.
2: Determine the start coefficient based on the residual distortion power
3: **for** certain number of iterations **do**
4: get $\hat{\alpha}_3^t = \frac{1}{N}\sum_{n=0}^{N-1} \frac{\bar{y}_n}{A_n}$.
5: set $\bar{y}_n = y_n - x_n^I * \hat{h}_n^I - \hat{\alpha}_3^t A_n$.
6: get $\hat{\alpha}_3^r = \frac{1}{N}\sum_{n=0}^{N-1} \frac{\bar{y}_n}{B_n}$.
7: set $\bar{y}_n = y_n - x_n^I * \hat{h}_n^I - \hat{\alpha}_3^r B_n - 3\hat{\alpha}_3^r \hat{\alpha}_3^t C_n$.
8: **end for**

4.4 Simulation Results and Discussions

In this section, the performance of the proposed cancellation scheme is numerically investigated under different operating conditions. The simulation setup is chosen as in WiFi 802.11n standard [43]. The indoor TGn channel model [54] is used to model the self-interference and signal-of-interest channels. The self-interference and signal-of-interest channel's Rician factors are set to 30dB and 3dB respectively. Two performance criteria are chosen: the achievable rate, and the residual interference plus distortion plus noise (RIDN) power. The

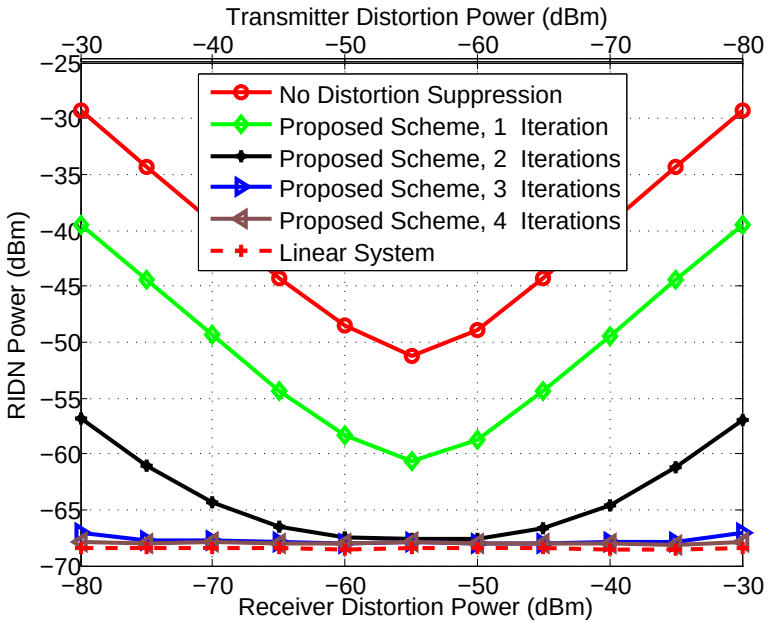

Figure 4.4: RIDN power at different distortion levels.

RIDN is calculated as

$$\mathsf{RIDN} = X_k^I \left(H_k^I - \hat{H}_k^I\right) + \left(D_k - \hat{D}_k\right) + \Phi_k + Q_k + Z_k. \tag{4.15}$$

The proposed algorithm is compared to two cases; first, the case of linear full-duplex system (the best case) where $D_k = 0$. Second, the case of nonlinear full-duplex system and no distortion removal is performed (as assumed in most current cancellation schemes).

In the first simulation scenario, we investigate the performance of the proposed scheme under different transmitter and receiver nonlinearity distortion levels. The target is to evaluate the performance of the proposed scheme under all distortion scenarios: (i) transmitter distortion is greater than receiver distortion, (ii) receiver distortion is greater than transmitter distortion, and (iii) transmitter and receiver distortion are comparable. Figure 4.4 shows the RIDN power at different transmitter and receiver distortion levels and phase noise power of -70dBm. The top and bottom x-axes show the transmitter and receiver distortion values respectively.

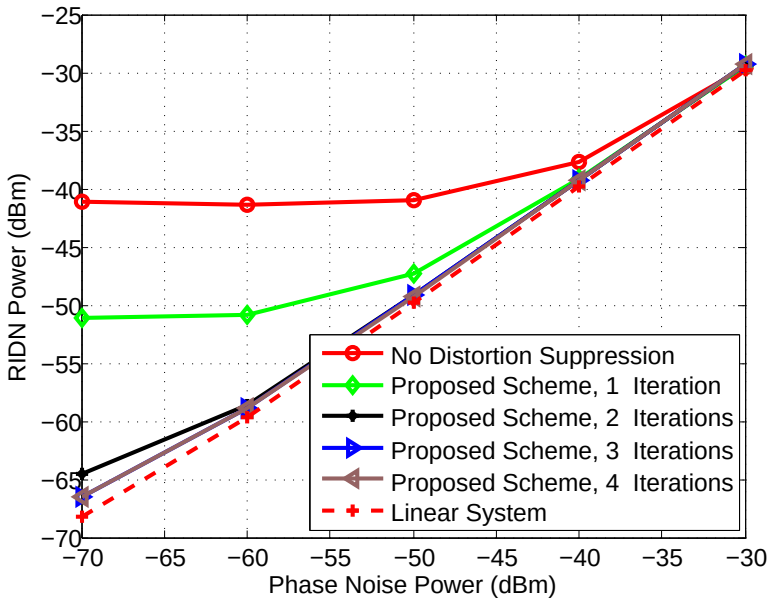

Figure 4.5: RIDN power at different phase noise levels.

The conclusions from Figure 4.4 are multifold: first, regardless of the distortion level, the proposed scheme is able to suppress the distortion to the level of the next bottleneck (e.g. phase noise in this case) and achieve performance that is highly close (less than 0.5dB difference) to the performance of a linear receiver. Second, when the difference between the distortion level and the level of the next bottleneck increases, the number of iterations required to suppress the distortion signal increases. The reason is that each iteration has a limited suppression gain controlled by the channel estimation error, thus more suppression require more iterations. Finally, comparing the left side of Figure 4.4 to the right side we note that, because the nonlinearity coefficients estimation algorithm adaptively selects the coefficient to start with, the proposed scheme performs the same way whether the transmitter distortion dominates receiver distortion or vise versa.

In the previous simulation scenario, the system is simulated in the case when the nonlinear distortion dominates other noise components. For complete performance evaluation, the performance is investigated under different phase noise power levels in order to inves-

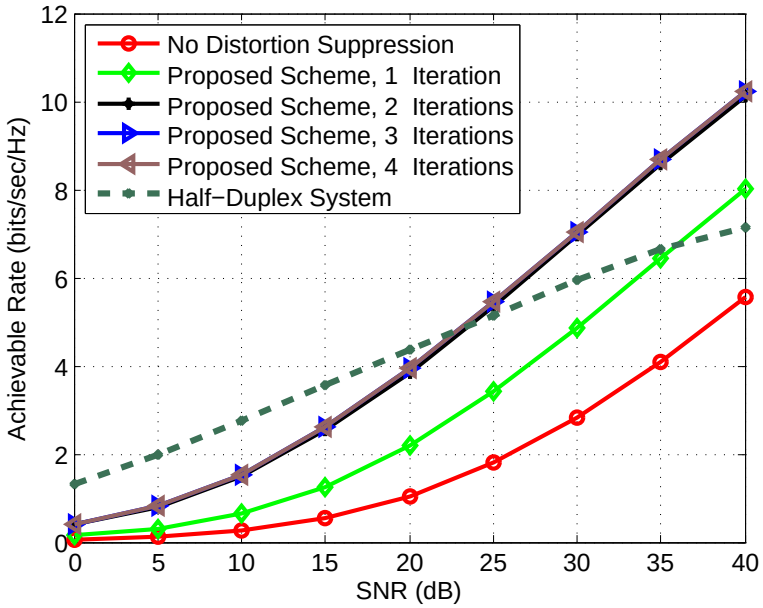

Figure 4.6: Full-duplex and half-duplex achievable rates at received self-interference signal strength = −30dBm, normalized transmitter and receiver distortion power = −45dB, and normalized phase noise power = −60dB.

tigate the case when the nonlinear distortion is not the limiting factor. Figure 4.5 shows the RIDN power at different phase noise levels with a −45dBm transmitter and receiver distortion power. The results show that when other noise component dominates nonlinear distortion, the proposed technique achieves the same performance as the case where no distortion suppression is performed. In other words, the proposed scheme does not degrade the performance at low distortion levels.

In the following simulation scenario, the overall full-duplex system performance is investigated and compared to the corresponding half-duplex system performance. Figure 4.6 shows the full-duplex and half-duplex system's achievable rate at different half-duplex signal-to-noise ratios (SNR). Since half-duplex system performance is usually limited by the receiver Gaussian noise, the SNR is defined as the received signal-of-interest power divided by the receiver Gaussian noise power. The parameters for this simulation scenario are shown in the figure caption. The results show that when the nonlinear distortion dominates other noise

components, performing distortion suppression using the proposed scheme significantly improves the full-duplex system's spectral efficiency and allows full-duplex systems to achieve a better rate than half-duplex systems at high SNR scenarios.

4.5 Conclusion

In this chapter, a digital-domain self-interference cancellation technique for full-duplex OFDM systems is proposed. The proposed technique increases the amount of cancellable self-interference power by suppressing the distortion caused by the transmitter and receiver nonlinearity. The proposed technique is able to suppress the nonlinear distortion to the level of the next significant noise component, and achieve performance that is less than 0.5dB off the performance of a linear full-duplex system.

Chapter 5

All-Digital Self-interference Cancellation Technique for Full-duplex Systems

5.1 Introduction

The analysis in chapter 2 shows that the cancellation capability of digital self-interference cancellation techniques is very limited, mainly due to the transceiver RF impairments. In chapter 3, and 4 we investigated the possibility of mitigating the two major limiting factors in full-duplex systems (i.e. phase noise and nonlinear distortion). The results in chapter 4 show that transceiver nonlinearity is manageable and could be significantly mitigated using nonlinearity estimation and suppression techniques. However, the analysis in chapter 3 shows that phase noise estimation and suppression techniques does not improve the cancellation capability of conventional digital cancellation techniques in practical operating conditions. Accordingly, improving the self-interference cancellation capability requires

other phase noise mitigation solutions to be investigated. In this chapter, we propose a novel digital self-interference cancellation technique that eliminates all transmitter impairments, and significantly mitigates the receiver phase noise and nonlinearity effects. With the proposed technique, digital self-interference cancellation is no longer limited by the transceiver phase noise or nonlinearities.

Recently, several full-duplex transceiver architectures are proposed to cancel out the impairments associated with the self-interference signal [20, 23]. The main idea in such architectures is to obtain a copy of the transmitted RF self-interference signal including all impairments and subtract it from the received signal in the RF domain. Since the obtained copy includes all transmitter impairments, the subtraction process is supposed to eliminate both the self-interference signal and the noise associated with it. In [20], a copy of the transmitted RF self-interference signal is passed through a variable attenuator and phase shifter then subtracted from the received signal in the RF domain. Since only one variable attenuator and phase shifter are used, these techniques will only mitigate the main component of the self-interference signal without mitigating the self-interference reflections. This issue has been handled in [23], where a multi-tap RF Finite Impulse Response (FIR) filter is used instead of the single attenuator. In this case, both main and reflected self-interference components (including the associated noise) are significantly mitigated at the receiver input. However, the size and power consumption of the RF FIR filter limits the applicability of such techniques.

In contrast with RF and analog cancellation techniques, we propose a novel all-digital self-interference cancellation technique based on a new full-duplex transceiver architecture that significantly mitigates transmitter and receiver impairments. In the proposed technique (shown in figure 5.1), an auxiliary receiver chain is used to obtain a digital-domain copy of the transmitted RF self-interference signal, which is then used to cancel out the self-interference signal and the associated transmitter impairments in the digital-domain. The auxiliary receiver chain has identical components as the ordinary receiver chain to emulate the effect

of the ordinary receiver chain on the received signal. Furthermore, in order to alleviate the receiver phase noise effect, the auxiliary and ordinary receiver chains share a common oscillator. The proposed technique is shown to significantly mitigate the transmitter and receiver impairments without the necessity for highly complex RF cancellation techniques. The main advantage of the proposed technique is that all signal processing is performed in the digital-domain, which significantly reduces the implementation complexity.

In this chapter, first, the performance of the proposed techniques is analytically and numerically investigated using a detailed full-duplex signal model that includes all major transmitter and receiver impairments. More specifically, transmitter and receiver nonlinearities, transmitter and receiver phase noise, receiver Gaussian noise, receiver quantization noise, and channel estimation errors are accounted for. Second, a thorough analytical and numerical analysis for the effect of each one of the transceiver impairments on the cancellation capability of the proposed technique is presented. Third, the performance and design tradeoffs involved with the proposed technique are also investigated. The analyses show that the proposed technique significantly mitigates the transceiver phase noise and nonlinearity effects, such that they are no longer the main performance limiting factors. Finally, the overall full-duplex system performance using a combination of the proposed digital cancellation technique and the practical passive suppression techniques proposed in [33] is numerically investigated.

5.2 System Model

In this section, the system model of the proposed full-duplex transceiver architecture is described in details. Figure 5.1 shows a detailed block diagram for the proposed digital self-interference cancellation technique based on a new full-duplex transceiver architecture. The transceiver consists of the ordinary transmit and receive chains in addition to one auxiliary

receiver chain used for self-interference cancellation. At the transmitter side, the information signal X is OFDM modulated, then up-converted to the RF frequency. The up-converted signal is then filtered, amplified, and transmitted through the transmit antenna. A fraction of the amplified signal is fed-back as input to the auxiliary receiver chain. The signal power at the auxiliary receiver input is controlled through the power splitter; therefore, the Low Noise Amplifier (LNA) could be omitted from the auxiliary receiver chain. The feed-back and ordinary-received signals are down-converted to base-band through the auxiliary and ordinary receiver chains respectively. The auxiliary and ordinary receiver chains are identical and share the same Phase Locked Loop (PLL). The channel transfer function H^{aux} represents the wired channel from the Power Amplifier (PA) output to the auxiliary receiver. While the channel transfer function H^{ord} represents the self-interference wireless channel.

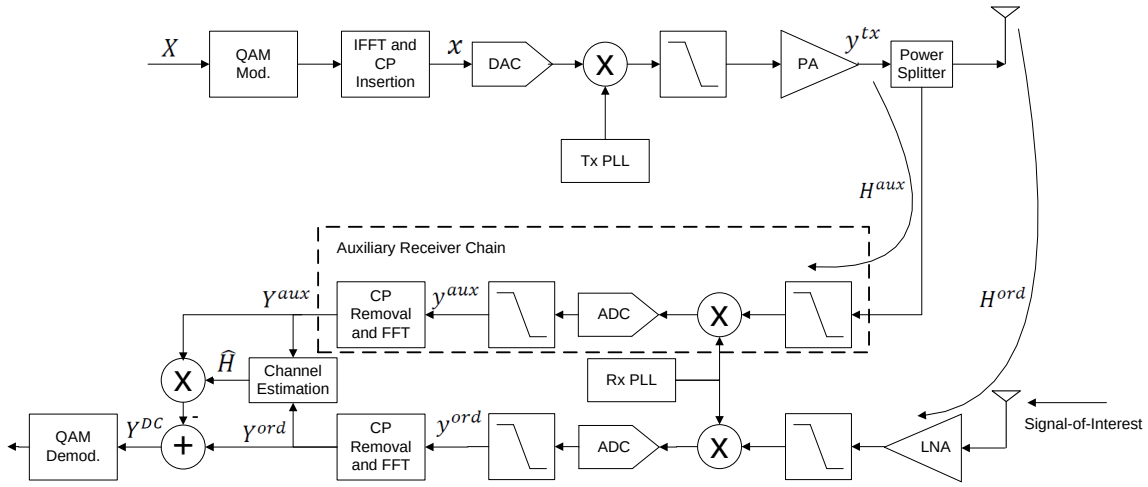

Figure 5.1: Detailed block diagram for the proposed digital self-interference cancellation technique.

The output of the auxiliary and the ordinary receiver chains are fed to a channel estimation block to obtain an estimate for the ratio between the ordinary and auxiliary channels (H^{ord}/H^{aux}). The channel estimation process is performed using time-orthogonal training sequences transmitted at the beginning of each data frame. The estimated channel is then multiplied with the auxiliary receiver output, and the multiplication output is subtracted

from the received signal to obtain an interference-free signal.

In this chapter, the main transmitter and receiver impairments are considered. More specifically, transmitter and receiver phase noise, transmitter and receiver nonlinearities, Analog-to-Digital Converter (ADC) quantization noise, and receiver Gaussian noise. Since the feed-back signal is obtained from the PA output which contains a copy of the transmitter impairments, the proposed architecture can significantly mitigate all transmitter impairments. In addition, the receiver phase noise effect is mitigated by means of sharing the same PLL between the auxiliary and ordinary receiver chains. In order to investigate the performance of the proposed technique, we first present a signal model with detailed modeling for each one of the transceiver impairments.

In the presence of the transmitter phase noise ϕ^{tx} and the PA nonlinear distortion signal d^{tx}, the transmitted signal at the PA output can be written as

$$y^{tx}(t) = x(t)e^{j\left(2\pi f_c t + \phi^{tx}(t)\right)} + d^{tx}(t), \tag{5.1}$$

where x is the transmitter base-band signal, d^{tx} is the transmitter nonlinear distortion due to the PA, and f_c is the carrier frequency. At the auxiliary receiver output, the digital base-band signal y^{aux} can be written as

$$y_n^{aux} = \left(y_n^{tx} * h_n^{aux}\right) e^{j\phi_n^{rx}} + q_n^{aux} + z_n^{aux}, \tag{5.2}$$

where $*$ denotes convolution process, n is the sample index, y_n^{tx} is the digital base-band representation of $y^{tx}(t)$, h^{aux} is the wired channel from the PA output to the auxiliary receiver input, ϕ^{rx} is the receiver phase noise process, q^{aux} is the auxiliary receiver ADC quantization noise, and z^{aux} is the auxiliary receiver Gaussian noise. Similarly, the digital

base-band signal y^{ord} at the ordinary receiver output can be written as

$$y_n^{ord} = \left(y_n^{tx} * h_n^{ord}\right) e^{j\phi_n^{rx}} + d_n^{rx} + q_n^{ord} + z_n^{ord} + s_n^{soi}, \tag{5.3}$$

where superscript ord refers to the ordinary receiver chain signals, d^{rx} is the receiver nonlinear distortion due to the LNA, and s^{soi} is the received signal-of-interest (including the signal-of-interest channel and all impairments). After digital self-interference cancellation, the interference-free signal Y^{DC} can be written as

$$Y_k^{DC} = Y_k^{ord} - Y_k^{aux}\hat{H}_k, \tag{5.4}$$

where uppercase letters denote the frequency domain representation of the corresponding signals, k is the subcarrier index, and $\hat{H}$ is an estimate for the ratio between the ordinary and auxiliary channels (H^{ord}/H^{aux}) calculated in the Least Square (LS) form as

$$\hat{H}_k = \frac{Y_k^{ord}}{Y_k^{aux}}. \tag{5.5}$$

For a complete signal model, a detailed description for the impairments and channel modeling is presented in the following subsections.

5.2.1 Transceiver nonlinearities

As described in chapter 4, for any nonlinear block, the output signal y can be written as a polynomial function of the input signal g as follows

$$y(t) = \sum_{m=1}^{M} \alpha_m g(t)^m. \tag{5.6}$$

With simple analysis, it can be easily shown that only the odd orders of the polynomial contribute to the in-band distortion [48]. Accordingly, equation (5.6) can be further simplified and written is the digital base-band domain as

$$y_n = \sum_{m=1,m\ is\ odd}^{M} \alpha_m g_n \left|g_n\right|^{m-1}, \tag{5.7}$$

where g_n and y_n are the digital base-band representation of the input and output of the nonlinear block. For the PA nonlinearity, the digital base-band representation of the input signal is $g_n = x_n e^{j\phi_n^{tx}}$. While, for the LNA nonlinearity, the LNA input is the transmitted signal after going through the wireless channel, i.e. $g_n = (y_n^{tx} * h_n^{ord})$.

5.2.2 Transceiver phase noise

A detailed description of the oscillator phase noise modeling for both free-running and PLL-based oscillators is presented in chapter 3 (section 3.2). Since PLL-based oscillators are commonly used in wireless systems, the numerical analysis in this chapter is performed using PLL-based oscillators.

5.2.3 Gaussian and quantization noise

A detailed description of the quantization and receiver Gaussian noise components is presented in chapter 2 (section 2.2). It has to be noted that, although the auxiliary and the ordinary receiver chains have identical components, the Gaussian and quantization noises are independent for the two receiver chains.

5.2.4 Wireless channel modeling

Generally, in full-duplex systems, the self-interference channel consists of two main components: The Line-of-Sight (LOS) component due to the direct link between the transmit and receive antennas, and the non-LOS component due to the signal reflections. Accordingly, the first tap of the self-interference channel could be modeled as Rician fading with Rician factor k and the remaining channel taps are modeled as Rayleigh fading with variance k. The Rician factor k represents the power ratio between the LOS and the reflective components of the channel. The experimental characterization presented in [33] show that for typical indoor environments with antenna separation of 35-50cm, the self-interference channel Rician factor is approximately 20-25dB.

The experimental results in [33] also show that the self-interference channel Rician factor is inversely proportional to the achieved passive suppression amount. For instance, using omni-directional antenna with antenna separation of 50cm could achieve up to 28dB passive suppression, and the self-interference channel Rician factor in this case is ∼25dB. On the hand, using directional antennas could achieve up to 45dB of passive suppression, however, the self-interference channel Rician factor decreases to ∼0dB. The main reason for this inverse relation is that passive suppression techniques tend to significantly mitigate the LOS component and slightly mitigates the reflections.

In this chapter, the analyses are based on the two-antenna transceiver architecture shown in figure 1. However, another architecture where the transmit and receive antennas are replaced by a circulator and a single antenna could be used [23]. In this case the achieved passive suppression will be limited by the circulator coupling (typically 20dB). On the other hand, the self-interference channel for the single-antenna architecture is expected to have larger Rician factor, mainly due to the fact that the reflections have to make a roundtrip in order to be reflected back to the same antenna. The impact of the passive suppression amount

and channel Rician factor on the cancellation performance is discussed in Section 5.3.

5.3 Self-interference Cancellation Analysis

The main idea of the proposed cancellation technique is to obtain a copy of the transmitted self-interference signal including all transmitter impairments, and use this copy for digital-domain self-interference cancellation at the receiver side. Hypothetically speaking, if both auxiliary and ordinary receiver chains are impairment-free, the proposed architecture should be able to totally eliminate both the self-interference signal and the transmitter impairments. However, due to the receiver impairments and the channel estimation errors, perfect self-interference cancellation is not possible. In fact, receiver impairments and channel estimation errors introduce certain limitations on the self-interference cancellation capability. In order to understand these limitations, we analytically and numerically investigate the impact of the receiver impairments and channel estimation errors on the self-interference cancellation capability of the proposed technique.

For a clear understanding of the impairments effect and the involved tradeoffs, each impairment is analyzed individually (i.e. the system is analyzed in the presence of one receiver impairment at a time). At the end, the overall performance in the presence of all impairments is investigated. In each analysis, all transmitter impairments are considered; only the receiver impairments are considered individually. During the analysis of the individual impairments, the auxiliary and ordinary channel transfer functions (H^{aux}, H^{ord}) are assumed to be perfectly known. The effect of channel estimation errors is studied in a separate subsection. The numerical analyses are based on a 20MHz OFDM-based system with 64 subcarriers per OFDM symbols as in IEEE802.11 systems [43]. The carrier frequency is set to 2.4GHz.

5.3.1 Impact of Gaussian and Quantization Noise

In the presence of only Gaussian and quantization noise, the auxiliary and ordinary receiver outputs (Equation (5.2) and (5.3)) can be rewritten as

$$y_n^{aux} = y_n^{tx} * h_n^{aux} + q_n^{aux} + z_n^{aux}, \tag{5.8}$$

$$y_n^{ord} = y_n^{tx} * h_n^{ord} + q_n^{ord} + z_n^{ord} + s_n^{soi}, \tag{5.9}$$

After self-interference cancellation, the frequency domain representation of the interference-free signal Y^{DC} can be written as

$$Y_k^{DC} = Y_k^{ord} - \frac{H_k^{ord}}{H_k^{aux}} Y_k^{aux} = S_k^{soi} + Q_k^{ord} + Z_k^{ord} - \bar{Q}_k^{aux} - \bar{Z}_k^{aux}, \tag{5.10}$$

where $\bar{Q}^{aux}$ and $\bar{Z}^{aux}$ are the modified auxiliary quantization and Gaussian noise after multiplication with the channel transfer function H^{ord}/H^{aux}.

Equation (5.10) sets the first performance limiting factor that results due to the Gaussian and quantization noise. In terms of power levels, since the noise terms are not correlated, the total noise power is calculated as the summation of the power of the four noise terms in (5.10). As shown in (2.3) the quantization noise power is inversely proportional to the LNA power gain and number of ADC bits. Therefore, one can easily get rid of the quantization noise limitation by increasing the number of ADC bits. For instance, using 14-bits ADC will result is quantization noise power of ~ -90dBm at 0dB LNA gain. However, increasing the number of ADC bits slightly increases the hardware complexity.

Typically, Gaussian noise dominates quantization noise, especially at high input power levels.

Equation (2.2) shows that the Gaussian noise power is a function of the input signal power level, and the noise figure of individual receiver components. At low input signal power levels (i.e. high LNA gain) the Gaussian noise power is dominated by the LNA noise figure which is designed to be relatively small. However, at high input signal power levels, the Gaussian noise power is dominated by the noise figure of the components following the LNA, which typically have relatively high noise figure. As a practical example, the NI5791 transceiver datasheet [71] show that the receiver Gaussian noise power is -163, and -145dBm/Hz at signal power levels of -25, and -5dBm respectively. This is equivalent to total noise power of -90 and -72dBm in a 20MHz bandwidth. Accordingly, decreasing the Gaussian noise effect requires low input signal power levels, which could be achieved through good passive self-interference suppression, or by decreasing the transmit power.

For more clarification, a numerical analysis is performed to investigate the impact of the Gaussian and quantization noise on the cancellation performance at different scenarios. In this analysis, the system is simulated using practical receiver parameters from the NI5791 transceiver datasheet [71]. More specifically, the number of ADC bits is set to 14bits, the receiver Gaussian noise is -90dBm for LNA gains $\geq$25dB, and -72dBm at 5dB LNA gain. Figure 5.2 shows the quantization and Gaussian noise power at different receiver input signal power levels. The half-duplex system noise floor is shown as a comparison reference. In half-duplex systems, since the input signal power is typically small, the noise floor is dominated by the LNA noise figure (-90dBm is this example). The results show that for input power levels ≤ -30dBm, the proposed full-duplex system has the same noise floor as compared to half-duplex systems. However, at high received signal power levels, the full-duplex system's noise floor linearly increases with the received signal power, mainly due to the decrease of the LNA gain, which increases the overall receiver noise figure as shown in (2.2).

Figure 3 show that at high received signal power levels, Gaussian noise is a considerable performance limiting factor. The Gaussian noise effect could be reduced by using either

good passive suppression techniques as in [33], or using the Balun RF cancellation proposed in [20]. In the Balun cancellation technique, part of the self-interference signal is mitigated before the signal goes through the LNA, which reduces the overall receiver noise figure and thus the Gaussian noise power.

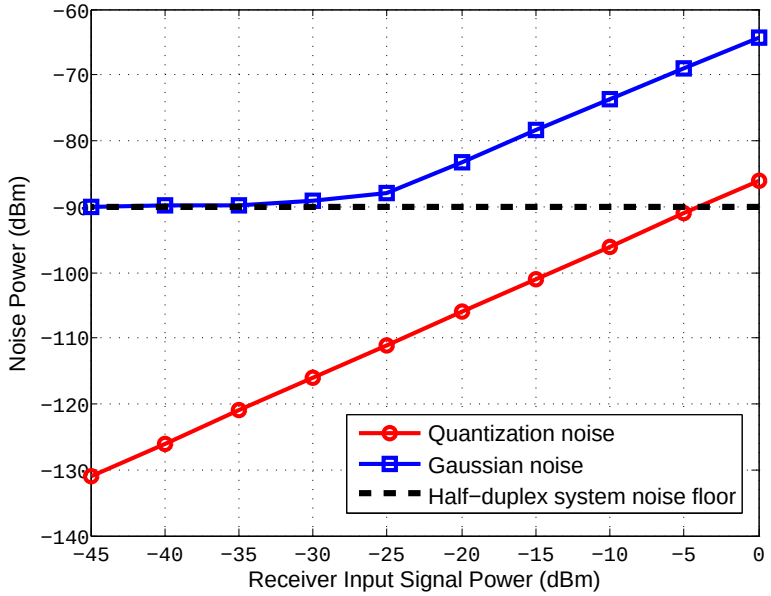

Figure 5.2: Quantization and Gaussian noise power at different receiver input signal power levels.

5.3.2 Impact of Receiver Phase Noise

In this analysis, the receiver is assumed to have only the phase noise impairment. Furthermore, the auxiliary and ordinary receiver chains are sharing the same PLL, and thus have the same phase noise signal. In the presence of only receiver phase noise, the auxiliary and ordinary receiver outputs (Equation (5.2) and (5.3)) can be rewritten as

$$y_n^{aux} = \left(y_n^{tx} * h_n^{aux}\right) e^{j\phi_n^{rx}}, \tag{5.11}$$

$$y_n^{ord} = \left(y_n^{tx} * h_n^{ord}\right) e^{j\phi_n^{rx}} + s_n^{soi}, \tag{5.12}$$

By performing Discrete Fourier Transform (DFT), the frequency domain representation of (5.11) and (5.12) can be written as

$$Y_k^{aux} = \sum_{l=0}^{N-1} Y_l^{tx} H_l^{aux} J_{k-l}^{rx}, \tag{5.13}$$

$$Y_k^{ord} = \sum_{l=0}^{N-1} Y_l^{tx} H_l^{ord} J_{k-l}^{rx} + S_k^{soi}, \tag{5.14}$$

where N is the number of subcarriers per OFDM symbol, and J^{rx} is the DFT coefficients of the phase noise process $e^{j\phi^{rx}}$ calculated as

$$J_k^{rx} = \sum_{n=0}^{N-1} e^{j\phi_n^{rx}} e^{-j2\pi\frac{nk}{N}}. \tag{5.15}$$

Since H^{aux} is a wired channel, it can be assumed that H^{aux} has a frequency flat response. Accordingly, equation (5.13) can be simplified as

$$Y_k^{aux} = H_k^{aux} \sum_{l=0}^{N-1} Y_l^{tx} J_{k-l}^{rx}. \tag{5.16}$$

After self-interference cancellation, the interference-free signal Y^{DC} can be written as

$$\begin{aligned} Y_k^{DC} &= Y_k^{ord} - \frac{H_k^{ord}}{H_k^{aux}} Y_k^{aux} = S_k^{soi} + \sum_{l=0}^{N-1} Y_l^{tx} H_l^{ord} J_{k-l}^{rx} - H_k^{ord} \sum_{l=0}^{N-1} Y_l^{tx} J_{k-l}^{rx} \\ &= S_k^{soi} + \sum_{l=0, l\neq k}^{N-1} \left(H_l^{ord} - H_k^{ord}\right) Y_l^{tx} J_{k-l}^{rx}. \end{aligned} \tag{5.17}$$

The second term in the right hand side of (5.17) represents the residual self-interference signal due to the receiver phase noise effect.

According to (5.17), the residual self-interference (RSI) power P_{RSI} can be calculated as

$$\begin{aligned} P_{RSI} &= E\left[\left|\sum_{l=0,l\neq k}^{N-1}\left(H_l^{ord}-H_k^{ord}\right)Y_l^{tx}J_{k-l}^{rx}\right|^2\right] \\ &= \sum_{l=0,l\neq k}^{N-1}E\left[\left|\left(H_l^{ord}-H_k^{ord}\right)\right|^2\right]E\left[\left|Y_l^{tx}\right|^2\right]E\left[\left|J_{k-l}^{rx}\right|^2\right] \\ &= P^{tx}\sum_{l=0,l\neq k}^{N-1}E\left[\left|\left(H_l^{ord}-H_k^{ord}\right)\right|^2\right]E\left[\left|J_{k-l}^{rx}\right|^2\right], \end{aligned} \tag{5.18}$$

where $E\left[\left|Y^{tx}\right|^2\right]=P^{tx}$ is the transmit power. Decomposing H^{ord} into LOS and non-LOS components where $H_k^{ord}=H^{ord,los}+H_k^{ord,nlos}$ equation (5.18) can be further simplified as

$$P_{RSI}=P^{tx}\sum_{l=0,l\neq k}^{N-1}E\left[\left|\left(H_l^{ord,nlos}-H_k^{ord,nlos}\right)\right|^2\right]E\left[\left|J_{k-l}^{rx}\right|^2\right]. \tag{5.19}$$

An upper bound for the residual self-interference power is obtained when $H_k^{ord,nlos}$ and $H_l^{ord,nlos}$ are uncorrelated for all $k\neq l$. In this case, the upper bound of the residual self-interference power in (5.19) is calculated as

$$P_{RSI}^{U}=P^{tx}\sum_{l=0,l\neq k}^{N-1}\left(E\left[\left|H_l^{ord,nlos}\right|^2\right]+E\left[\left|H_k^{ord,nlos}\right|^2\right]\right)E\left[\left|J_{k-l}^{rx}\right|^2\right]=2P^{tx}P^{nlos}P^{PN}. \tag{5.20}$$

where P^{nlos} is the power of the non-LOS component of the self-interference channel, P^{PN} is the total in-band phase noise power, and the factor of 2 is due to the subtraction of uncorrelated random variables. On the other hand, it is obvious that the lower bound of the residual self-interference power is zero. The lower bound is achieved when the self-interference channel has frequency-flat transfer function. Between the upper and lower bounds, the

residual self-interference power is determined by the self-interference channel characteristics, mainly the correlation between the channel frequency response at different subcarriers.

Typically, the correlation between the channel frequency response at different subcarriers is determined by the coherence bandwidth (CBW) of the channel. By definition, the CBW is defined as the frequency band in which the channel could be considered frequency flat. According to this definition, equation (5.19) can be rewritten as

$$P_{RSI} = P^{tx} \sum_{l=0,|k-l|>CBW}^{N-1} E\left[\left|\left(H_l^{ord,nlos} - H_k^{ord,nlos}\right)\right|^2\right] E\left[\left|J_{k-l}^{rx}\right|^2\right], \tag{5.21}$$

where $H_l^{ord,nlos} - H_k^{ord,nlos} = 0$ within the CBW of the channel. Furthermore, as shown in chapter 3 (figure 3.4, and 3.5), the phase noise process has a decaying power spectral density, such that the majority of the phase noise power is located around the DC carrier (i.e. J_0). Accordingly, the remaining terms where $|k-l| > CBW$ will be weighted by small phase noise values $|J_{k-l}|^2$.

Equation (5.21) shows that the proposed digital cancellation technique totally eliminates the phase noise associated with the LOS component of the channel in addition to part of the phase noise associated with the non-LOS component depending on the CBW. This is considered a significant improvement compared to conventional digital cancellation techniques where no phase noise elimination is achieved. For example, if the self-interference channel has a Rician factor of 20dB (i.e. the non-LOS component is 20dB lower than the LOS component), the proposed technique will mitigate the phase noise by at least 20dB more than the conventional digital cancellation techniques. In addition, more mitigation will be achieved according to the CBW of the channel.

In order to quantify the phase noise mitigation gain achieved due to the CBW of the channel, the system is simulated under three different channel models with different maximum delay spread (i.e. different CBW). The simulated channel models are the 'B', 'C', and 'D' TGn

channel models defined in [54]. The 'B', 'C', and 'D' channel models have a maximum delay spread of 80, 200, and 390ns respectively. Figure 5.3 shows the residual self-interference power for the three channel models at different non-LOS component power levels, with total phase noise power of -40dBc. The results show that, larger CBW results in lower residual self-interference power (i.e. more phase noise mitigation). In terms of numbers, approximately 15-30dB reduction in residual self-interference power compared to the upper bound is achieved due to the correlation between the channel frequency responses within the CBW of the channel.

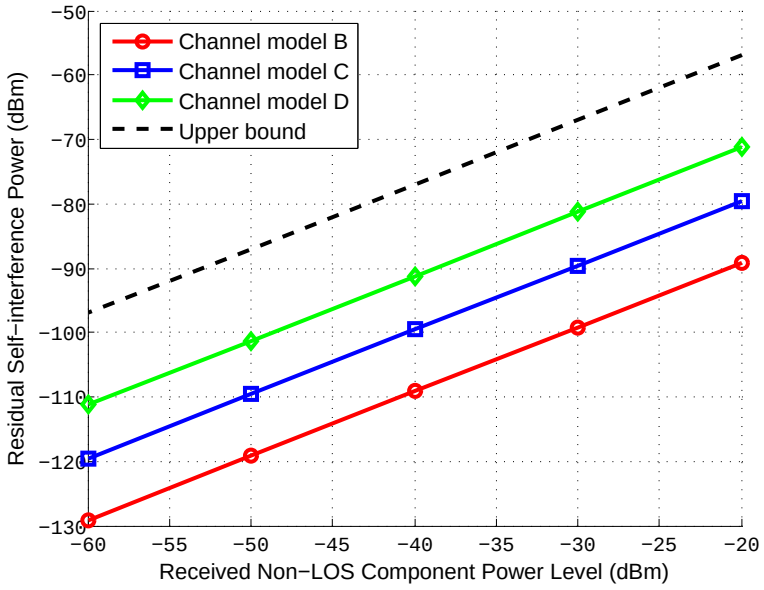

Figure 5.3: Residual self-interference power due to receiver phase noise effect for different channel models with −40dBc total in-band phase noise power.

5.3.3 Impact of Channel Estimation Errors

In the previous analyses, the channel transfer function H^{ord}/H^{aux} was assumed to be perfectly known. However, in practical systems, the channel transfer function is obtained through a channel estimation process that results in channel estimation errors. In this

section, the effect of the channel estimation errors on the cancellation performance is investigated.

In practical indoor applications [43], the channel is estimated using training symbols transmitted at the beginning of each data frame. During the training interval, the Least Square (LS) estimator is used to obtain an estimate for the channel transfer function as

$$\hat{H}_k = \frac{Y_k^{ord}}{Y_k^{aux}}. \tag{5.22}$$

Since LS estimator is known to have estimation errors that are directly proportional to the noise level, channel estimation error effect should be analyzed in the presence of all system impairments.

In the presence of receiver Gaussian, quantization, and phase noise, the frequency domain representation of the ordinary and auxiliary receiver outputs Y^{ord}, Y^{aux} during the training interval can be written as [1]

$$\begin{aligned} Y_k^{ord} &= \sum_{l=0}^{N-1} Y_l^{tx} H_l^{ord} J_{k-l}^{rx} + Q_k^{ord} + Z_k^{ord} \\ &= H_k^{ord} \sum_{l=0}^{N-1} Y_l^{tx} J_{k-l}^{rx} + \sum_{l=0}^{N-1} Y_l^{tx} \left(H_l^{ord} - H_k^{ord} \right) J_{k-l}^{rx} + Q_k^{ord} + Z_k^{ord} \\ &= H_k^{ord} \sum_{l=0}^{N-1} Y_l^{tx} J_{k-l}^{rx} + \eta_k, \end{aligned} \tag{5.23}$$

[1] Note that the signal-of-interest is not transmitted during the self-interference training interval

$$
\begin{aligned}
Y_k^{aux} &= \sum_{l=0}^{N-1} Y_l^{tx} H_l^{aux} J_{k-l}^{rx} + Q_k^{aux} + Z_k^{aux} \\
&= H_k^{aux} \sum_{l=0}^{N-1} Y_l^{tx} J_{k-l}^{rx} + Q_k^{aux} + Z_k^{aux} \\
&= H_k^{aux} \sum_{l=0}^{N-1} Y_l^{tx} J_{k-l}^{rx} + \zeta_k, \qquad (5.24)
\end{aligned}
$$

where η, and ζ are the composite noise component in the ordinary and auxiliary receiver chains calculated as

$$
\eta_k = \sum_{l=0}^{N-1} Y_l^{tx} \left(H_l^{ord} - H_k^{ord} \right) J_{k-l}^{rx} + Q_k^{ord} + Z_k^{ord}, \qquad (5.25)
$$

$$
\zeta_k = Q_k^{aux} + Z_k^{aux}. \qquad (5.26)
$$

The first noise component in (5.25) represents the residual self-interference due to the receiver phase noise effect as described in (5.17). Dividing (5.23) by (5.24) to obtain $\hat{H}$ we get

$$
\hat{H}_k = \frac{H_k^{ord} \sum_{l=0}^{N-1} Y_l^{tx} J_{k-l}^{rx} + \eta_k}{H_k^{aux} \sum_{l=0}^{N-1} Y_l^{tx} J_{k-l}^{rx} + \zeta_k}. \qquad (5.27)
$$

Since $\zeta_k \ll H_k^{aux} \sum_{l=0}^{N-1} Y_k^{tx} J_{k-l}^{rx}$, using the approximation of $(1+x)^{-1} \simeq 1 - x, x \ll 1$, equation (5.27) can be approximated as

$$
\hat{H}_k = \frac{H_k^{ord}}{H_k^{aux}} + \frac{\eta_k - \zeta_k}{H_k^{aux} \sum_{l=0}^{N-1} Y_l^{tx} J_{k-l}^{rx}} = \frac{H_k^{ord}}{H_k^{aux}} + E_H, \qquad (5.28)
$$

where E_H is the channel estimation error due to the receiver impairments. Equation (5.28) shows that the channel estimation error is directly related to the summation of all noise components in both the auxiliary and ordinary receiver chains. One simple way to improve

the channel estimation quality is by averaging the estimated channel $\hat{H}$ over multiple OFDM symbols as follows

$$\hat{H}_k = \frac{1}{M} \sum_{m=1}^{M} \frac{Y_{m,k}^{ord}}{Y_{m,k}^{aux}}. \tag{5.29}$$

In this case, since the noises at different OFDM symbols are not correlated, the channel estimation error will be reduced by a factor of M, where M is the number of training OFDM symbols. On the other hand, increasing the number of training symbols will negatively impact the overall system capacity.

After self-interference cancellation, the channel estimation error will be added to the existing receiver impairments, thus increasing the residual self-interference power. Figure 5.4(a) shows the increment in the residual self-interference power due to imperfect channel estimation as compared to the case of perfect channel knowledge. The results show that, the residual self-interference power is doubled when the channel is estimated using one training symbol. However, averaging over 4 symbols reduces the degradation to only 1dB compared to the perfect channel case

Another important factor is the channel estimation error due to the time varying nature of the wireless channel. In practical indoor applications, the channel is estimated once at the beginning of each data frame, and then assumed to be constant within the frame. While this might be sufficient for half-duplex systems, this assumption does not hold for the self-interference channel in full-duplex systems. The reason is that, in half-duplex systems, the signal-of-interest arrives at relatively small power levels such that the channel error due to fading effect will be much smaller than the noise floor. However, in full-duplex systems, the power of the self-interference signal is significantly high, such that the channel error due to the fading effect might dominate other noise components, especially with long data frames.

Figure 5.4(b) show the increment in the residual self-interference power due to the fading

effect as compared to the case of perfect channel knowledge. The fading effect is investigated at different frame lengths with 5Hz Doppler frequency channel. The results show that for long data frames, the fading effect significantly increases the residual self-interference power compared to the perfect channel case. More specifically, up to 6.5dB performance degradation is expected for frame lengths of 150 symbols (i.e. 600us based on the simulated system parameters). It can also be noticed that the performance degradation is decreasing with the decrease of the received signal power level. The reason is that, at low received signal power levels, the fading effect becomes negligible compared to the receiver impairments and the performance becomes noise limited. However, at high received signal power levels, the fading effect dominates other noise components. This behavior also explains why the fading effect is a significant concern in full-duplex systems, while it is not a concern in half-duplex systems.

From figures 5.4(a), (b) we can conclude that reducing the channel estimation error requires more training symbols and shorter frame lengths. Both requirements negatively impact the overall system capacity. In fact, capacity degradation is related to the training overhead, which is defined as the ratio between the number of training symbols to the number of useful data symbols. At the same training overhead, several combinations of the number of training symbols and frame lengths could be used. For example, 4% training overhead could be achieved with 2 training symbols every 50 data symbols, or 4 training symbols every 100 data symbols, etc. The appropriate choice should be made based on the receiver operating point, mainly the received signal power level. For instance, at high received signal power levels, using shorter frames with small number of training symbols is better than using long frames with large number of training symbols and vice versa. This tradeoff is clear in figures 5.4(a), (b), where it is shown that at high received signal power levels, doubling the frame length from 50 to 100 symbols degrades the performance by 2.5dB, while reducing the number of training symbols from 4 to 2 symbols only degrades the performance by 1dB. In this scenario, for 4% training overhead, using 50-symbols frame with 2 training symbols is

better than using 100-symbols frame with 4 training symbols. On the other hand, at low received signal power levels, the degradation due to the fading effect is smaller than the degradation due to the receiver impairments. In this case, using more training symbols is more beneficial than using short frames.

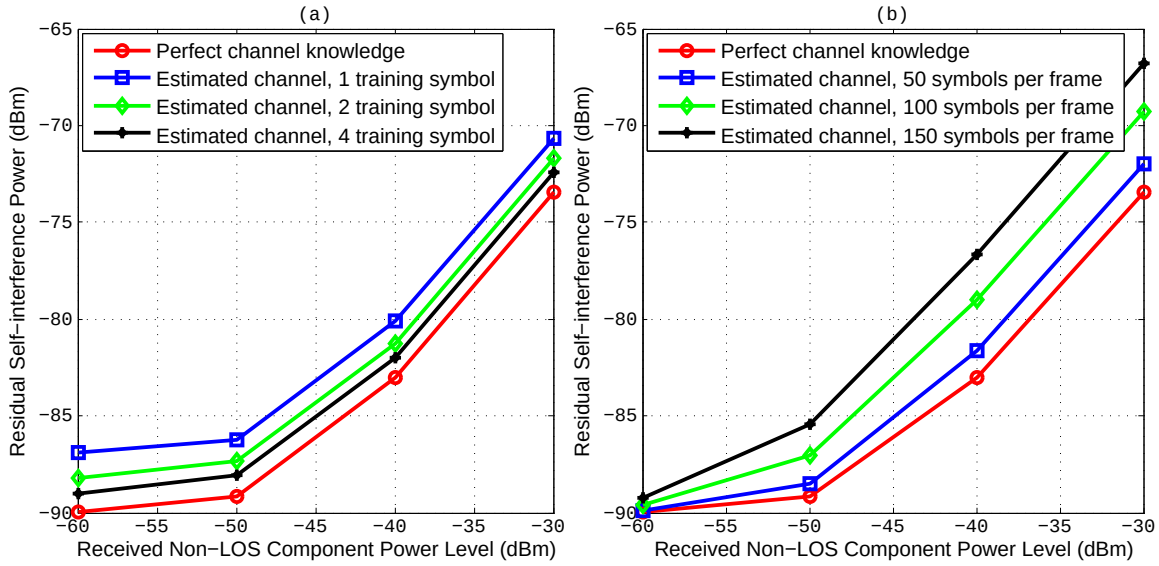

Figure 5.4: Residual self-interference power due to channel estimation error effect: (a) channel estimation error due to receiver noise, (b) channel estimation error due to fading effect.

5.3.4 Impact of Receiver Nonlinearities

In the presence of only receiver nonlinearities, the auxiliary and ordinary receiver outputs (Equation (5.2) and (5.3)) can be rewritten as

$$y_n^{aux} = y_n^{tx} * h_n^{aux}. \tag{5.30}$$

$$y_n^{ord} = y_n^{tx} * h_n^{ord} + d_n^{rx} + s_n^{soi}. \tag{5.31}$$

Then, after self-interference cancellation, the interference-free signal Y^{DC} can be written as

$$Y_k^{DC} = Y_k^{ord} - \frac{H_k^{ord}}{H_k^{aux}} Y_k^{aux} = Y_k^{tx} H_k^{ord} + D_k^{rx} + S_k^{soi} - \frac{H_k^{ord}}{H_k^{aux}} \left(Y_k^{tx} H_k^{aux} \right) = D_k^{rx} + S_k^{soi}, \quad (5.32)$$

Where D_k^{rx} is the frequency domain representation of the LNA nonlinear distortion signal d^{rx}. In this analysis, we are assuming that the LNA is the major contributor to the receiver nonlinearity. Therefore, the auxiliary receiver chain is assumed to be highly linear, since there is no LNA in the auxiliary receiver chain. According to (5.32), it can be easily shown that the residual self-interference power is directly proportional to the nonlinear distortion level. Accordingly, receiver nonlinearity suppression is essential for better self-interference cancellation capability. The nonlinearity estimation and suppression technique presented in chapter 4 could be modified to be used with the proposed architecture for receiver nonlinearity suppression as follows.

According to the nonlinearity model in (5.7), and considering only third order nonlinearities, the receiver nonlinear distortion signal d^{rx} can be written in terms of the transmitted signal y^{tx} as

$$d_n^{rx} = \alpha_3 \left(y_n^{tx} * h_n^{ord} \right) \left| y_n^{tx} * h_n^{ord} \right|^2 . \quad (5.33)$$

Using (5.1), the base-band representation of the transmitted signal $y^{tx}(t)$ can be written as

$$y_n^{tx} = x_n e^{j\phi_n^{tx}} + d_n^{tx} = x_n + j x_n \phi_n^{tx} + d_n^{tx}, \quad (5.34)$$

Where $e^{j\phi} \simeq 1 + j\phi, \phi \ll 1$. The second and third terms in the right hand side of (34) is mainly the transmitter phase noise and distortion signals that are typically $\ll x_n$ in terms of power. According to (5.34), the transmitter phase noise and distortion signals will contribute to the receiver nonlinear distortion d^{rx}. However, their contribution will be much smaller than the distortion due to the main transmitted signal x_n. Therefore, the transmitter phase

noise and distortion signals could be ignored while substituting from (5.34) into (5.33). Accordingly, equation (5.33) can be approximated as

$$d_n^{rx} = \alpha_3 \left(x_n * h_n^{ord}\right) \left|x_n * h_n^{ord}\right|^2. \tag{5.35}$$

In (5.35), x_n is known and h^{ord} could be estimated during the channel estimation training period. The only unknown in (5.35) is the nonlinearity coefficient α_3, which could be estimated using simple LS estimator. As described before, channel estimation error is directly proportional to the receiver impairments. Accordingly, in the presence of receiver nonlinearity, the channel estimation error will be also a function of the receiver nonlinearity. Therefore, any nonlinearity estimation and suppression technique should consider the channel estimation error due to receiver nonlinearity.

Referring back to (5.30) and (5.31), the channel estimation in the presence of only receiver nonlinearity is performed as

$$\hat{H}_x = \frac{Y_k^{ord}}{Y_k^{aux}} = \frac{Y_k^{tx} H_k^{ord} + D_k^{rx}}{Y_k^{tx} H_k^{aux}} = \frac{H_k^{ord}}{H_k^{aux}} + \frac{D_k^{rx}}{Y_k^{tx} H_k^{aux}}. \tag{5.36}$$

In order to estimate the nonlinearity coefficient, one additional training symbol is transmitted after the channel estimation training symbol. Superscript $tr1$, and $tr2$ is given to the different signals within the channel estimation training symbol and the additional training symbol respectively. During the additional training symbol, the received signal after self-interference cancellation can be written as

$$\begin{aligned} Y_k^{DC,tr2} &= Y_k^{ord,tr2} - \hat{H}_k Y_k^{aux,tr2} \\ &= Y_k^{tx,tr2} H_k^{ord} + D_k^{rx,tr2} - \left(\frac{H_k^{ord}}{H_k^{aux}} + \frac{D_k^{rx,tr1}}{Y_k^{tx,tr1} H_k^{aux}}\right) \left(Y_k^{tx,tr2} H_k^{aux}\right) \\ &= D_k^{rx,tr2} - \frac{Y_k^{tx,tr2}}{Y_k^{tx,tr1}} D_k^{rx,tr1}. \end{aligned} \tag{5.37}$$

Using the same approximation as in (5.35), equation (5.37) can be approximated as

$$Y_k^{DC,tr2} = D_k^{rx,tr2} - \frac{X_k^{tr2}}{X_k^{tr1}} D_k^{rx,tr1} = \alpha_3 \left(\bar{D}_k^{rx,tr2} - \frac{X_k^{tr2}}{X_k^{tr1}} \bar{D}_k^{rx,tr1} \right), \tag{5.38}$$

and

$$\bar{D}_k^{rx,i} = DFT \left[\left(x_n^i * h_n^{ord} \right) \left| x_n^i * h_n^{ord} \right|^2 \right], \quad i \in \{tr1, tr2\}. \tag{5.39}$$

Finally, an estimate for the nonlinearity coefficient α_3 is obtained as

$$\hat{\alpha}_3 = \frac{1}{N} \sum_{k=0}^{N-1} \frac{Y_k^{DC,tr2}}{\bar{D}_k^{rx,tr2} - \frac{X_k^{tr2}}{X_k^{tr1}} \bar{D}_k^{rx,tr1}}. \tag{5.40}$$

During the data symbols, the estimated nonlinearity coefficient $\hat{\alpha}_3$ is used to reconstruct the distortion signal and subtract it from the received signal. Note that, the nonlinearity coefficients change very slowly such that it could be estimated once every several frames, which reduces the training overhead due to the use of the additional training symbol.

The proposed nonlinearity estimation and suppression technique is numerically investigated at different operating conditions. Figure 5.5 shows the residual self-interference power at different nonlinear distortion power levels in three cases: i) the linear receiver case, ii) the nonlinear receiver case without performing nonlinearity suppression, and iii) the nonlinear receiver case with the proposed nonlinearity suppression technique. In the linear receiver case, the performance is limited by other receiver impairments and channel estimation errors. The results show that without nonlinearity suppression, the residual self-interference power is limited by the distortion power level. However, performing nonlinearity suppression using the proposed technique could achieve $\sim$23dB more reduction in the residual self-interference power. Furthermore, at distortion power levels ≤ -45dBm, the proposed technique is shown to achieve almost the same performance as in the linear receiver case, which means that the

23dB improvement are sufficient to eliminate the nonlinearity effect at such distortion power levels.

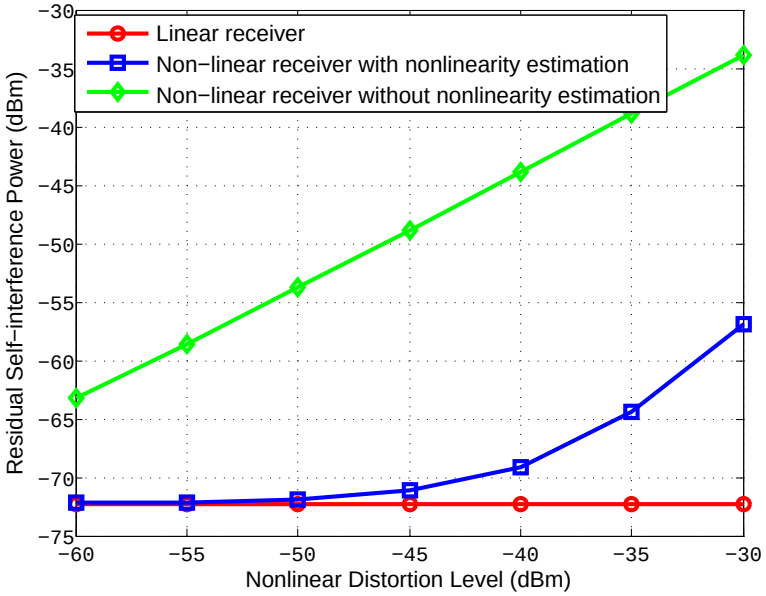

Figure 5.5: Residual self-interference power due to receiver nonlinearities with and without nonlinearity estimation.

5.3.5 Overall Cancellation Performance

In this section, the overall self-interference cancellation performance of the proposed technique is numerically investigated in the presence of all transmitter and receiver impairments. The design tradeoffs and the factors contributing to the residual self-interference power are discussed. In the previous analyses, we show that the residual self-interference power highly depends on the following factors: i) the power level of each one of the receiver impairments, ii) the received self-interference power level, iii) the channel Rician factor which determines the power of the received non-LOS component, and iv) the self-interference channel characteristics (e.g. coherence bandwidth, Doppler frequency). In practical full-duplex systems, those four parameters are not totally independent. For instance, the experimental results in [33] show that, the self-interference channel Rician factor is inversely proportional to the

achieved passive suppression amount which determines the received self-interference signal power. Accordingly, for reliable conclusions, such dependency should be considered while investigating the overall cancellation performance.

To be pragmatic, all presented system parameters are chosen based on practical transceivers and real-time experimental results. More specifically, the values for the transmitter and receiver impairments are chosen based on the datasheet of the NI5791 transceiver [71] as follows: i) the integrated in-band transmitter and receiver phase noise power is -40dBc, ii) the number of ADC bits is 14bits, iii) the Gaussian noise power is -90dBm and -72dBm at receiver input power levels of -25dBm and -5dBm respectively, and iv) the transmitter and receiver third order distortion power level is -45dB from the linear component power level. The system is simulated with the indoor TGn channel model 'D' [54] at 5Hz Doppler frequency. The training overhead is set to 4%.

From a passive suppression perspective, three practical scenarios are investigated: a) the use of omni-directional antenna with 35cm antenna separation. In this scenario, 25dB of passive self-interference suppression is achieved, and the self-interference channel Rician factor is 20dB [33]. b) The use of directional antennas with absorbing material between the transmit and receive antennas [33]. In this scenario, 45dB of passive suppression is achieved, and the self-interference channel Rician factor drops to 0dB. c) The use of reconfigurable directional antennas (presented in chapter 6 in this thesis). In this secnario, up to 60dB of passive suppression is achieved, and the self-interference channel Rician factor is 0dB. The main difference between the three scenarios is the received self-interference power, and the received non-LOS component power level. For example, at transmit power of 20dBm, the first scenario will have a received self-interference power of -5dBm and non-LOS component power level of -25dBm. While in the second scenario, both the received self-interference power and the non-LOS component power levels are at -25dBm.

In each scenario, the performance of the proposed digital cancellation technique is investi-

gated at different transmit power values. The performance is also compared to the conventional digital cancellation techniques [17]. The residual self-interference power due to each one of the receiver impairments is also presented to identify the main bottleneck in each region of operation. In all analyses, the half-duplex system's noise floor is shown for comparison purposes. Figure 5.6(a)-(c) shows the residual self-interference power at different transmit power values for the three scenarios. The conclusions from these results are multifold: first, in all scenarios, the proposed self-interference cancellation technique significantly mitigates the phase noise and nonlinearity effects to below the receiver noise floor. Therefore, in contrast with conventional digital cancellation techniques, the cancellation capability of the proposed techniques is no longer phase noise or nonlinearity limited.

Second, in the first scenario, due to the relatively high received self-interference power, the receiver Gaussian noise dominates other noise components and becomes the performance limiting factor. However, as the transmit power decreases, the Gaussian noise decreases which reduces the residual self-interference power. Accordingly, in such scenarios with relatively low passive suppression amounts, the proposed technique is more suitable to be used in low transmit power applications (e.g. up to 5dBm transmit power levels). Furthermore, simple analog cancellation techniques (e.g. Balun technique [20]) could be used to alleviate the Gaussian noise effect in such scenarios. On the other hand, when good passive suppression techniques are used (e.g. second and third scenarios), the Gaussian noise is no longer the limiting factor, and the self-interference signal could be significantly mitigated to $\sim$3dB above the half-duplex system's noise floor.

Third, following the receiver Gaussian noise, the channel error due to the fading effect is found to be the next performance bottleneck. The good thing about the error due to the fading effect is that, in contrast to other receiver impairments, there are many ways to reduce the fading effect. For example, i) interpolating the channel between different data frames, ii) inserting pilots within the OFDM symbol to track the channel variations, iii) using

shorter frames lengths, or iv) using pilot-based frame structure instead of the preamble-based frame structure. In the pilot-based frame structures, pilot subcarriers are inserted within the OFDM symbols to be used for the channel estimation purposes. Such pilot subcarriers allow for fast tracking of the channel variations.

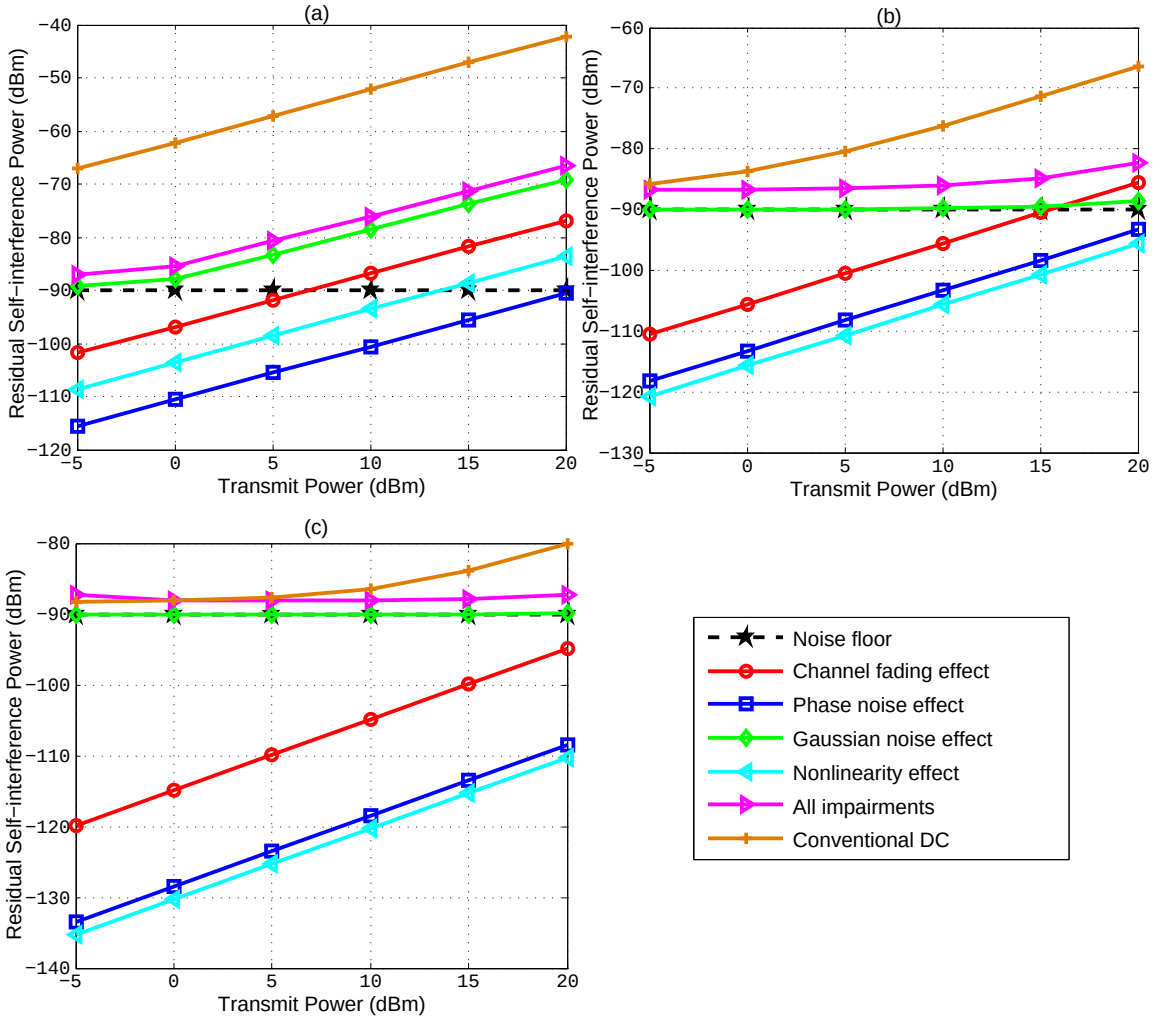

Figure 5.6: Residual self-interference power due to different receiver impairments at different transmit power values: (a) 1^{st} scenario, (b) 2^{nd} scenario, (c) 3^{rd} scenario.

5.4 Achievable Rate Analysis

In this section, the overall full-duplex system performance using the proposed digital cancellation technique is investigated in terms of the achievable rate gain compared to conventional half-duplex systems. The performance is investigated in the same three operating scenarios described in Section 5.3.5. Both full-duplex and half-duplex system performances are investigated in the presence of all transmitter and receiver impairments. The performance is investigated at two transmit power values: 20dBm, and 5dBm.

Generally, the achievable rate for both full-duplex and half-duplex systems can be calculated as

$$R^{FD} = E\left[log_2\left(1 + SINR^{FD}\right)\right], \tag{5.41}$$

$$R^{HD} = \frac{1}{2}E\left[log_2\left(1 + SNR^{HD}\right)\right], \tag{5.42}$$

where $E[\,]$ denotes expectation process, R^{FD}, R^{HD} is the full-duplex and half-duplex system's achievable rate, $SINR^{FD}$ is the signal-of-interest to interference plus noise ratio in full-duplex systems, and SNR^{HD} is the signal to noise ratio in half-duplex systems. The factor of $1/2$ in the half-duplex rate equation is due to the fact that the resources are divided between the two communicating nodes.

Figure 5.7(a)-(c) shows the achievable rate for the three scenarios at different SNR values. The conclusions from these results are multifold: first, the results show that the proposed technique significantly outperforms the conventional digital cancellation technique in all operating scenarios. The only exception is the case of 5dBm transmit power in the third scenario, where both the proposed technique and the conventional digital cancellation tech-

nique achieves the same performance. The reason is that, at 5dBm transmit power with the 60dB passive suppression assumed in the third scenario, only 35dB of digital cancellation are required to suppress the self-interference signal to the noise floor. Those 35dB could be easily achieved using conventional digital cancellation techniques. However, as the transmit power increases, the proposed technique will be able to achieve more self-interference cancellation, while the cancellation achieved using the conventional techniques will saturate. Second, figure 5.7(a) shows that, in the first scenario where the passive suppression amount is relatively low, the proposed technique can only be used in low transmit power applications.

Third, in the second and third scenarios, the proposed technique achieves significant rate improvement compared to conventional half-duplex systems, especially in high SNR regimes. In order to quantify the achievable rate gain of the proposed full-duplex system compared to the conventional half-duplex system, we calculate the average rate gain over the whole SNR range from 0 to 40dB for all scenarios, and the results are shown in table 5.1. The results in table 5.1 are average results; however, exact rate gain for each SNR value could be obtained from figure 5.7(a)-(c). Negative rate gain means that operating in full-duplex mode will degrade the overall system performance.

Table 5.1: Average full-duplex rate improvement compared to half-duplex system in different operating scenarios

	5dBm Transmit Power		20dBm Transmit Power	
	Proposed Technique	Conventional DC	Proposed Technique	Conventional DC
1^{st} Scenario 25dB passive suppression	14%	−58%	−58%	−98%
2^{nd} Scenario 45dB passive suppression	61%	11%	23%	−63%
3^{rd} Scenario 60dB passive suppression	76%	72%	67%	14%

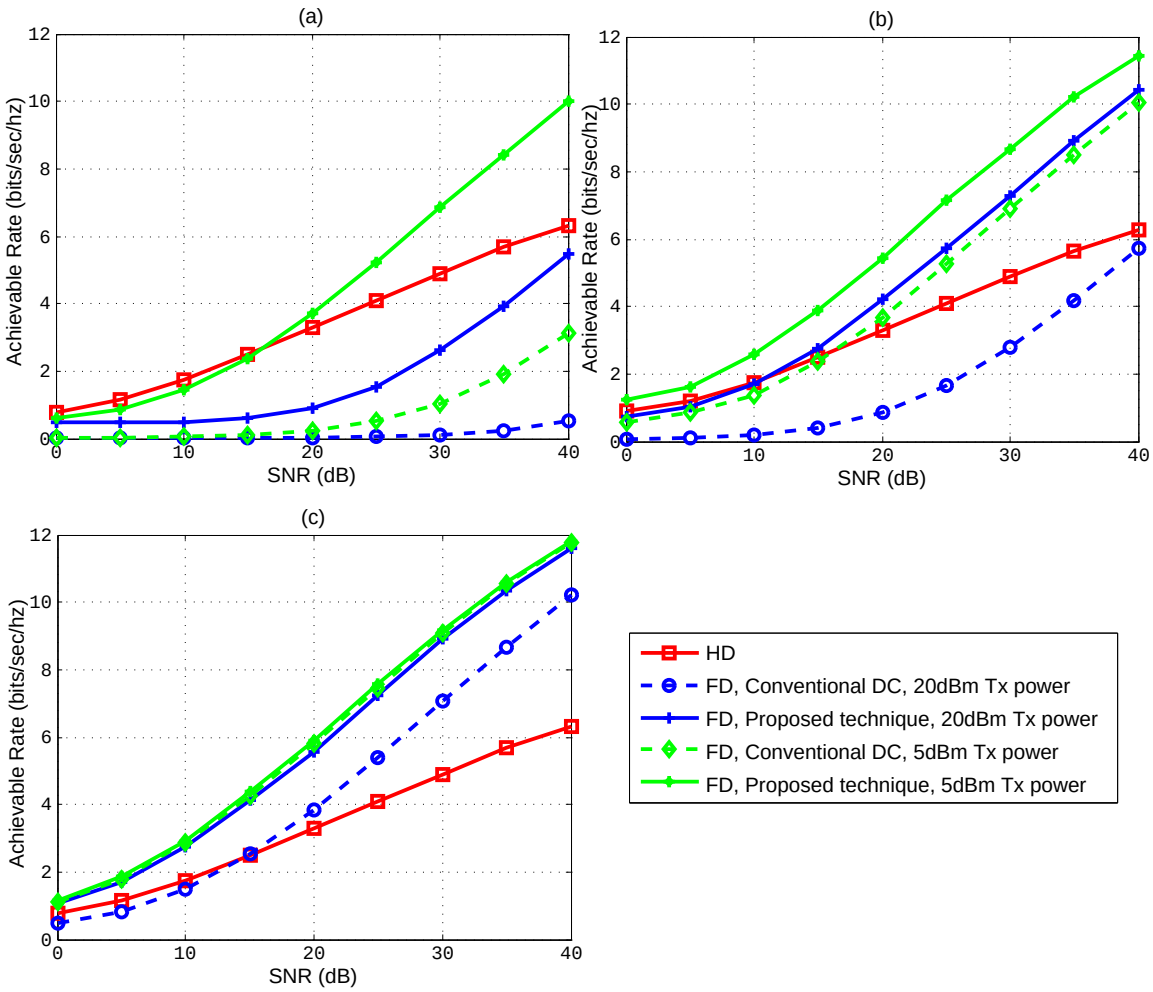

Figure 5.7: Full-duplex and Half-duplex achievable rates at different transmit power and SNR values: (a) 1^{st} scenario, (b) 2^{nd} scenario, (c) 3^{rd} scenario.

5.5 Conclusion

In this chapter, a novel all-digital self-interference cancellation technique for full-duplex systems is proposed. The proposed technique uses an auxiliary receiver chain to obtain a digital-domain copy of the transmitted RF self-interference signal including all transmitter impairments. The self-interference signal copy is then used in the digital-domain to cancel out both the self-interference signal and the transmitter impairments. In order to alleviate the receiver phase noise effect, a common oscillator is shared between the auxiliary and ordinary receiver chains. In addition, a nonlinearity estimation and suppression technique is

proposed to mitigate the receiver nonlinearity effects. A thorough analytical and numerical analysis for the effect of the transmitter and receiver impairments on the cancellation capability of the proposed technique is presented. The analyses show that the proposed technique significantly mitigates the transceiver phase noise and nonlinearity effects. The overall full-duplex system performance using a combination of the proposed digital cancellation technique and practical passive suppression techniques is numerically investigated. The results show that, the proposed technique significantly mitigates the self-interference signal to $\sim$3dB higher than the receiver noise floor, which results in up to 76% rate improvement compared to conventional half-duplex systems at 20dBm transmit power values.

Chapter 6

Passive Self-interference Suppression Using MRA

6.1 Introduction

Typically, full-duplex systems deploy both passive suppression and active cancellation techniques to significantly mitigate the self-interference signal. In chapter 3-5, we discussed several solutions to improve the cancellation capability of active self-interference cancellation techniques by either impairments mitigation or using novel transceiver architectures. For a complete investigation of the self-interference cancellation problem, this chapter proposes a novel passive self-interference suppression technique that is capable of achieving up to 65dB of passive suppression at 10 cm antenna separation. In addition, the proposed passive suppression technique is integrated with the conventional digital cancellation techniques to build a complete full-duplex system that is experimentally proven to achieve 90% rate improvement over half-duplex systems.

6.1.1 Contribution

The main contributions of this chapter are as follows: first, we introduce the design and operating mechanism of a 2.5GHz MRA antenna. MRA is a dynamically reconfigurable antenna that is capable of changing its proprieties (e.g. radiation pattern, polarization, and operating frequency) according to certain input configurations. The MRA has 4096 possible radiation patterns. A pattern selection mechanism to select the optimum pattern among the various MRA patterns is presented. Since the MRA has many radiation patterns, one can select the pattern that minimizes the received self-interference power. However, this method can not guarantee the optimal overall system performance, mainly because the selected pattern also affects the received signal-of-interest (the desired signal) power. To guarantee the best overall system performance, we developed a pattern selection mechanism that maximizes the received Signal-of-interest to Interferer Ratio (SIR) at the receiver input. The performance of the MRA-based passive self-interference suppression is experimentally investigated. The results show that, the MRA can achieve an average of 65dB of passive self-interference suppression, with a 45dB SIR gain compared to the case when an omni-directional antenna is used.

Second, a detailed experimental analysis for the required MRA training time and training overhead in different indoor environmental conditions. In addition, a heuristic-based approach is proposed to reduce the training overhead by selecting a small suboptimal set of patterns among all MRA patterns. The results show that using the proposed heuristic, at 1% training overhead with a suboptimal set of 300 patterns, 62dBs of passive suppression can be achieved with only a 3dB performance loss as compared to the optimal case.

Finally, a complete full-duplex system with a combined MRA-based passive suppression and conventional active self-interference cancellation is presented. The overall system performance is evaluated in different indoor environmental conditions. The results show that at

1% training overhead, a total of 95dB self-interference cancellation is achieved in typical indoor environments. The 95dB self-interference cancellation is experimentally shown to be sufficient for 90% full-duplex rate improvement compared to half-duplex systems at 5dBm transmit power.

6.1.2 Related Work

Throughout the literature, passive self-interference suppression is achieved through one or a combination of the following four methods: (i) antenna separation, (ii) antenna isolation, (iii) antenna directionality, and (iv) antenna polarization. The applicability of each one of these methods depends on the application, and the physical constraints of the system. For example, in mobile applications with small device dimensions, the passive suppression achieved using antenna separation and isolation is very limited. However, in others systems (e.g. relay systems) where the transmit and receive antennas are not necessary collocated, antenna separation and isolation could achieve significant passive suppression. For instance, in [45, 46], the use of a single pattern directional antenna and $4-6$ m of antenna separation achieves $\sim$85dB of passive suppression. While in [47], using 5 m of antenna separation in addition to antenna isolation achieves 70dB of passive suppression. This large antenna separation might be acceptable in relay systems, but it is not acceptable in practical mobile applications. A more practical passive self-interference suppression method with relatively small antenna separation (e.g $20-40$ cm) was introduced in [30, 31]. The results show a maximum of 60dB passive suppression at $\sim$40cm antenna separation with cross polarization, and a metal shield between the antennas.

Recently, a comprehensive study of the achieved passive suppression using different combinations of the previously mentioned methods was introduced in [33]. In [33], the passive suppression performance is characterized using two single-pattern directional antennas placed

at different orientations, with different antenna separations ranging from 35-50 cm. The results show that in a non-reflective environment (e.g. Anechoic Chamber), a maximum of 72dB passive suppression could be achieved when absorptive shielding is present between the two antennas. While in a reflective room the maximum achievable passive suppression is reduced to 45dB due to the self-interference signal reflections.

In contrast with the prior work, we focus on the deployment of full-duplex transmission in mobile indoor applications where the allowed antenna separation is very limited. Our approach could achieve 65dB of passive suppression at only 10 cm antenna separation in a reflective indoor environment, without any antenna shielding. Moreover, the directional antenna used in all prior work is a single pattern directional antenna. The lack of beam steering capability in such antennas might affect the signal-of-interest power in certain scenarios (e.g. when the desired signal is coming from the opposite direction of the antenna). On the other hand, the reconfigurability feature in the full-duplex systems utilizing MRA attempts to maximize the SIR for any given scenario.

6.2 Antenna Structure and Working Mechanism

6.2.1 MRA Structure

The 3-D schematic and cross section view of the MRA are depicted in figure 6.1. This MRA employed an aperture-coupled feed mechanism for RF feeding similar to the MRA presented in [72]. The main two components of the MRA architecture are, namely, the driven patch antenna and parasitic layer. The driven patch (19.3x19.3 mm^2) is designed to operate in the frequency band of 2.4-2.5 GHz and fed by a 50-Ohm microstrip line through an aperture (21.4x1.4 mm^2) etched on the center of the common ground plane. The feed layer (90x90x0.508 mm^3) and patch layer (90x90x3.048 mm^3) are built respectively by using the

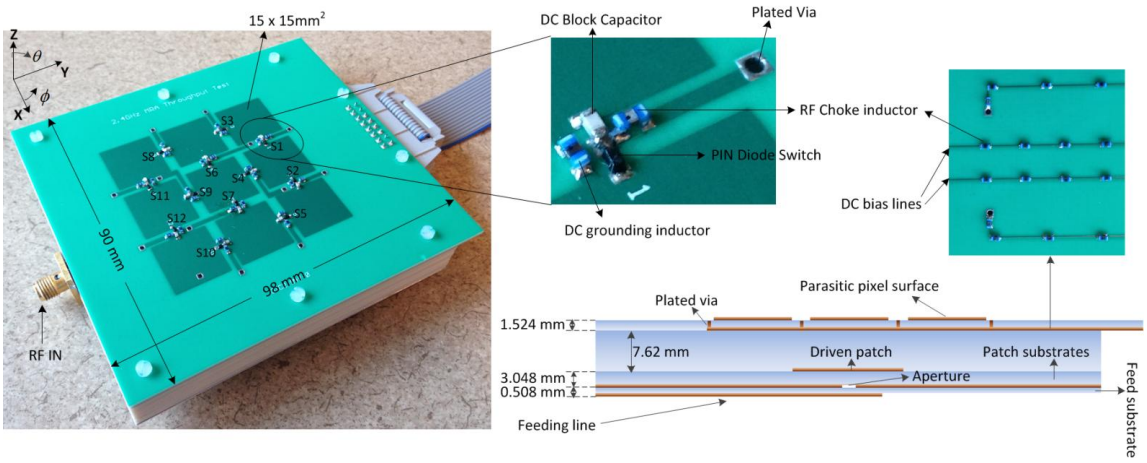

Figure 6.1: 3-D schematic and the cross section view of the MRA.

substrate Rogers 4003C ($\epsilon_r = 3.55$, $tan\ \delta = 0.0027$) [73]. The same substrate (98x90x1.524 mm^3) is used to form the parasitic layer above the driven patch. Notice that there is a 7.62 mm gap between parasitic layer and driven patch antenna, where the gap is filled with the RO4003C.

The reconfigurable parasitic surface, which consists of 3x3 square-shaped metallic pixels connected by 12 PIN diode switches with ON/OFF status, is formed on the top surface of the parasitic layer with individual pixel size being 15x15 mm^2. Thus the geometry of the parasitic surface can be configured by switching ON/OFF the 12 PIN diode switches, which are marked as S1-S12 in figure 6.1. DC bias lines for controlling the PIN diode switches are also formed on the parasitic layer but on the backside of the substrate. Vias are placed through the parasitic layer so that DC bias lines can be connected to the PIN diode switches on the parasitic surface.

Four different kinds of lumped components are used on the parasitic layer as shown in figure 6.1: 1) PIN diode switches are used in between all rectangular pixels. Metallic pixels are connected/disconnected by switching ON/OFF the PIN diode switches to change the geometry of the parasitic surface, which in turn change the current distribution, and thus

RF characteristic. 2) Inductors are placed along the DC bias lines as RF chokes. The SRF (self resonant frequency) of the RF choke is chosen to be around 2.5 GHz, thus RF chokes would appear as high impedance in the ISM band to minimize the current on the bias lines, thus minimizing the effect of the bias lines on the antenna performance. 3) Inductors are also placed in between all the rectangular pixels to connect all the pixels together. In this manner, all the pixels can be DC grounded together to provide Ground for DC biasing purpose. The SRF of these inductors was chosen to be the same value as RF chokes to keep the high RF impedance between pixels. 4) DC block capacitors are used to properly bias the PIN diode switches as shown in figure 6.1. The SRF of DC block capacitor is around 2.5 GHz to provide low RF impedance in the ISM band. In this way, the effect of DC block capacitor on RF performance is minimized.

6.2.2 Working Mechanism

The working mechanism of the antenna system, which is composed of one driven antenna and multiple parasitic elements, can be described by the theory of reactively controlled directive arrays developed by R. F. Harrington [74]. It was shown that the main beam direction of the driven antenna can be directed into a desired direction by the proper reactive loading of the parasitic elements. In the presented MRA, the proper reactive loading corresponds to a specific geometry of the parasitic pixel surface, which is obtained by switching ON/OFF the PIN diode switches between adjacent pixels of this surface. Switching ON and OFF the PIN diode switches placed on the MRA surface creates 4096 different modes of operation each with unique MRA radiation pattern. As an example, figure 6.2 shows the simulated and measured MRA radiation pattern for four different modes of operation, showing good agreement between the simulated and measured patterns.

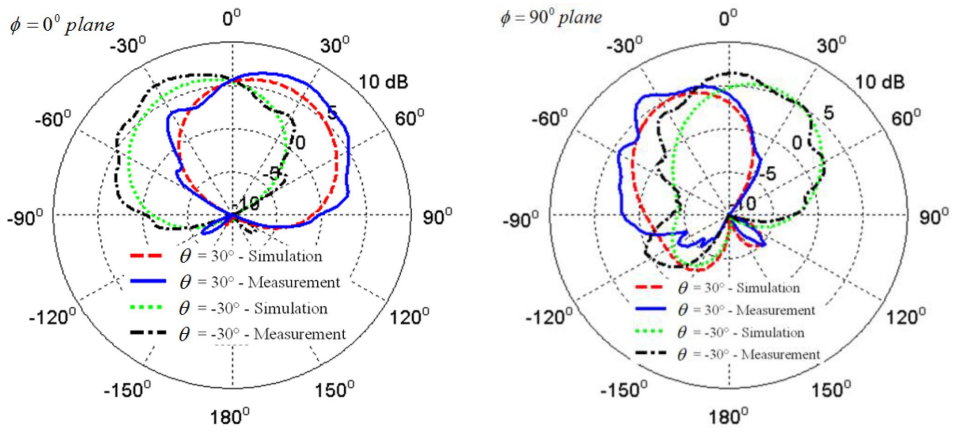

Figure 6.2: Simulated and measured radiation patterns for four different MRA modes at 2.45 GHz.

6.3 Experimental Framework and Environment

Due to the significant dependence of the full-duplex system performance on hardware impairments and the surrounding environments, experimental analysis is extremely important for performance characterization in full-duplex systems. In addition to hardware impairments, the use of a directional antenna at such small antenna separation creates a near-field effect that is difficult to account for at every possible scenario. In this section, the experimental setup, framework, and experimental environment are described in details.

6.3.1 Experimental setup

A complete full-duplex system is constructed using the Universal Software Radio Peripheral (USRP) software defined radio (SDR) platform [64]. Each USRP contains RF transceiver and Field Programmable Gate Array (FPGA). All USRP's are connected to a host PC through a Gigabit Ethernet connection. The baseband signal processing is performed over the host PC. The baseband signals are streamed to/from the USRPs at a rate of 25M sample/sec. The RF transceivers are then used for real-time signal transmission and reception. All experiments

are performed in the ISM band at 2.5Ghz carrier frequency with a 10Mhz signal bandwidth. All USRPs are synchronized to one reference clock.

As shown in figure 6.3, the full-duplex system consists of two nodes communicating in a full-duplex manner. Each node is equipped with one transmit antenna and one receive antenna. In this analysis, a dipole omni-directional antenna is used as transmit antenna, while the MRA is used as receive antenna. Both transmit and receive antennas have the same antenna polarization[1]. The MRA antenna has a total of 4096 different radiation patterns. The pattern selection is performed through a 12-lines digital control cable driven from an FPGA on a Zedboard [75]. The timing of all USRPs and the FPGA that drives the antenna switches are aligned with one reference Pulse Per Second (PPS) signal. Figure 6.4 shows a typical structure for a full-duplex node using MRA antenna. Another full-duplex system architecture where both transmit and receive antennas are omni-directional antennas is used for comparison purposes

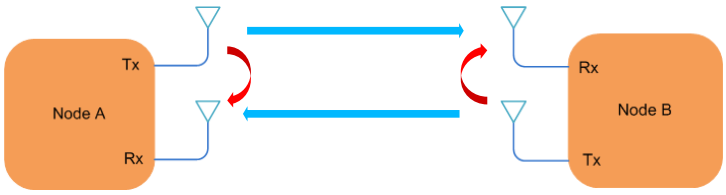

Figure 6.3: Two nodes full-duplex system.

6.3.2 Experimental framework

In this chapter, two different frameworks are used for performance characterization: the passive suppression characterization framework, and the complete system framework. In

[1]There are many other antenna configurations that could be used. For example, the MRA could be use as transmit antenna, or both transmit and receive antennas. Furthermore, cross antenna polarization could be used.

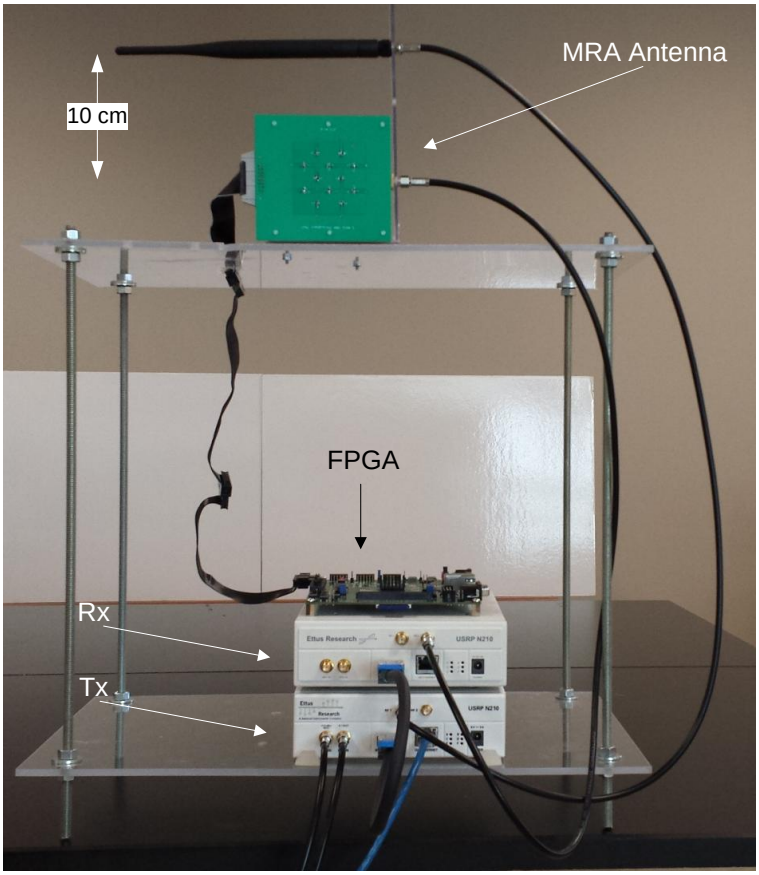

Figure 6.4: Full-duplex wireless node with MRA.

the passive suppression characterization framework, the full-duplex system is used to characterize the achieved passive self-interference suppression for each MRA radiation pattern at different environmental conditions. For measurement purposes, in this framework, the received SIR defined as the ratio between the received signal-of-interest power and the received self-interference power is used as a performance metric. The passive suppression characterization frame structure is shown in figure 6.5. Each transmission frame consists of L segments, where L is the number of antenna patterns that need to be characterized. Each segment contains three intervals: Gap interval, Data interval, and Null interval. The Data and Null intervals have the same length and are alternating between the two nodes. The MRA radiation pattern is changed at the segment edge. The Gap interval is used to account for the MRA switching time. During the Data interval, the node is transmitting a

training sequence, while during the Null interval the node is silent. At the receiver side, the transmitted frames from each node are combined and received by the MRA antenna. In the combined frame, each segment will contain a self-interference portion and a signal-of-interest portion. The received signal strength is calculated for each portion to obtain an estimate for the received self-interference and signal-of-interest power.

The complete system framework is used to characterize the overall full-duplex system performance when the MRA-based passive self-interference suppression is combined with the conventional digital cancellation technique. In this framework, two different performance metrics are used: the overall self-interference cancellation, and the achievable full duplex rate. The transmission frame structure in the complete system framework consists of two main intervals: the MRA training interval, and the data transmission interval. During the MRA training interval, the MRA patterns are trained and the optimum pattern is selected. During the data transmission interval, the full-duplex data transmission takes place between the two communicating nodes. During MRA training interval, a frame structure similar to the one described in the passive suppression characterization framework is used. On the other hand, the data transmission interval consists of several data frames that have the same frame structure as in the 802.11n systems [43]. Each frame consists of several OFDM symbols with 64 subcarriers in each symbol. At the beginning of each data frame, training symbols are transmitted for channel estimation purposes. After channel estimation, digital self-interference cancellation is performed to mitigate the residual self-interference signal.

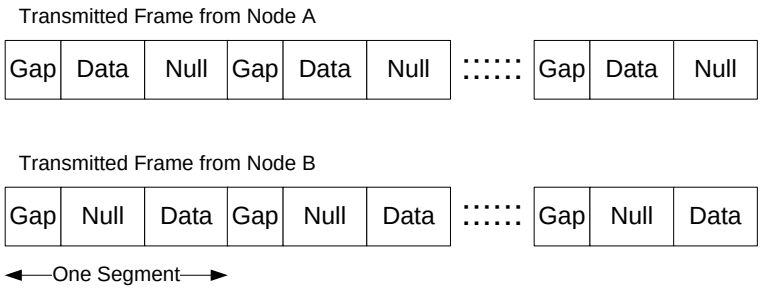

Figure 6.5: MRA training frame structure.

6.3.3 Practical aspects

Since the optimum pattern selection process involves extensive training, training time and training overhead are important parameters that have to be investigated. According to the MRA training frame structure, the training time and training overhead are a function of two main parameters: the number of MRA patterns that have to be trained, and the segment length. In this section, the required minimum segment duration is discussed (discussion related to the number of MRA patterns that have to be trained is presented in the Section 6.4).

The segment duration is a function of the Gap and the Data intervals' length. The Gap interval length is directly proportional to the MRA switching time which is a function of the MRA switching circuitry. In the current design, the MRA switching time is ∼0.5us. The length of the Data interval depends on how the received signal strength is calculated. For example, if the received signal strength is calculated in the digital domain, the Analog to Digital Converter (ADC) sampling rate and the allowable timing offset will determine the minimum Data interval length. Based on our extensive experiments, approximately 30 time-domain samples are enough to obtain a good estimate for the received signal strength. Therefore, using 40Mhz ADC sampling rate, the required minimum segment duration is 2us (0.5us for antenna switching, and 1.5us for Data and Null intervals per segment). This time could be reduced to 1.25us if the ADC sampling rate is doubled to 80Mhz, which is a practical sampling rate in current wireless systems

6.3.4 Experimental environment

The experimental analysis is conducted in the Wireless Systems and Circuits Laboratory (WSCL) within Engineering Hall at the University of California, Irvine. Figure 6.6 shows a floor plan for the area where the experiments are performed, and presents a typical laboratory

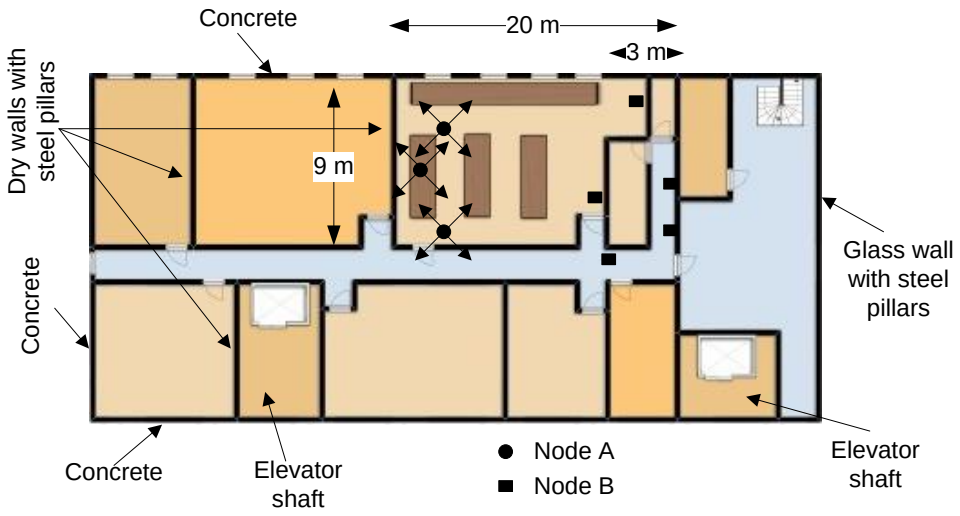

Figure 6.6: Floor plan for the area where the experiments are conducted.

environment with measurement workstations, tables, metallic surfaces, etc. The outer walls of the building are either concrete walls or glass walls with steel pillars. While, the inner walls are dry walls with steel pillars.

To enrich the experimental analysis, the two communicating nodes are placed at different positions inside and outside the laboratory to create a variety of Line Of Sight (LOS) and non-LOS environments. In addition, different MRA orientations are tested such that the two communicating nodes are facing each other, opposite to each other, or side to side. To emulate typical conditions, the experiments are performed in both semi-static and dynamic environments. In a semi-static environment, the area is static with no moving personnel in the near area. While in dynamic environments, normal laboratory activities are maintained with moving personnel during the experiment time.

6.4 Experimental Results

In this section, the performance of the MRA-based passive suppression is characterized and discussed. The performance is also compared to the conventional omni-directional antenna based passive suppression. In addition, we present a heuristic-based approach to reduce the overall MRA training time by reducing the number of MRA patterns that need to be trained. The performance of the heuristic-based approach is compared to the optimal case where all MRA patterns are trained. Finally, the MRA training overhead and training periodicity are characterized and discussed.

6.4.1 MRA-based passive self-interference suppression

In this part, the passive suppression characterization framework is used to characterize the achieved MRA-based passive Self-interference suppression. The performance is evaluated at different transmit power values ranging from -10dBm to 10dBm. Each run lasts for several seconds. In each run, all the 4096 MRA patterns are trained, and the pattern that maximizes the SIR is selected.

Figure 6.7 shows the empirical Cumulative Distribution Function (CDF) of the achieved passive self-interference suppression for both MRA and omni-directional antenna cases. The passive suppression is defined as the ratio between the transmit power and the received self-interference power at the antenna output. The CDF is calculated over time for all different runs and transmit power values. The results show that, using MRA achieves an average of 65dB passive suppression, with 45dB passive suppression gain compared to omni-directional antenna.

Since the selected MRA pattern affects the received signal-of-interest power, the achieved passive suppression amount is not sufficient to characterize the overall system performance.

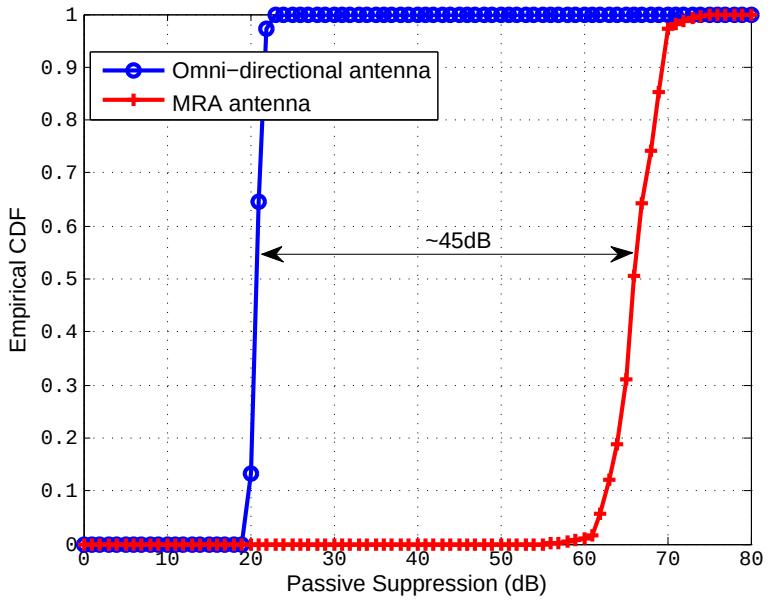

Figure 6.7: CDF of omni-directional antenna and MRA-based passive self-interference suppression.

Instead, the effect of the MRA on the received signal-of-interest power should be also considered. The received signal-of-interest power is affected by both the MRA pattern, and the distance between the two communicating nodes. Therefore, to eliminate the distance factor and focus only on the MRA effect, the signal-of-interest power loss is used as a performance metric instead of the absolute value of the received signal-of-interest power. The signal-of-interest power loss is defined as the received signal-of-interest power ratio between the MRA case and the omni-directional antenna case for the same experimental environment.

Figure 6.8 shows the empirical CDF of the signal-of-interest power loss for three different experimental environments, in addition to the average CDF for all environments. The description of the three different environments is as follows: in the opposite orientation environment, the MRA antennas in the two communicating nodes are placed back-to-back, such that the back side of the MRA at a node is facing the other node. The face-to-face orientation is the contrary of the opposite orientation. In the side-to-side orientation, the side of the MRA at one node is facing the other node. The main difference between the opposite

orientation and the face-to-face orientation is that in the opposite orientation, the MRA is receiving most of the signal-of-interest power through its back loops which generally has small antenna gain. However, in the face-to-face orientation, most of the power is received through the main loops of the MRA which generally has high gain due to antenna directivity. Therefore, it is expected to have signal-of-interest power loss in the opposite orientations, while in the face-to-face orientation, the MRA is supposed to achieve signal-of-interest power gain. As shown in figure 6.8, an average of 5dB loss in the signal-of-interest power is expected in the opposite orientation environments, while an average signal-of-interest power gain of 4dB and 1dB is achieved in face-to-face and side-to-side orientations respectively. As an average over all different orientations, an average signal-of-interest power loss of 1dB is expected when the MRA is used. Compared to the 45dB self-interference suppression gain achieved by MRA, 1dB signal-of-interest power loss is negligible.

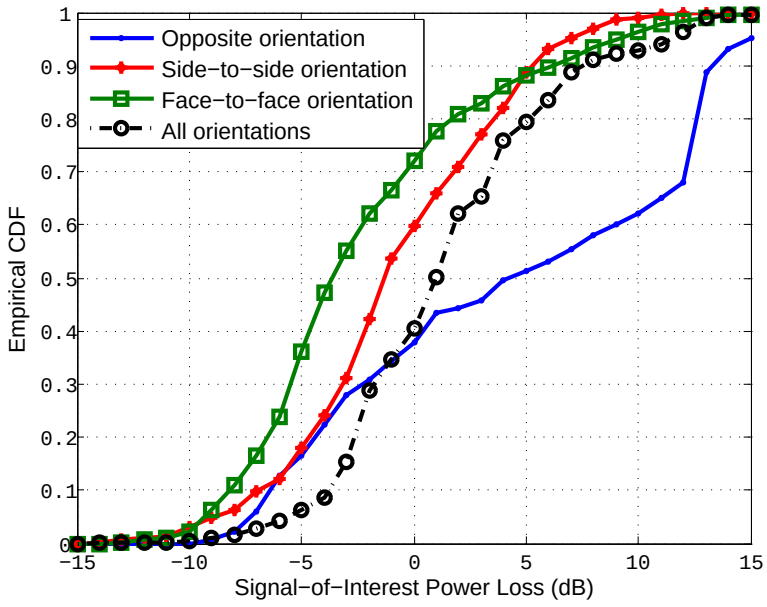

Figure 6.8: CDF of the Signal-of-interest power loss for different experimental environments.

6.4.2 Suboptimal pattern-set selection heuristic

While using the MRA as described leads to significant gains, the investment required to obtain 4096 modes is prohibitive. The goal of this section is to identify a heuristic that can reduce training overhead. To address this issue, we calculate the distribution of the optimal MRA pattern over time and for different environmental conditions. The calculated distribution is used to check if the optimal pattern index is localized or spans the whole range from 1 to 4096. The results in figure 6.9 show that, the optimum pattern index spans the whole range, but it is not uniformly distributed. In fact, the results show that there are some patterns that have low or even zero probability to be among the optimum patterns, while other patterns have high probability to be among the optimum ones.

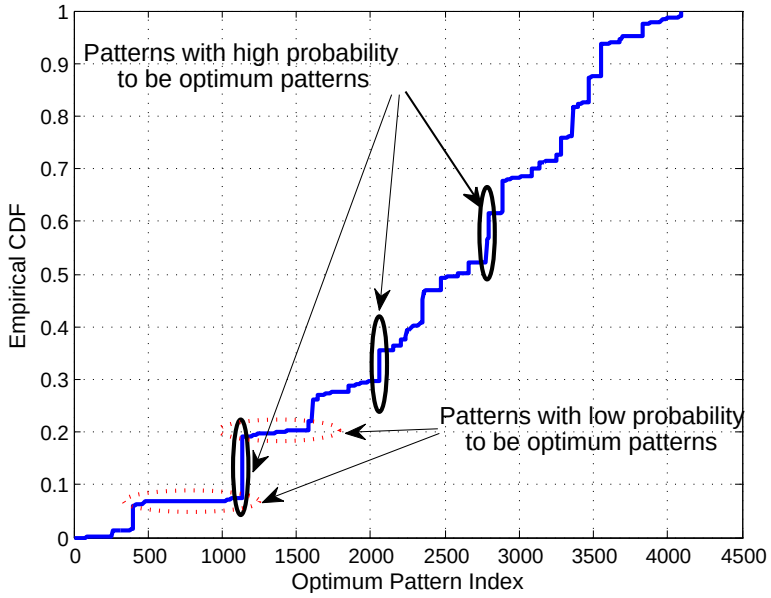

Figure 6.9: CDF of the index of the optimal MRA pattern.

While one viable choice may be to exclude patterns with low probability of being optimal, it is important to take into account the degree of "sub-optimalty". In fact, for a pattern, to have a low (or zero) probability of being optimum does not necessary means that the pattern achieves poor performance. For instance, among those low probability patterns there are two

categories: i) patterns that achieve good performance that is slightly less than the performance of the optimal pattern, and ii) patterns with poor performance that is significantly less than that of the optimal pattern. Although they have significant performance difference, the probability criterion does not differentiate between those two categories because they are both considered non-optimal. Accordingly, a better selection criterion should involve the self-interference suppression performance for each pattern, not only the probability of being among the optimum patterns or not.

For further clarification, consider that in full-duplex systems, the self-interference signal arrives at the receive antenna in two main components: the LOS component through the direct link between the transmit and receive antennas, and the non-LOS component due to the reflections. Due to the close proximity of the transmit and receive antennas, the LOS component is much higher than the non-LOS component. Therefore any MRA pattern with high gain in the LOS direction most likely will achieve poor performance, thus this pattern has to be avoided. In fact, the optimal patterns are the patterns that are capable of suppressing not only the LOS component but also part of the non-LOS component.

Accordingly, based on the achieved self-interference suppression for each MRA pattern, we developed a heuristic-based approach to select a suboptimal set of patterns that are expected to achieve the best performance. First, we run the system in 16 different environments that include a variety of LOS, non-LOS, semi-static, and dynamic scenarios each with 4 different orientations (opposite, face-to-face, and two side-to-side orientations). In each run, the achieved passive self-interference suppression for each one of the 4096 MRA patterns is calculated. We set a certain threshold X that represents a desired passive self-interference suppression amount. Then, the patterns that achieve passive suppression $> X$ at any time in any environment are selected. Basically, we select the patterns that are capable of achieving passive suppression $> X$ at least once. Therefore, any pattern that is not selected is guaranteed to have passive suppression less than X in all tested scenarios. The results in

figure 6.10 show the number of patterns that are capable of achieving passive suppression $> X$ at least once for different values of the threshold X. For instance, the results show that there are 1000, and 300 patterns capable of achieving passive suppression $>$ 52dB and 58dB respectively.

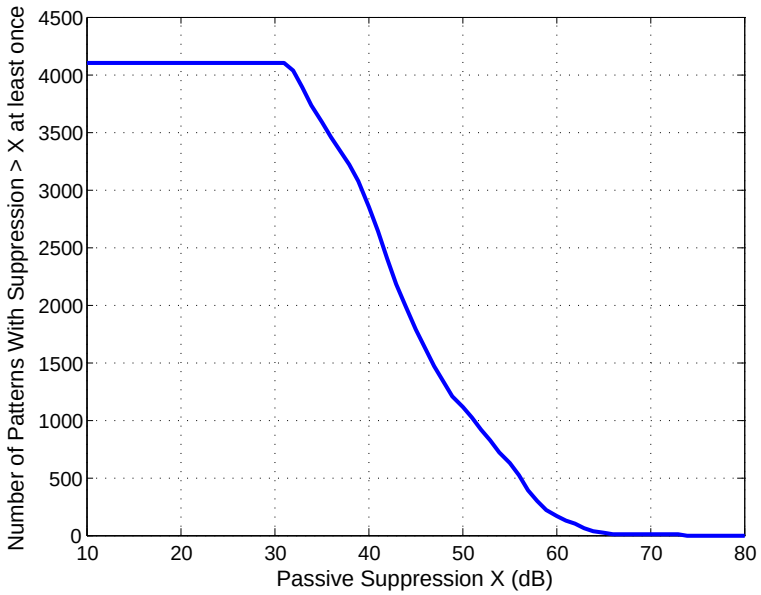

Figure 6.10: Number of MRA patterns that are capable of achieving passive suppression ¿ X in at least one of the tested scenarios.

In order to test the accuracy of the proposed heuristic we selected two different suboptimal set of patterns with passive suppression threshold $X = 52$dB and 58dB respectively. The first set contains 1000 patterns, and the second set contains 300 patterns. The performance of the selected sets is characterized in more than 20 different experimental environments that are different from the 16 environments used to select the suboptimal sets[2]. Figure 6.11 shows the CDF of both passive self-interference suppression and signal-of-interest power loss for the selected sets as well as the optimal 4096-patterns set. The results show that the 300-patterns set achieves an average of 62dB passive self-interference suppression with 3dB

[2]The experimental environments in this/following analysis are different from the environments used to select the suboptimal sets in the sense that the positions of the two communicating nodes are changed and different orientations spanning the whole 360^o are used.

loss compared to the optimum 4096 patterns set, but at ∼14 times less training time. Also, at ∼4 times less training time, the 1000-patterns set achieves an average of 64dB passive self-interference suppression. On the other hand, from signal-of-interest perspective, the results show that the 1000- and 300-patterns sets achieve almost the same performance as the optimal 4096-patterns set.

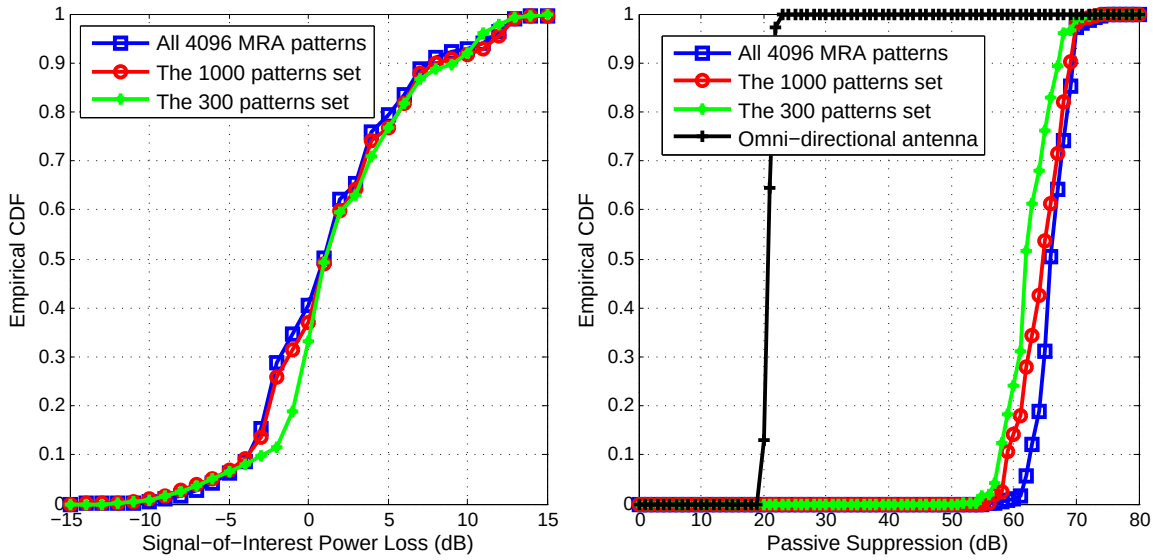

Figure 6.11: CDF of passive self-interference suppression and signal-of-interest power loss with different MRA pattern sets.

6.4.3 MRA training overhead

Due to its significant effect on the overall system capacity, training overhead is an important parameter that should be investigated. The training overhead is defined as the ratio between the training duration and the useful data duration. In the proposed full-duplex system, the training overhead is a function of two main parameters: the number of MRA patterns that need to be trained, and the re-training period. The re-training period is defined as the minimum time between two successive training intervals.

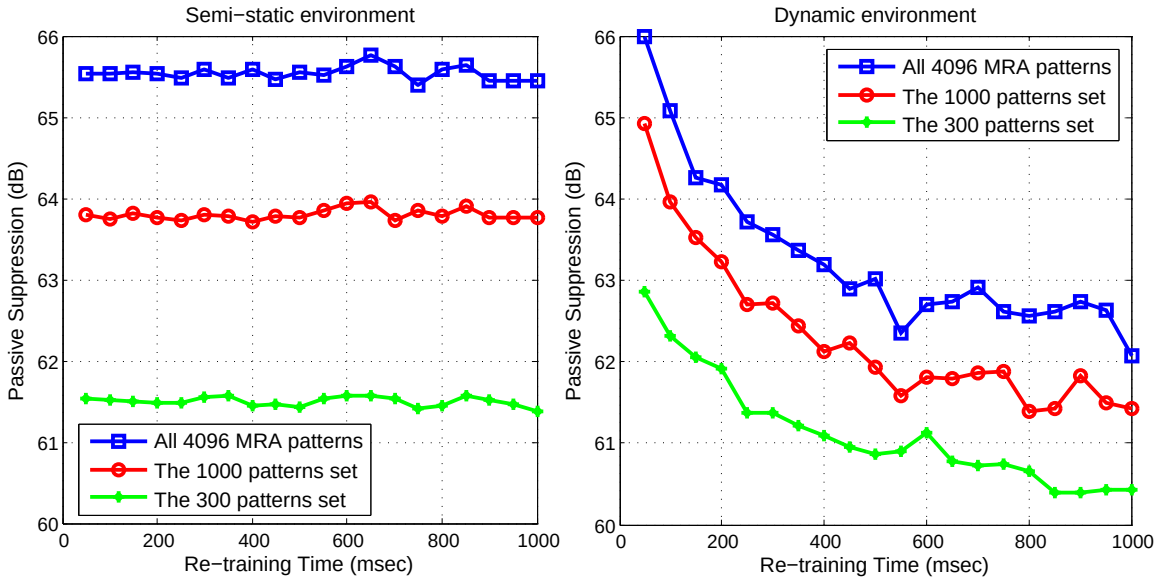

Figure 6.12: Passive self-interference suppression at different MRA re-training time.

In this analysis, we characterize the MRA training overhead in different environmental conditions. The system performance is evaluated for the selected suboptimal sets as well as the optimal 4096-pattern set. In this analysis, experiments are conducted in two main environments: semi-static environment and dynamic environment. Figure 6.12 shows the achieved average passive self-interference suppression at different re-training times for the semi-static and dynamic environments. The conclusions from these results are multifold: first, due to the slow channel variations in the semi-static environment, the system performance is almost constant with respect to the re-training time. In this kind of environments, the MRA could be trained once per second with no performance loss. Assuming that each pattern requires 2us training time, the training duration for the 4096-, 1000-, and 300-patterns sets are ∼8ms, 2ms, and 0.6ms respectively. If the MRA is trained once per second, the training overhead for the 4096-, 1000-, and 300-patterns sets will be 0.8%, 0.2%, and 0.06% respectively, which is negligible overhead compared to the expected 100% capacity gain achieved by full-duplex systems.

Second, in the dynamic environment, due to the relatively fast channel variations, the system

starts to lose performance with the increase of the re-training time. The results show that, 2-3dB passive self-interference suppression loss is expected when the re-training time increases from 50ms to 500ms. However, for fair comparison of the different pattern sets, the overall training overhead should be considered. Thus, rather than focusing on the re-training time, it is desired to observe the performance at a fixed training overhead. For example, if the training overhead is fixed at 1% with a 2us pattern training interval then, the 4096-, 1000-, and 300-patterns sets should be compared at re-training times of ∼800ms, 200ms, and 60ms respectively. Comparing the performance of the different sets at the previous re-training times we note that all different sets achieve approximately the same performance.

Another practical aspect that should be considered when discussing re-training time is useful data frame length. Although the performance of the optimum 4096-patterns set is best among the other sets, however, for reasonable training overhead, the required re-training time for the 4096-patterns set is very high. For instance, from the previous examples, we show that for the optimal 4096-patterns set at 1% training overhead, re-training time of 800ms is required regardless of the useful data length transmitted within the 800ms. In other words, to guarantee 1% training overhead, a useful data frame length of ∼800ms should be transmitted between the two successive MRA training intervals. Therefore, in multi-user networks, each user should be assigned a continuous 800ms interval for data transmission, which is relatively large interval. On the other hand, the 300-patterns set requires only 60ms re-training time. Accordingly, from a practical perspective, using smaller pattern sets alleviates the constraints on the overall network performance.

6.5 Overall Full-duplex System Performance

In this section, we characterize the overall performance of the full-duplex system utilizing MRA. For full system performance characterization, the MRA-based passive suppression is

combined with a conventional digital self-interference cancellation technique. In the full-duplex system, the received signal in the time and frequency domains can be written as

$$y_n = h_n^I * \left(x_n^I + z_n^T\right) + h_n^S * \left(x_n^S + z_n^T\right) + z_n^R, \tag{6.1}$$

$$Y_k = H_k^I \left(X_k^I + Z_k^T\right) + H_k^S \left(X_k^S + Z_k^T\right) + Z_k^R, \tag{6.2}$$

where x^I, x^S are the transmitted time domain self-interference and signal-of-interest signals, h^I, h^S are the self-interference and signal-of-interest channels, z^T represents the transmitter noise, z^R represents the receiver noise, n is the time index, k is the subcarrier index, * denotes convolution process, and uppercase letters denote the frequency-domain representation of the corresponding time-domain signals. The digital cancellation is performed by subtracting the term $\hat{H}_k^I X_k^I$ from the received signal in (6.2). $\hat{H}^I$ is an estimate for the self-interference channel, obtained using training sequences transmitted at the beginning of each data frame [17].

6.5.1 Overall self-interference cancellation

In this analysis, the overall self-interference cancellation achieved using MRA-based passive suppression followed by digital cancellation (DC) is characterized. The complete system framework discussed in section 6.3 is used to characterize the overall self-interference cancellation performance as follows. In the beginning, the MRA is trained and the optimum pattern is selected. Then, a sequence of data frames are transmitted from one node and the other node remains silent. Now, the received data frame contains only the self-interference signal, and the noise associated with it. The self-interference channel is estimated at the beginning

of each data frame, then digital cancellation is performed. The total self-interference suppression is calculated as the ratio between the transmit power and the residual self-interference power after digital cancellation.

Figure 6.13 shows the residual self-interference power before and after DC at different transmit power values. The results show that, in addition to the ∼63dB passive suppression, digital cancellation could achieve up to 32dB more self-interference cancellation for a total of 95dB self-interference cancellation. At high transmit power values, the 32dB gain is mainly limited by the transmitter noise which can not be eliminated using conventional digital cancellation techniques. On the other hand, at low transmit power values, the achieved digital cancellation amount is limited by the receiver noise floor. At lower transmit power levels, the self-interference signal is totally suppressed to below the receiver noise floor, and the full-duplex systems is expected to achieve ∼100% rate gain compared to half-duplex systems.

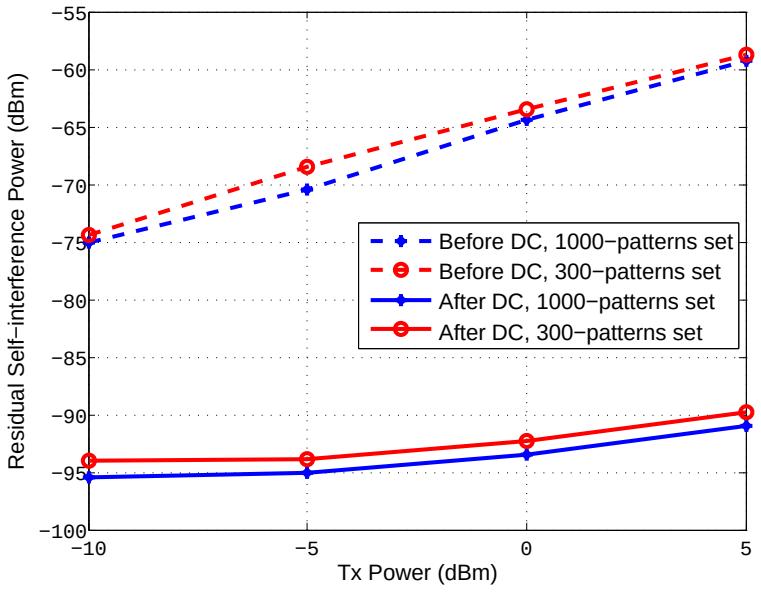

Figure 6.13: Residual self-interference power before and after DC at different transmit power values.

6.5.2 Achievable rate gain

The most important performance metric in full-duplex systems is the achievable rate gain compared to half-duplex systems. In this analysis, the achievable rate of the proposed full-duplex system is characterized in different experimental environments at different transmit power values. The performance is compared to the half-duplex system performance in the same environments. The achievable rate is calculated as a function of the effective Signal to Noise Ratio (SNR) as $R = log_2(1 + SNR)$. One way to calculate the effective SNR in an experimental analysis is by calculating the Error Vector Magnitude (EVM) defined as the distance between the received symbols (after equalization and digital cancellation) and the original transmitted symbols. Using the EVM to SNR conversion method in [26], the SNR is calculated as $SNR = 1/(EVM)^2$. The average achievable rate for both full-duplex and half-duplex systems is calculated as

$$R^{FD} = \frac{1}{NMK} \sum_{n=1}^{N} \sum_{m=1}^{M} \sum_{k=1}^{K} log_2 \left[1 + SINR_{n,m,k}\right], \tag{6.3}$$

$$R^{HD} = \frac{1}{NMK} \sum_{n=1}^{N} \sum_{m=1}^{M} \sum_{k=1}^{K} \frac{1}{2} log_2 \left[1 + SNR_{n,m,k}\right], \tag{6.4}$$

where R^{FD}, R^{HD} are the average achievable rate for full-duplex and half-duplex systems, $SINR$ is the effective signal to interference plus noise ratio in full-duplex system, SNR is the effective signal to noise ratio in the half-duplex system, N, M, K are the total number of data frames, OFDM symbols per frame, subcarriers per OFDM symbol respectively. The factor of $\frac{1}{2}$ in the half-duplex rate equation is due to the fact that each half-duplex node is transmitting only half of the time.

Figure 6.14 shows the achievable rate and the rate gain for the full-duplex and half-duplex

systems at different transmit power values. The results show that, the proposed full-duplex system achieves 80−90% rate gain compared to the half-duplex system at 5dBm transmit power in typical indoor environments. The reason why the proposed full-duplex system could not achieve the 100% rate gain even at low transmits power values is due to the 1dB signal-of-interest power loss shown in figure 6.11. This signal-of-interest power loss makes the full-duplex SINR less than the half-duplex SNR by 1dB even if the self-interference signal is totally suppressed below the noise floor. On the other hand, the performance difference between the 1000-patterns and the 300-patterns sets is due to the difference in the achieved self-interference cancellation amount as shown in figure 6.13.

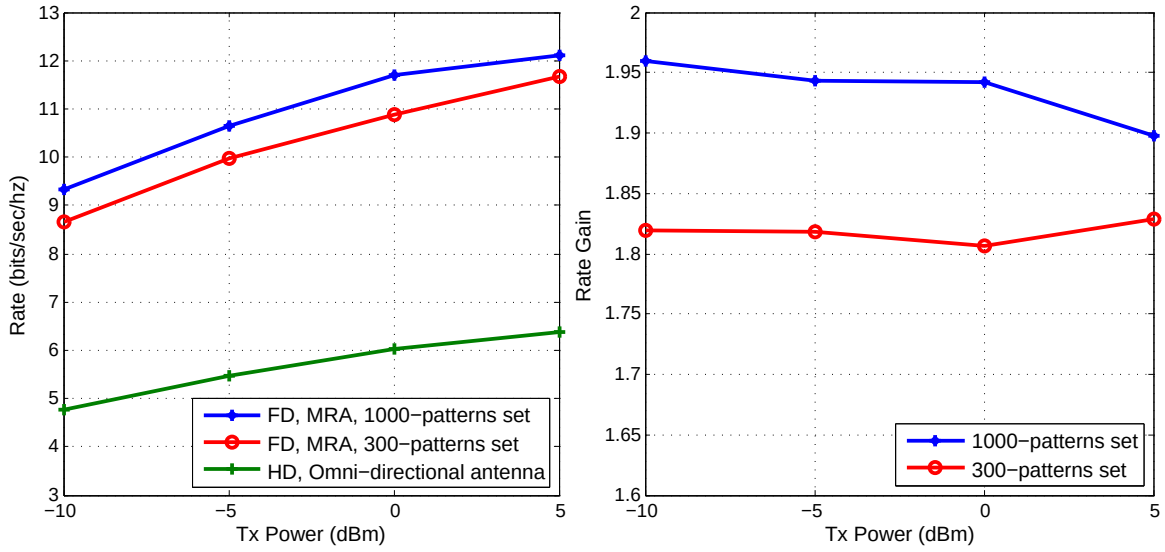

Figure 6.14: Overall achievable rate and rate gain for full-duplex and half-duplex systems.

6.6 Conclusion

In this chapter, A passive self-interference suppression technique using MRA is proposed. The proposed technique shows to achieve up to 65dB of passive suppression at 10 cm antenna separation. The proposed technique is combined with a conventional digital self-interference

cancellation technique to build a complete full-duplex system. The system performance is experimentally investigated in different indoor environments. The results show that, a total of 95dB self-interference cancellation is achieved by combining the MRA-based passive suppression technique with the conventional digital self-interference cancellation technique. In addition, the full-duplex achievable rate is experimentally investigated in typical indoor environments showing that, the proposed full-duplex system achieves up to 90% rate improvement compared to half-duplex systems in typical indoor environments.

Chapter 7

Conclusions and Summary

In this thesis, we considered the problem of self-interference cancellation in full-duplex systems.

First, we constructed a signal model that includes most of the transmitter and receiver RF impairments. Based on the model, we analytically and numerically investigated the effect of RF impairments on the cancellation capability of conventional self-interference cancellation techniques. In this analysis, the main performance limiting factors are identified. The results show that oscillator phase noise and transceiver nonlinearity are the two main limiting factors in full-duplex systems.

Then, we proposed several phase noise and nonlinearity estimation and suppression techniques to improve the overall self-interference cancellation capability. The nonlinearity suppression technique is shown to suppress the nonlinear distortion to the level of the next significant noise component, and achieve performance that is less than 0.5dB off the performance of a linear full-duplex system. On the other hand, phase noise estimation and suppression in full-duplex systems is shown to be very challenging and complexity consuming problem. More specifically, the results show that at a complexity of order $O(32^2)$ a

maximum of 3dB more self-interference cancellation is achieved compared to the case where no phase noise suppression in performed. Accordingly, to achieve significant phase noise suppression, other solutions should be investigated.

To overcome the phase noise limitation, we proposed a novel all-digital self-interference cancellation technique that is capable of significantly mitigating the transceiver phase noise and nonlinearity effects. The analyses show that using the proposed technique, full-duplex systems are no longer phase noise or nonlinearity limited. In addition, the overall full-duplex system performance using a combination of the proposed digital cancellation technique and practical passive suppression techniques is numerically investigated. The results show that, the proposed technique significantly mitigates the self-interference signal to ∼3dB higher than the receiver noise floor, which results in up to 76% rate improvement compared to conventional half-duplex systems at 20dBm transmit power values.

Since typical full-duplex systems deploy both passive suppression and active cancellation techniques to significantly mitigate the self-interference signal, the thesis concludes with proposing a novel MRA-based passive self-interference suppression technique that is capable of achieving 65dB of passive suppression at 10 cm antenna separation. The proposed technique is combined with a conventional digital self-interference cancellation technique to build a complete full-duplex system. The system performance is experimentally investigated in different indoor environments showing that, the proposed full-duplex system achieves up to 90% rate improvement compared to half-duplex systems in typical indoor environments.

Bibliography

[1] Cisco Visual Networking Index: Global Mobile Data Traffic Forecast Update, 2013-2018, Cisco, 2014.

[2] A. Fehske, G. Fettweis, J. Malmodin, and G. Biczok, "The global footprint of mobile communications: The ecological and economic perspective," *Communications Magazine, IEEE*, vol.49, no.8, pp.55,62, August 2011.

[3] D. W. Bliss, P. A. Parker, and A. R. Margetts, "Simultaneous transmission and reception for improved wireless network performance," *Conference Proceedings of the IEEE Statistical Signal Processing Workshop*, Aug. 2007.

[4] T. Riihonen, S. Werner, and R. Wichman, "Spatial loop interference suppression in full-duplex mimo relays," *Signals, Systems and Computers, 2009 Asilomar Conference on*, pp. 15081512, November 2009.

[5] T. Riihonen, S. Werner, and R. Wichman, "Residual self-interference in full-duplex MIMO relays after null-space projection and cancellation," *Signals, Systems and Computers, 2010 Asilomar Conference on*, pp. 653657, November 2010.

[6] D. Senaratne and C. Tellambura, "Beamforming for space division duplexing," *in Proceedings of IEEE International Conference on Communications (ICC)*, pp. 15, June 2011.

[7] T. Riihonen, S. Werner, and R. Wichman, "Mitigation of loopback self-interference in

full-duplex MIMO relays," *IEEE Transactions on Signal Processing*, vol. 59, pp. 5983 5993, Dec. 2011

[8] J. Ma, G. Li, J. Zhang, T. Kuze, and H. Iura, "A new coupling channel estimator for cross-talk cancellation at wireless relay stations," *IEEE Global Telecommunications Conference*, pp. 16, 2009.

[9] E. A. Rodriguez, R. L. Valcarce, T. Riihonen, S. Werner, and R. Wichman, "Adaptive self-interference cancellation in wideband full-duplex decode-and-forward MIMO relays," *IEEE Workshop on Signal Processing Advances in Wireless Communications (SPAWC)*, June 2013.

[10] E. A. Rodriguez, R. L. Valcarce, T. Riihonen, S. Werner, and R. Wichman, "Autocorrelation-based adaptation rule for feedback equalization in wideband full-duplex amplify-and- forward MIMO relays," *IEEE International Conference on Acoustics, Speech and Signal Processing (ICASSP)*, May 2013

[11] P. Lioliou, M. Viberg, M. Coldrey, and F. Athley, "Self-interference suppression in full-duplex MIMO relays," *Signals, Systems and Computers, 2010 Asilomar Conference on* , pp.658-662, Nov. 2010.

[12] S. Li, and R. D. Murch, "Full-Duplex Wireless Communication Using Transmitter Output Based Echo Cancellation," *Global Telecommunications Conference (GLOBECOM 2011)*, 2011 IEEE , pp.1-5, Dec. 2011.

[13] M. Duarte, and A. Sabharwal, "Full-duplex wireless communications using off-the-shelf radios: Feasibility and first results," *Signals, Systems and Computers, 2010 Asilomar Conference on*, pp.1558-1562, Nov. 2010.

[14] J. I. Choi, M. Jain, K. Srinivasan, P. Levis, and S. Katti, "Achieving single channel, full duplex wireless communication," *in MobiCom*, 2010.

[15] B. P. Day, A. R. Margetts, D. W. Bliss, and P. Schniter, "Full-Duplex Bidirectional MIMO: Achievable Rates Under Limited Dynamic Range," *Signal Processing, IEEE Transactions on*, vol.60, no.7, pp.3702-3713, July 2012.

[16] B. P. Day, A. R. Margetts, D. W. Bliss, and P. Schniter, "Full-Duplex MIMO Relaying: Achievable Rates Under Limited Dynamic Range," *Selected Areas in Communications, IEEE Journal on*, vol.30, no.8, pp.1541-1553, September 2012.

[17] M. Duarte, C. Dick, and A. Sabharwal, "Experiment-driven Characterization of Full-Duplex Wireless Systems," *Wireless Communications, IEEE Transactions on*, vol.11, no.12, pp.4296,4307, December 2012.

[18] S. Chen, M. A. Beach, and J. P. McGeehan, "Division-free duplex for wireless applications," *IEEE Electronics Letters*, vol. 34, 1998.

[19] B. Radunovic, D. Gunawardena, P. Key, A. P. N. Singh, V. Balan, and G. Dejean, "Rethinking indoor wireless Mesh Design: Low power, low frequency, full duplex," *Wireless Mesh Networks (WIMESH 2010), 2010 Fifth IEEE Workshop on*, pp.1-6, June 2010.

[20] M. Jain, J. I. Choi, T. Kim, D. Bharadia, K. Srinivasan, S. Seth, P. Levis, S. Katti, and P. Sinha, "Practical, Real-time, Full Duplex Wireless," *in Proceeding of the ACM Mobicom*, Sept. 2011.

[21] M.E. Knox, "Single antenna full duplex communications using a common carrier," *Wireless and Microwave Technology Conference (WAMICON), 2012 IEEE 13th Annual*, 15-17 April 2012.

[22] A. Balatsoukas-Stimming, P. Belanovic, K. Alexandris, and A. Burg, "On Self-interference Suppression Methods for Low-complexity Full-duplex MIMO," *Signals, Systems and Computers, 2013 Asilomar Conference on*, pp.992,997, Nov. 2013.

[23] D. Bharadia, E. McMilin, and S. Katti, "Full Duplex Radios, " in *ACM SIGCOMM*, Aug. 2013.

[24] H. Suzuki, K. Itoh, Y. Ebine, and M. Sato, "A booster configuration with adaptive reduction of transmitter-receiver antenna coupling for pager systems," *IEEE Vehicular Technology Conference, Fall 1999*, vol. 3, pp. 1516 1520 vol.3, 1999.

[25] K. Lin, Y. E. Wang, C.-K. Pao, and Y.-C. Shih, "A Ka-Band FMCW radar front-end with adaptive leakage cancellation," *IEEE Transactions on Microwave Theory and Techniques*, vol. 54, no. 12, pp. 40414048, 2006.

[26] J.-W. Jung, H.-H. Roh, J.-C. Kim, H.-G. Kwak, M. S. Jeong, and J.-S. Park, "TX leakage Cancellation via a micro controller and high TX-to-RX ssolations covering an UHF RFID frequency band of 908 to 914 MHz," *IEEE Microwave and Wireless Components Letters*, vol. 18, no. 10, pp. 710712, 2008.

[27] G. Lasser, R. Langwieser, and A. L. Scholtz, "Broadband suppression properties of active leaking carrier cancellers," *IEEE International Conference on RFID*, pp. 208212, IEEE, 2009.

[28] P. Pursula, M. Kiviranta, and H. Seppa, "UHF RFID reader with reflected power canceller," *IEEE Microwave and Wireless Components Letters*, vol. 19, no. 1, pp. 4850, 2009.

[29] A. Sahai, G. Patel, and A. Sabharwal, "Pushing the limits of full-duplex: Design and real-time implementation, http://arxiv.org/abs/1107.0607," in *Rice University Technical Report TREE1104*, June 2011.

[30] A. Sahai, G. Patel, and A. Sabharwal, "Asynchronous full-duplex wireless," *Communication Systems and Networks (COMSNETS), 2012 Fourth International Conference on* , pp.1-9, Jan. 2012.

[31] M. Duarte, A. Sabharwal, V. Aggarwal, R. Jana, K.K. Ramakrishnan, C.W. Rice, and N.K. Shankaranarayanan, "Design and Characterization of a Full-Duplex Multiantenna System for WiFi Networks," *Vehicular Technology, IEEE Transactions on*, vol.63, no.3, pp.1160,1177, March 2014.

[32] E. Everett, M. Duarte, C. Dick, and A. Sabharwal, "Empowering full-duplex wireless communication by exploiting directional diversity," *Signals, Systems and Computers, 2011 Asilomar Conference on*, pp.2002-2006, Nov. 2011.

[33] E. Everett, A. Sahai, and A. Sabharwal, "Passive Self-Interference Suppression for Full-Duplex Infrastructure Nodes," *Wireless Communications, IEEE Transactions on*, vol.13, no.2, pp.680,694, February 2014.

[34] W. Cheng, X. Zhang, and H. Zhang, "Full Duplex Wireless Communications for Cognitive Radio Networks," [Online]. Available: http://arxiv.org/abs/1105.0034.

[35] M. A. Khojastepour, K. Sundaresan, S. Rangarajan, X. Zhang, and S. Barghi, "The case for antenna cancellation for scalable full-duplex wireless communications," *in Proceedings of the 10th ACM Workshop on HotNets*, 2011.

[36] J. I. Choi, S. Hong, M. Jain, S. Katti, P. Levis, and J. Mehlman, "Beyond full duplex wireless," *Signals, Systems and Computers, 2012 Asilomar Conference on*, pp.40,44, 4-7 Nov. 2012.

[37] A. Sahai, G. Patel, C. Dick, and A. Sabharwal, "Understanding the impact of phase noise on active cancellation in wireless full-duplex," *Signals, Systems and Computers, 2012 Asilomar Conference on*, pp.29,33, 4-7 Nov. 2012.

[38] D.W. Bliss, T.M. Hancock, and P. Schniter, "Hardware phenomenological effects on cochannel full-duplex MIMO relay performance," *Signals, Systems and Computers, 2012 Asilomar Conference on*, pp.34,39, 4-7 Nov. 2012.

[39] T. Riihonen, P. Mathecken, and R. Wichman, "Effect of oscillator phase noise and processing delay in full-duplex OFDM repeaters," *Signals, Systems and Computers, 2012 Asilomar Conference on*, Nov. 2012.

[40] A. Sahai, G. Patel, C. Dick, and A. Sabharwal, "On the Impact of Phase Noise on Active Cancellation in Wireless Full-Duplex," *Vehicular Technology, IEEE Transactions on*, vol.62, no.9, pp.4494,4510, Nov. 2013.

[41] V. Syrjala, M. Valkama, L. Anttila, T. Riihonen, and D. Korpi, "Analysis of Oscillator Phase-Noise Effects on Self-Interference Cancellation in Full-Duplex OFDM Radio Transceivers," *Wireless Communications, IEEE Transactions on*, vol.13, no.6, pp.2977,2990, June 2014.

[42] A. Sabharwal, P. Schniter, D. Guo, D. Bliss, S. Rangarajan, and R. Wichman, "In-band Full-duplex Wireless: Challenges and Opportunities," *Selected Areas in Communications, IEEE Journal on*, vol.PP, no.99, June 2014.

[43] "IEEE Standard for Information technology–Telecommunications and information exchange between systems Local and metropolitan area networks–Specific requirements Part 11: Wireless LAN Medium Access Control (MAC) and Physical Layer (PHY) Specifications," *IEEE Std 802.11-2012 (Revision of IEEE Std 802.11-2007)*, March 2012.

[44] Femto Forum, "Interference Management in UMTS Femtocells," February 2010.

[45] W. Slingsby, and J. McGeehan, "Antenna isolation measurements for on-frequency radio repeaters," *ntennas and Propagation, 1995., Ninth International Conference on (Conf. Publ. No. 407)*, 4-7 Apr 1995.

[46] C. Anderson, S. Krishnamoorthy, C. Ranson, T. Lemon, W. Newhall, T. Kummetz, and J. Reed, "Antenna isolation, wideband multipath propagation measurements, and interference mitigation for on-frequency repeaters," *SoutheastCon, 2004. Proceedings. IEEE*, 26-29 March 2004.

[47] K. Haneda, E. Kahra, S. Wyne, C. Icheln, and P. Vainikainen, "Measurement of loop-back interference channels for outdoor-to-indoor full-duplex radio relays," *Antennas and Propagation (EuCAP), 2010 Proceedings of the Fourth European Conference on*, 12-16 April 2010.

[48] T. Schenk, RF Imperfections in High-rate Wireless Systems, Impact and Digital Compensation. New York: Springer-Verlag, 2008.

[49] B. Razavi, Design of Analog CMOS Integrated Circuits. New York:McGraw-Hill, 2001.

[50] M. Lu, N. Shanbhag, and A. Singer, "BER-optimal analog-to-digital converters for communication links," *Circuits and Systems (ISCAS), Proceedings of 2010 IEEE International Symposium on*, pp.1029-1032, May 30 2010-June 2 2010.

[51] ``http://datasheets.maximintegrated.com/en/ds/MAX2828-MAX2829.pdf''.

[52] ``http://datasheets.maximintegrated.com/en/ds/MAX19757.pdf''.

[53] S. Shekhar, D. Gangopadhyay, W. Eum-Chan, and D. J. Allstot, "A 2.4-GHz Extended-Range Type-I $\Sigma\Delta$ Fractional-N Synthesizer With 1.8-MHz Loop Bandwidth and 110-dBc/Hz Phase Noise," *Circuits and Systems II: Express Briefs, IEEE Transactions on*, vol.58, no.8, pp.472-476, Aug. 2011.

[54] V. Erceg, and L. Schumacher et al., "TGn channel models," IEEE 802.11-03/940r4, May 2004.

[55] S. S. Ghassemzadeh, L. J. Greenstein, A. Kavcic, T. Sveinsson, and V. Tarokh, "UWB indoor path loss model for residential and commercial buildings," *Vehicular Technology Conference, 2003. VTC 2003-Fall. 2003 IEEE 58th*, vol.5, pp.3115-3119 Vol.5, Oct. 2003.

[56] S. Zhou, and J. K. Pollard, "Position measurement using Bluetooth," *Consumer Electronics, IEEE Transactions on*, vol.52, no.2, pp.555-558, May 2006.

[57] SIG, "Specification of the Bluetooth System", http://www.bluetooth.com.

[58] A. Mehrotra, "Noise analysis of phase-locked loops," *Circuits and Systems I: Fundamental Theory and Applications, IEEE Transactions on*, vol.49, no.9, pp. 1309-1316, Sep 2002.

[59] C. Andrews, and A.C. Molnar, "A passive-mixer-first receiver with baseband-controlled RF impedance matching, $\ll$ 6dB NF, and $\gg$ 27dBm wideband IIP3," *Solid-State Circuits Conference Digest of Technical Papers (ISSCC), 2010 IEEE International*, pp.46,47, 7-11 Feb. 2010.

[60] D. Murphy, A. Hafez, A. Mirzaei, M. Mikhemar, H. Darabi, M.F. Chang, and A. Abidi, "A blocker-tolerant wideband noise-cancelling receiver with a 2dB noise figure," *Solid-State Circuits Conference Digest of Technical Papers (ISSCC), 2012 IEEE International*, pp.74,76, 19-23 Feb. 2012.

[61] T. Kwon, S. Lim, S. Choi, and D. Hong, "Optimal Duplex Mode for DF Relay in Terms of the Outage Probability," *Vehicular Technology, IEEE Transactions on*, vol.59, no.7, pp.3628-3634, Sept. 2010.

[62] A. Demir, A. Mehrotra, and J. Roychowdhury, "Phase noise in oscillators; a unifying theory and numerical methods for characterization," *IEEE Trans. Circuits Syst. I*, vol. 47, pp. 655-674 May 2000.

[63] "Rice University WARP project," http://warp.rice.edu.

[64] "Universal Software Radio Peripheral (USRP), " https://www.ettus.com/product/category/USRP-Networked-Series.

[65] D. Petrovic, W. Rave, and G. Fettweis, "Effects of Phase Noise on OFDM Systems With and Without PLL: Characterization and Compensation," *Communications, IEEE Transactions on*, vol.55, no.8, pp.1607-1616, Aug. 2007.

[66] S. Wu, P. Liu, and Y. Bar-Ness, "Phase Noise Estimation and Mitigation for OFDM Systems," *Wireless Communications, IEEE Transactions on*, vol.5, no.12, pp.3616-3625, December 2006.

[67] S. Bittner, W. Rave, and G. Fettweis, "Joint Iterative Transmitter and Receiver Phase Noise Correction using Soft Information," *Communications, 2007. ICC '07. IEEE International Conference on*, pp.2847-2852, 24-28 June 2007.

[68] V. Syrjala, and M. Valkama, "Receiver DSP for OFDM Systems Impaired by Transmitter and Receiver Phase Noise," *Communications (ICC), 2011 IEEE International Conference on*, June 2011.

[69] V. Syrjala, and M. Valkama, "Iterative receiver signal processing for joint mitigation of transmitter and receiver phase noise in OFDM-based cognitive radio link," in Proc. *CROWNCOM12, Stockholm, Sweden*, Jun. 2012.

[70] Y. Kang, K. Kim, and H. Park, "Efficient DFT-based channel estimation for OFDM systems on multipath channels," *Communications, IET*, vol.1, no.2, pp.197,202, April 2007.

[71] NI 5791R User Manual and Specifications. http://www.ni.com/pdf/manuals/373845d.pdf.

[72] Z. Li, D. Rodrigo, L. Jofre, B. Cetiner, "A new class of antenna array with a reconfigurable element factors," *IEEE Trans. Antennas Propag.*, vol. 61, no. 4, pp. 1947-1955, Apr. 2013.

[73] Rogers Corp., Microwave Products Tech. Information 2012, One Technology Drive, CT 06263.

[74] R. F. Harrington, "Reactively controlled directive arrays," submitted to *IEEE Trans. Antennas Propag.*, vol. 26, no. 3, pp. 390-395, May 1978.

[75] "The ZedBoard," http://www.zedboard.org/.

[76] H. Arslan, and H. Mahmoud, "Error vector magnitude to SNR conversion for nondata-aided receivers," *IEEE Transactions on Wireless Communications*, vol. 8, no. 5, pp. 26942704, May 2009.